BARYON-BARYON INTERACTIONS IN A CHIRAL CONSTITUENT QUARK MODEL

BRUNO JULIÁ DÍAZ

UNIVERSIDAD DE SALAMANCA

FACULTAD DE CIENCIAS

Departamento de Física, Ingeniería y Radiología Médica

Grupo de Física Nuclear

D. ALFREDO VALCARCE MEJÍA, PROFESOR TITULAR DE FÍSICA ATÓMICA, MOLECULAR Y NUCLEAR, MIEMBRO DEL DEPARTAMENTO DE FÍSICA, INGENIERÍA Y RADIOLOGÍA MÉDICA,

Autoriza la presentación de la tesis doctoral titulada "Baryon-Baryon interactions in a chiral constituent quark model", realizada bajo su dirección por D. Bruno Juliá Díaz.

Salamanca, 11 de Febrero de 2003

Fdo: A. Valcarce

Durante estos cuatro años ha habido mucha gente que me ha ayudado y que me ha animado a seguir en esta empresa. Algunos muy activamente, colaborando, enseñándome cosas, otros sencillamente hablando, compartiendo sus historias, otros están cerca desde hace tiempo. Me gustaría no olvidar a ninguno, aunque esto no parece fácil, disculpadme pues los omitidos.

Quisiera agradecer a mi director, Alfredo Valcarce, por introducirme en el mundo de los quarks, por su dedicación y trabajo que han hecho posible esta tesis y por su confianza a lo largo de todo el proceso.

A Pedro González por su ayuda y colaboración en mucho de lo que hay expuesto en esta tesis y por las agradables dos semanas en Valencia. A Paco Fernández por su apoyo a lo largo de estos años. A David R. Entem por permitirme utilizar su trabajo y por su ayuda en varios de los temas tratados en la tesis. A Eliecer y Vijande por su amistad. A Luis, Barquilla y Verde por su compañerismo, así como al resto de miembros del grupo.

Thanks to Johann Haidenbauer for welcoming me in Jülich, for the nice working atmosphere and for the very interesting collaboration we had. Also to the theory group at the KFA (Jülich), specially to J. Oller and Achot. I also want to thank Sergei, Walid and Wassan for the time we shared in Nordstraße 3.

Thanks to Peter Sauer for allowing me to join his group and enjoy their endless matrix elements in their warming environment in Appelstraße 2. And of course to Karlsten Chmielewski, L. Yuan and Malte Oelsner for their very pleasant company in Hannover.

I want to thank Harry Lee for teaching me, for his friendship and for the nice collaboration we started. I also want to thank the people at the Theory Division in ANL: Bob, Steve, Peter, Bogdan, Murray, etc. Special mention to Jonathan, Stephane and Marty whose company I enjoyed during my stays at Argonne.

Thanks to S. Hirenzaki for helping me to reproduce his calculations.

Gracias a la gente con la que he compartido los congresos y escuelas.

A J. Villarroel, M. Matias, la gente del futbito, los charro-ópticos y al resto de gente de la Facultad por hacerme más agradable mi paso por Salamanca.

También me gustaría agradecer a toda la gente que ha convivido conmigo durante este tiempo: Carlos, Norma, Manu, Baptiste, Dagmar, Rodolfo, Anabelle, Jamo, Alejandro y a la gente con la que he pasado buenos ratillos: Steffano, Ursula, Javi, Cruz, Rebecca, Audrey, Denis, Sergio, Conraduss, Fernando, Zahara, Ben, Capuccine, Dominique&Claude.

A mi familia por andar por ahí y seguir mis pasos en cada evento familiar.

A toda la gente con la que he disfrutado hablando/discutiendo de física y de cualquier otra cosa: Barroso, el Ferre, J. Luis Franco, Demetrio, Morillas, Assum, Spela, Alfons, Humberto, Bernard, Raphäel, Javi Vignote, Laura, ...

Y por su puesto a mis amigos y compañeros de carrera: Nacho, Fernandito, Rubio, Luna, Andrés, Beatriz, Lainez, Cristinita, Melas, Julián, Borja, Amanda y Edu.

A ti, ma chérie Charlotte, por estar ahí!

Y cómo no!,

A mi madre, por mostrarme otros mundos.

Contents

Notation

In the following several symbols will appear which are summarized here for a better reading,

BO	Born-Oppenheimer
RGM	Resonating Group Method
EST	Ernst-Shakin-Thaler

λ_i	Color Gell-Mann matrix, particle i
σ_i	Pauli spin matrix, particle i

m_N	Nucleon mass
m_π	Pion mass
α_{ch}	Chiral coupling constant
Λ_{ch}	Chiral symmetry breaking scale
α_s	Strong coupling constant
b	Harmonic oscillator parameter

S	Spin
T	Isospin
J	Total angular momentum
L	Orbital angular momentum
$^{2S+1}L_J$	Spectroscopic notation

N	Nucleon
$N^*(1440)$	Roper resonance
Δ	$\Delta(1232)$

OPE	One-pion exchange
OSE	One-sigma exchange
OGE	One-gluon exchange

1 A BIT OF HISTORY: MOTIVATION

Understanding the forces that bind nuclei and prevent them from breaking apart due to the electromagnetic repulsion between the protons is still an open issue though their existence has already been known for almost a hundred years.

The pioneering experiments of Rutherford [1] [1] by 1910 led to the discovery of the inner structure of atoms. That step started the exploration of a new field of physics which could not be described with the existing ideas at that time: the very small was completely different from the world we are dealing with on our day life and also to the world of the very large exemplified by the movement of planets and stars. This new world needed new ways of thinking, basic concepts had to be revisited and redefined in an entirely different way.

Quantum mechanics proved to be extremely successful in explaining the properties of atoms allowing a quantitative understanding. Atomic spectra were explained with astonishing precision assuming a very simple model, atoms were made up of a heavy nucleus with positive charge sitting in the center of a quite empty space with a group of electrons orbiting around it obeying the laws of quantum mechanics. The force that was preventing electrons to escape from the nucleus was the electromagnetic force. Soon after, the interaction between atoms that make possible the existence of molecules, clusters of atoms, could also be understood as remnant forces, Van der Waals forces, of the electromagnetic attraction between the electrons and the nuclei.

The next natural step was to keep increasing the collision energies such that the possible structure of the nucleus itself could be explored. Nuclei basicly consist of protons and neutrons [2] tightly packed to form a dense core inside atoms. The forces that keep neutrons and protons together have to be of very short-range, otherwise they would show up at higher scales, and of great intensity compared to the electromagnetic repulsive interaction between the protons. These forces that keep nucleons bound together to form nuclei are called *strong forces.*

---

[1]Rutherford found that the only way to understand the results of the experiments carried out by E. Marsden and H. Geiger, under his supervision, where they bombarded thin layers of materials with alpha particles, was to assume a positively charged nucleus of very short size, 10^{-14} meters, residing inside the atoms whose peculiar sizes where about 10^4 times larger. In his own words *'It was almost as if you fired a fifteen-inch shell at a piece of tissue paper and it bounced back and hit you'.*

[2]The discovery of neutrons by Chadwick [2, 3] was much later than that of the proton.

	Symbol	Mass, MeV	Spin	Parity	Isotopic spin, T, T_3	Strange-ness, s	Baryon number, N	Lifetime, sec	Principal decay schemes
Photon	γ	0	1	-1	–	–	0	∞	
Leptons	ν_e, $\bar{\nu}_e$	0	$\frac{1}{2}$		–	–	0	∞	
	ν_μ, $\bar{\nu}_\mu$	0	$\frac{1}{2}$		–	–	0	∞	
	e±	0.510976 ± 0.000007	$\frac{1}{2}$	∓ 1	--	–	0	∞	
	$\mu\pm$	105.653 ± 0.002	$\frac{1}{2}$	∓ 1	--	--	0	$(2.200 \pm 0.002)10^{-6}$	$\mu \to e + \nu_\mu + \bar{\nu}_e$
Mesons	$\pi\pm$	139.58 ± 0.05	0	-1	$(1, \pm 1)$	0	0	$(2.55 \pm 0.03)10^{-8}$	$\pi \to \mu + \bar{\nu}_\mu$
	π^0	134.99 ± 0.05			$(1, 0)$			$(1.1 \pm 0.2)10^{-16}$	$\pi^0 \to 2\gamma$
	K^+	493.8 ± 0.2	0	-1	$(\frac{1}{2}, \frac{1}{2})$ $(\frac{1}{2}, -\frac{1}{2})$	$+1$ -1	0	$(1.23 \pm 0.01)10^{-8}$	$K \to$ $\begin{cases} 2\pi \\ 3\pi \\ \pi + \mu + \bar{\nu}_\mu \\ \pi + e + \bar{\nu}_e \\ \mu + \bar{\nu}_\mu \end{cases}$
	K^-								
	K^0, $\overline{K^0}$	497.8 ± 0.6			$(\frac{1}{2}, \mp\frac{1}{2})$	± 1		$(0.91 \pm 0.02)10^{-10}$ or $(6 \pm 2)10^{-8}$	
Baryons	p	938.21 ± 0.01	$\frac{1}{2}$	1	$(\frac{1}{2}, +\frac{1}{2})$	0	1	∞	
	n	939.50 ± 0.01	$\frac{1}{2}$	1	$(\frac{1}{2}, -\frac{1}{2})$	0	1	$(1.01 \pm 0.03)10^{+3}$	$n \to p + e + \bar{\nu}_e$
	Λ	1115.4 ± 0.1	$\frac{1}{2}$	1	0	-1	1	$(2.6 \pm 0.2)10^{-10}$	$\Lambda \to$ $\begin{cases} p + \pi^- \\ n + \pi^0 \end{cases}$
	Σ^+	1189.2 ± 0.2	$\frac{1}{2}$	1	$(1, +1)$	-1	1	$(0.77 \pm 0.03)10^{-10}$	$\Sigma^+ \to$ $\begin{cases} n + \pi^+ \\ p + \pi^0 \end{cases}$
	Σ^-	1197.6 ± 0.5	$\frac{1}{2}$	1	$(1, -1)$	-1	1	$(1.6 \pm 0.1)10^{-10}$	$\Sigma^- \to n + \pi^-$
	Σ^0	1193.2 ± 0.7	$\frac{1}{2}$	1	$(1, 0)$	-1	1	$< 10^{-11}$	$\Sigma^0 \to \Lambda + \gamma$
	Ξ^-	1321.0 ± 0.2	$\frac{1}{2}$?	?	$(\frac{1}{2}, -\frac{1}{2})$	-2	1	$(1.6 \pm 0.1)10^{-10}$	$\Xi \to \Lambda + \pi$
	Ξ^0	1321 ± 4	$\frac{1}{2}$?	?	$(\frac{1}{2}, \frac{1}{2})$	-2	1	$(4 \pm 1)10^{-10}$	

Figure 1.1: The particle zoo. We show the particles with lifetimes longer than 10^{-16}s known by 1964. The figure is taken from Ref. [9].

Too many particles

Yukawa postulated in the 30s that this force between nucleons (neutrons and protons) should be mediated by a massive particle, unknown at that time, in analogy to the photon and the electromagnetic interaction. Based on considerations about the range of this interaction [3] he predicted that its mass should be of around 100 MeV [4]. This carrier of the strong force was called the pion (π). The pion was discovered experimentally a decade later by Lattes et al. [5]. This discovery, together with that of the muon by Neddermeyer and Anderson [6] and Street and Stevenson [7] [4] settled the beginning of particle physics.

By the middle of the past century a lot of very short-lived new particles were produced in accelerators around the world in what was soon baptized as *the particle zoo*, see Fig. 1.1. This huge amount of different particles reminded the times of Mendeleiev when there were more than 70 *elements* that seemed to be all of them equally elementary showing that a much simpler interpretation of all the particles would probably be on the way. This happened in the 60s when M. Gell-Mann, Y. Ne'eman and G. Zweig, postulated the idea

---

[3]The range of an interaction is related to the inverse of the mass of the exchanged particle, that makes electromagnetic interaction very long ranged -photons cannot be at rest- so that with a mass of a few hundred MeV the range of the interaction was on the region of the 10^{-15} meters.

[4]The muon was thought for some time to be the pion itself due to the similar masses of both particles. The keypoint to distinguish between them was the mean life of the detected particle that was much longer than the expected one for the pion. See Ref. [8] for a historical description of the discoveries of muons and pions.

of quarks [10, 11]. These particles were first introduced as a mathematical artifact to give some sort of order to the zoo [5]. This idea not only could explain most of the particles (hadrons) as compound states of three basic ones but also allowed Gell-Mann to predict a new particle with its mass in what was one of the great successes of the quark model, the Ω^- (1672), discovered experimentally by Barnes et al. [12] a few months after it was theoretically predicted. Years after, it appeared the idea of these particles being the actual microscopic constituents of all matter that could feel strong forces. The quark picture was introduced; protons, neutrons, and the rest of baryons, were made up of three quarks while mesons, such as the pion, were composed of a quark and an antiquark. This simple idea, assuming some quantum numbers for the quarks, allowed to understand the quantum numbers of all the known particles and also gave an impressive result when magnetic moments were studied.

Thus, the first thing that was studied within the quark picture were static properties of the particles already known by that time. The next goal was to understand the forces between the quarks, the dynamics. The basic questions that had to be answered were, Why do quarks only appear in groups of three or as quark-antiquark and never alone? How could one explain high-energy experiments where jets of particles were found? Which is the mechanism that binds these quarks together?

QCD

There it came *Quantum Chromodynamics* (QCD). The necessity of a new degree of freedom, color, was soon postulated. It was introduced to preserve the Pauli antisymmetrization principle in this new world of inside nucleons. The 'new' [6] theory, QCD, has been able to explain all the data in the high-energy regions being now considered as the *true* theory of the strong interaction. However this theory has some important impediments, mostly due to the non-abelian structure of the gauge group from which it is derived, and has remained only partially solved until today. The main problem comes from the fact that a perturbative understanding of the theory can only be done properly at very high energies where the coupling constant between quarks and gluons is small and a perturbative solution of the theory makes sense (see Fig. 1.2). It is this region the one that is tested in very high energy experiments where jets of particles are found. They can be naively understood assuming that when, for example, an electron hits a proton with great energy, each quark of the proton is hit independently and then dressed with quarks from the vacuum forming new hadrons and resulting in three (each for each original quark in the proton) jets, see Fig. 1.3.

---

[5]The original idea came when they realized that most of the particles already known could be accommodated in certain representations of the $SU(3)_f$ group giving support to the idea of some basic pieces being the vectors of the fundamental representations of the group.
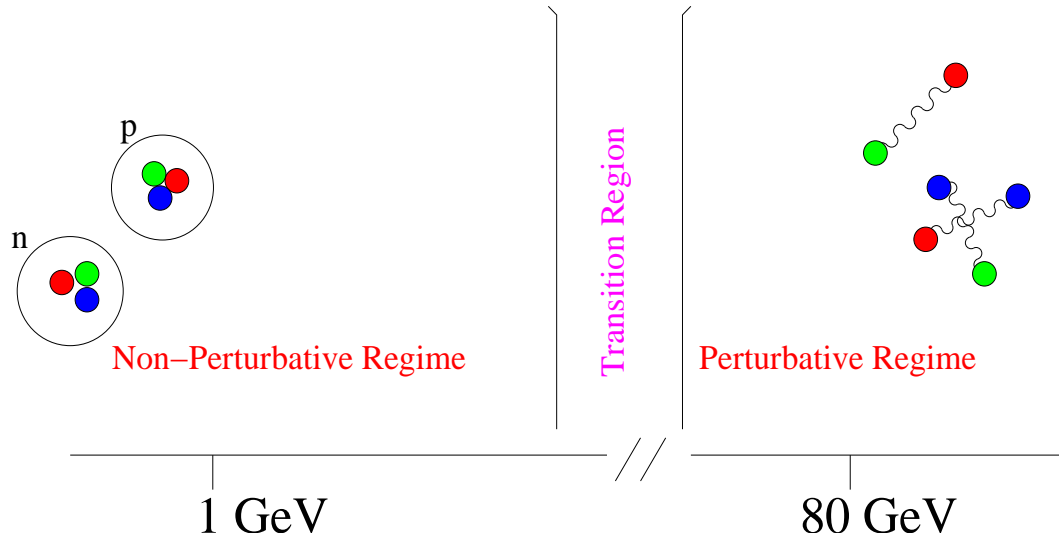
[6]QCD is already 30 years old.

Figure 1.2: Naive distinct regimes in QCD.

Difficulties at low energies

A completely different scenario occurs in the energy domain where we are interested in medium-energy nuclear physics. In this region we are dealing with energies of the order of the masses of low-lying hadrons, typically 1 GeV. At these energies the coupling between gluons and quarks grows making impossible any perturbative description. This problem has given rise to a whole variety of models, such as constituent quark models, skirmion models, bag models; approaches, such as the study of chiral symmetry as a tool to obtain low-energy theories, and also to some new branches like *lattice QCD.*

This energy domain is nowadays of great interest because of mainly two reasons:

- The transition between QCD and nuclear physics, that is, between the scale where a description in terms of quarks and gluons and the description in terms of mesons and baryons, is expected to lie in this region.

- It is the region of confinement where quarks are tightly bound together to form hadrons and also where chiral symmetry has been proved to be crucial.

There is where constituent quark models enter into the game. They recover the initial naive picture for hadrons, baryons being composed by three quarks and mesons by a quark and an antiquark, and derive the forces acting between these *constituent* quarks taking into account the main properties of the underlying theory, QCD. This *naive* idea finds great support in the heavy quark sector and allows a very good understanding of, for instance, the charmonium ($c\bar{c}$) spectrum. The spectrum of charmonium turns out to be approximately just a rescaling of the spectrum of positronium (electron-positron, of electromagnetic origin) as can be seen in Fig. 1.4 [13].
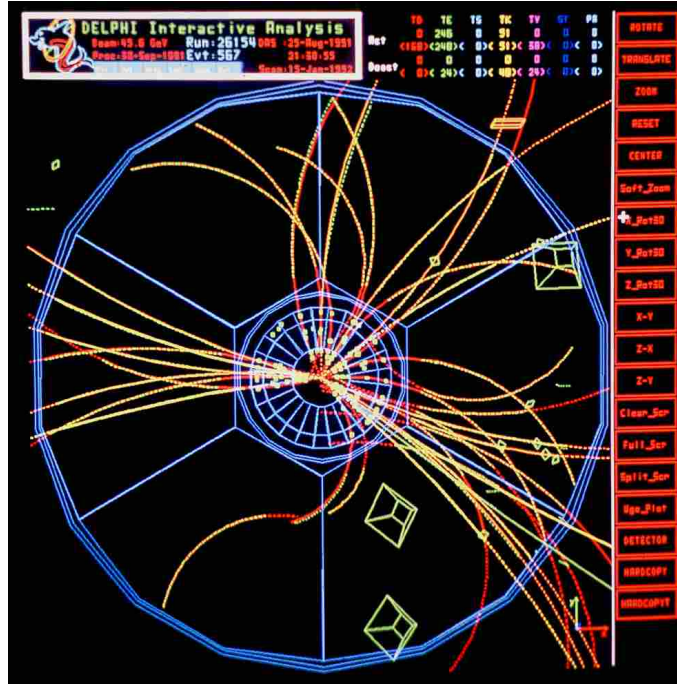
Figure 1.3: Resulting hadrons in a high energy collision. Jets are clearly recognized. Picture taken from the CERN photo database, `http://www.cern.ch`.

During the last 30 years several of such *QCD inspired* models have been proposed. These models provide a consistent framework which can link two different phenomenologies as are on the one hand the baryon-baryon interactions and with them the origin of nuclear forces and on the other hand the study of low-lying hadronic spectra and the nature of resonances.

In this thesis we consider a constituent quark model which has been employed to study many features in the low-energy regime. In the following we go through several open issues in this energy range and briefly describe the contribution of this work to each of them.

In Chapter 2 we start describing the basic elements of the chiral constituent quark model and summarize some of the previous calculations that have already been done with it. The model we use in this work is the one of Refs. [14, 15] [7]. The differences between the model and other available in the literature will be discussed. The main success of the model concerns the understanding of both the low-energy hadron spectrum and the

---

[7]Some authors name this model as *hybrid quark model* due to the model containing both the exchange of gluons and Goldstone bosons. We do not use it as it creates confusion with true hybrid models where the interactions between quarks are supplemented with effective interactions at baryonic level.
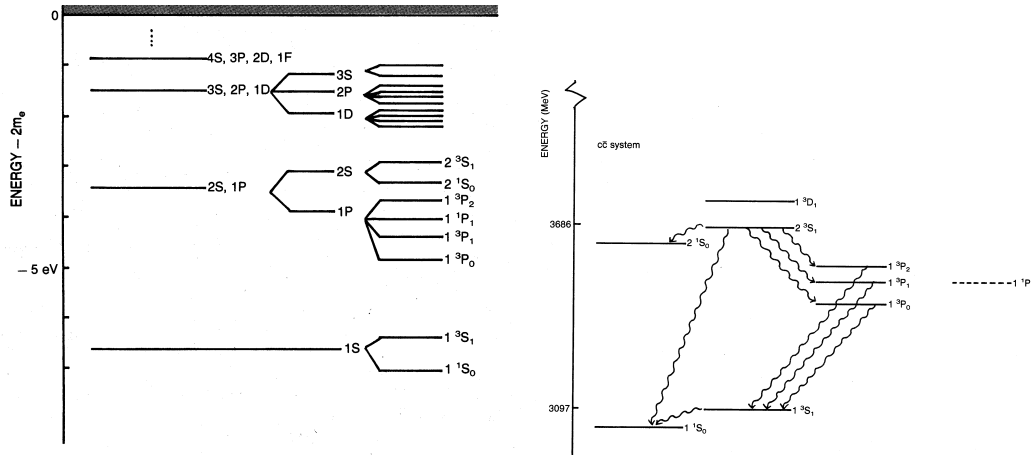
Figure 1.4: On the left the spectrum of positronium, driven by the coulomb interaction. On the right the experimental spectrum of charmonium $c\bar{c}$. In solid the states already observed, in wavy lines the electromagnetic transitions. Figures taken from Ref. [13].

nucleon-nucleon (NN) interaction.

Baryon-Baryon interactions

The study of baryon-baryon interactions has received much effort during the last decades. On the one hand there was the great success of *one boson exchange* (OBE) models such as the Nijmegen or Bonn potentials (see [16, 17], and references therein). These models had as starting point the Yukawa theory. They constructed the NN interaction by assuming the exchange of mesons between the nucleons at a baryonic level, without any mention to the inner structure of nucleons. They made a clear distinction between three regions of the NN interaction which are the short ($R < 1$ fm), medium (1 fm < R < 2 fm) and long-range parts ($R > 2$ fm). Understanding the short-range was not considered a main goal of baryonic models as there the substructure of nucleons is expected to play a role. For example the Paris potential [18], which was built based on dispersion theory, parametrizes the short-range part with no physics underneath while the Bonn potential uses the exchange of more massive mesons to generate repulsion at short distances. The medium and long ranges were mostly explained in terms of the exchange of pions (long-range) and more massive mesons, such as the σ (medium-range). These models have several free parameters: the coupling constants between the nucleons and the exchanged mesons, the cut-offs used to regularize the potentials and also the structure of the vertex functions (monopole, dipole, etc.).

The reasons to study the NN interaction (and in general of any baryon-baryon interaction) with a constituent quark model are many folded. Historically it was thought as a clear way to try to obtain the short-range of the NN interaction which had to be parametrized

in OBE models [19, 20, 21]. In this line the first studies were devoted to understand the repulsive core of the NN interaction as a consequence of the antisymmetrization principle at the quark level [22]. These studies were mostly focused on a correct description of the symmetries so that the repulsive behavior of the NN interaction at short distances could be explained. The next step was to try to understand the interaction at all distances. An interesting fundamental approach was the one followed by Fujiwara and Hecht [23]. They incorporated explicit $q\bar{q}$ and $(q\bar{q})^2$ pairs to the model and studied the resulting NN interaction. Their results showed some attraction in the long-range but not enough to understand the experimental data. Soon later some hybrid models containing constituent quarks and also an *effective* baryonic potential between the center of mass of the clusters were constructed in order to get a good description of the interaction also at long distances [24, 25]. The lack of consistency of this last hybrid approach makes it not very appealing. Then chiral symmetry ideas made their way into this problem and forced the appearance of *chiral constituent quark models*. These models, that we explain in more detail in the next chapter, incorporate in a natural way the exchange of mesons between the constituent quarks. They were also the first models that successfully pursued a simultaneous understanding of both the low-lying hadron spectra and the NN interaction based on a unique microscopic quark-quark interaction [14, 26, 27].

The construction of baryon-baryon interaction potentials from the dynamics of the constituents is a crucial point for the results described in this thesis. In Chapter 3 the way two-baryon potentials are constructed using the Born-Oppenheimer (BO) method is discussed. This method is later on employed to build the transition and direct potentials to the $N^*(1440)$.

Few-body observables

Once two-baryon systems have been studied a next step could be to explore the quality of such potentials when applied to the study of few-body observables. Studying few-body systems a much deeper understanding of the baryon-baryon interactions can be pursued. For example, the NN interaction is constrained by all the existing experimental data, phase shifts and deuteron properties, which only depend on the *on-shell* part of the T matrix. The *off-shell* part of the interaction cannot be fixed by any nucleon-nucleon phenomenology and it is thus unknown. Several two-nucleon interactions may have the same on-shell behavior, and therefore reproduce equally well the phase shifts and deuteron properties, but have a completely different off-shell behavior. On the other hand this off-the-energy-shell part of the T matrix can be explored by studying few-body observables such as the triton binding energy [8]. An interesting point is to explore the implications of constructing the NN potential from a quark model regarding the off-shell behavior of the potential. In particular, this different off-shell behavior of the T matrix could explain part of the missing binding of the triton as compared to calculations which are completely

---

[8]In many-body problems one of the nucleons can exist, by virtue of the Heisenberg uncertainty principle, off the energy shell, that is, the energy momentum dispersion relation $E^2 = p^2 + m^2$ does not hold.
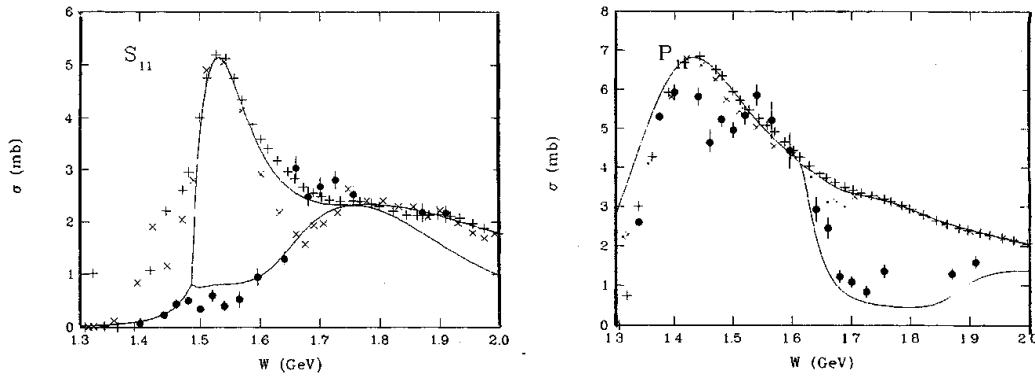
Figure 1.5: πN cross sections versus the invariant mass of the system. "X" and "+" are the results from the partial wave analyses of Refs. [30, 31]. The solid line corresponds to the analysis of Ref. [32] where the picture is taken from. On the left we see the S_{11} channel where the $N^*(1535)$ appears as a clear peak in the cross section. On the right the same for the case of the $N^*(1440)$ resonance. The solid circles are contributions to $\pi\pi N$ channels.

local [28] or with the off-shell behavior fixed arbitrarily. In Ref. [29] a calculation of the triton binding energy was performed employing a two-body NN interaction derived partly from a quark model. However, they had to include an effective force between the center of the clusters to provide medium-range attraction to the resulting potential.

In Chapter 4 we focus on a few-body observable, the triton binding energy. We calculate for the first time the triton binding energy making use of NN potentials derived from a constituent quark model. We perform a calculation with BO derived NN potentials and also with potentials derived through the resonating group method (RGM). The motivation to perform such a calculation is two-sided, on the one hand we show that the model used can get a reasonable result for the binding energy of the triton, on the other hand we analyze the results obtained with the non-local potential derived from the RGM as compared to those derived within the BO scheme, studying the effect of the non-local contributions to the interaction.

Hadronic resonances

The existence of a spectrum of hadrons is a clear signal of the presence of substructure. These resonances appear as peaks in scattering experiments such as πN, ep, pp, and many others. In Fig. 1.5 we show some examples of such experiments. The peaks observed at certain energies show the existence of resonant states whose properties, such as width, mass and quantum numbers, can be extracted from the experimental data. Some of the baryonic resonances can very well be understood from a quark model picture as excitations

Baryon	Mass (MeV)	Parity	Spin	Isospin	Experiment
N	939	+	1/2	1/2	
Δ	1232	+	3/2	3/2	π, e
$N^*(1440)$	1440	+	1/2	1/2	π, e

Table 1.1: Properties of low-lying baryons. The 'Experiment' shows in which experiment has the resonance been observed, π refers to πN scattering while e refers to (e, N) processes.

both radial or orbital and of spin-isospin of the constituent quarks. But there are some cases where the nature of the resonance is not so clear and several interpretations still coexist, this is the case of the Roper ($N^*(1440)$) resonance, see Table 1.1. Its nature is elusive and there exist nowadays several interpretations of its origin which motivate part of the experimental works at JLab [33]. In this work we shall assume the $N^*(1440)$ to be an excitation of the constituent quarks with no other Fock state components and will see what can be inferred from it. Very recent lattice calculations [34] support this quark model picture of the $N^*(1440)$ resonance. Let us note that the naive quark model cuts the Fock space keeping only states with three valence quarks, for instance the nucleon wave function in the quark model is:

$$|N\rangle = |qqq\rangle \,, \tag{1.1}$$

but it could also contain terms of the type,

$$|N\rangle = |qqq\rangle + |qqq q\bar{q}\rangle + |qqqg\rangle + \dots . \tag{1.2}$$

The success of the naive model in explaining the phenomenology, spectra and baryon interactions, supports the truncation of the Fock series according to Eq. (1.1).

In the case of the $N^*(1440)$ some authors claim it can be generated *dynamically* when they study the πN system from a baryonic point of view [35]. This fact can be rephrased in a quark model language as saying that more Fock components are needed than the three quark one, or also, that the coefficients of the other components of the Fock state are bigger than the *naive* one [9].

Apart from the nature of resonances there is also the problem of determining to what extent they affect the dynamics of neutrons and protons in nuclear reactions. The first resonance to be studied and that is nowadays accepted to play an essential role to understand NN dynamics at higher energies is the $\Delta(1232)$. In the quark model this is just a spin-isospin excitation of the nucleon and can be very well understood in the quark model picture. Recently also the role of the $N^*(1440)$ has been studied from a baryonic point of view in several reactions such as $p(\alpha, \alpha')$ or $p(d, d')$ [36, 37] scattering or when studying the dynamics of nucleons and resonances with a Boltzmann equation formalism [38]. In both

---

[9]This was one of the points of discussion in the meeting "The physics of the Roper resonance" (Trento, 2002). M. Lutz defended the idea of most of the resonances being generated dynamically. W. Weise, D. O. Riska, E. Oset and others seemed to have more conciliatory points of view.

cases it is customary to have a good model for the transition between the different baryons involved. The quark model provides a good starting point for obtaining these transition potentials in a well defined and consistent way. The basic assumption needed, once the microscopic interaction between the constituents is settled, resides in the construction of the Fock vector for the resonances.

The BO method exposed in Chapter 3 will be employed to obtain both the direct $NN^*(1440) \rightarrow NN^*(1440)$ and the transition $NN \rightarrow NN^*(1440)$ potentials in Chapter 5. In both cases an ample description of the features of both potentials is given. In Chapter 6 we make use of the potentials obtained in Chapter 5 and present three applications: first we calculate the probability of $NN^*(1440)$ and $N\Delta$ components on the deuteron, secondly we obtain the coupling constants between the $N^*(1440)$ and the N and the two Goldstone bosons present in the model making use of the transition potential described in Chapter 5, finally we explore the *Roper excitation in the target* mechanism proposed in Ref. [37] to understand part of the differential cross section of the process $p(d, d')X$. Chapter 7 is devoted to explore the implications of our transition potentials, the ones calculated in Chapter 5 together with the $NN \rightarrow N\Delta$ transition potentials already obtained in Refs. [39, 40], in the investigation of the NN interaction at energies above the Δ region.

2 THE QUARK MODEL

In this thesis we make use of the constituent quark model developed by the Salamanca-Tübingen group [14, 15]. This model was constructed a decade ago and has already been applied to the study of different aspects of the low-energy regime of the strong interaction.

The model belongs to the category of *QCD inspired models*. Therefore, its main assumptions can be understood from the relevant features of the theory we want to model, QCD. First, we explain in some detail the relevant properties of QCD which are important to build the constituent quark model. We describe a theoretical scenario that can serve as a bridge between the theory and our model. Secondly a deeper perspective on the actual quark model is given. We go through all the important points defining the quark model as are the confinement procedure, the residual interactions, the dynamics of the constituents and the way the few parameters occurring in the model have already been fixed. Finally we show some results from previous works where the same constituent quark model was employed so that the reader retains a glimpse of the variety of phenomena that can be correlated and studied.

2.1   From QCD to constituent quarks

There are many theoretical scenarios that provide hints pointing to the existence of a regime where constituent quarks emerge as the *natural* degrees of freedom from the underlying theory. To understand them we have to look carefully into the main aspects of QCD.

QCD is a gauge theory. This means that the interaction lagrangian can be derived in the following way: Let us start with a free lagrangian for a certain number of quark families (flavors),

$$\mathcal{L}_0 = \sum_f \bar{q}_f \left(i\gamma^\mu \partial_\mu - m_f \right) q_f \,. \tag{2.1}$$

q_f and $\bar{q}_f$ are the quark and antiquark fields with flavor f, defined as three vectors of the color field, that is, $q_f \equiv \mathrm{column}(q_f^1, q_f^2, q_f^3)$ with q_f^α being a quark field of color α and flavor f.

Let us then impose gauge invariance to this lagrangian, that is, force the lagrangian to be invariant under the following transformation of the fields,

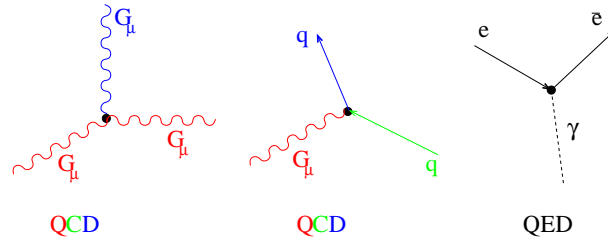$$q_f^\alpha \rightarrow U_\beta^\alpha \, q_f^\beta \,, \tag{2.2}$$

Figure 2.1: Some of the vertexes appearing in QCD.

where $UU^\dagger = 1$ and $\det U = 1$. The $SU(3)_c$ color matrices U can be written in the form,

$$U = \exp\left\{-ig_s \frac{\lambda^a}{2}\Lambda_a(x)\right\}, \tag{2.3}$$

with λ^a the generators of the fundamental representation of $SU(3)$(Gell-Mann matrices) and $\Lambda_a(x)$ real space-time functions. In order to fulfill the above requirement, Eq. (2.2), a certain number of gauge fields [1] need to be added to the theory in direct analogy to what happens in the gauge derivation of quantum electrodynamics.

However there is a major difference between the two theories and it is the symmetry group which is imposed on the free lagrangian. In the case of QED the symmetry group is $U(1)$ while in the case of QCD the group is $SU(3)_c$. $U(1)$ is an abelian group while $SU(3)$ is not abelian. As a consequence, the resulting interactions between the constituents and the gauge fields are much more involved than in the case of electrodynamics, see Fig. 2.1. In particular, we can see that unlike in QED this lagrangian contains interactions between the particles which carry the strong force, the gluons, which also carry the charge of the gauge group, color. This makes the theory non-linear and is the main reason for most of the difficulties one encounters when trying to solve it.

There are three relevant properties that correspond to three different limits where some important characteristics of the theory have already been settled.

Asymptotic freedom

This corresponds to the limit of very high energies. In this limit the quarks are carrying a huge momentum and are thus moving very fast, or correspondingly they can be very close together, at very short distances. In this limit the running coupling between quarks and gluons drops very fast and a perturbative treatment of the theory is in order. Actually, the coupling drops asymptotically to zero so that in the limit of very high momenta quarks move essentially as free particles, see Fig. 2.2. This is what is known as *asymptotic freedom*. This very special feature of QCD allows a clear understanding of most of high

---

[1]The number of gauge fields necessary to preserve gauge invariance is equal to the number of generators of the group, in the case of $SU(3)$ this number is eight. The explicit gauge derivation of the QCD lagrangian can be seen in Ref. [41].
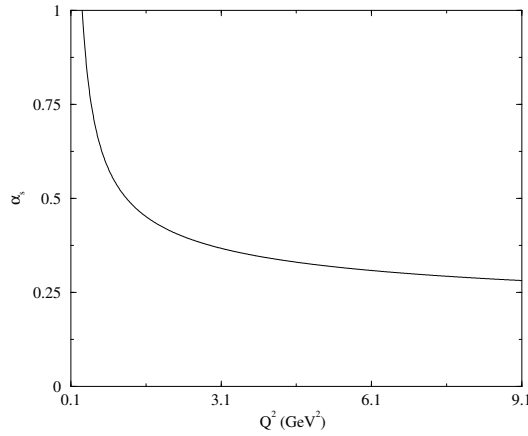
Figure 2.2: Behavior of the running coupling between quarks and gluons calculated up to one-loop corrections, α_s, as a function of the momentum transfer, see for instance Ref. [42].

energy collision experiments where jets of hadrons are found in concordance with the idea of free quarks being hit independently and getting *dressed* with $q\bar{q}$ pairs of the vacuum as their energies decrease.

Chiral Symmetry

This is a property of the QCD lagrangian that is being studied extensively nowadays. The reason is that it is one of the few tools that permits us to study the physics of the strong interaction at low energies from QCD in a more or less systematic way.

The main point lies on the empirical fact that the current masses (the masses appearing in the QCD lagrangian) of the lowest lying quarks, up, down (and strange), are very small compared to the scale of masses of low lying hadrons [2] - 10 (100) MeV vs. 1 GeV. This led to the idea of studying the theory in the limit of those quark masses being actually zero, which is almost the case for up and down quarks. In this limit it can be easily shown that the QCD lagrangian splits up into two different pieces which conserve chirality and which do not mix together. This chiral symmetry of the QCD lagrangian in the limit of the masses of the quarks being exactly zero would imply (if realized *a la Wigner-Weil* [3]) several features that could be tested experimentally. The first one would be the existence of chiral partners, that is, for each low lying hadron there would exist another one with equal mass and opposite parity, secondly, the masses of all low lying mesons would be degenerate in mass in that limit. This is not observed in nature and leads to the idea of a *dynamical chiral symmetry breaking* in QCD [3]. This has a tremendous relevance due

---

[2]This is completely accepted for quarks u and d. For the s quark, whose mass is 80-155 MeV [43], its smallness deserves some discussion.

[3] There are two main ways in which actual symmetries of the lagrangian can show up in the spectrum. The first one is the standard, Wigner-Weil, realization when the generators of the group annihilate the

to the existence of a theorem by Goldstone [46] which states that when a lagrangian is invariant under a certain group there must exist a massless boson for each generator of the group that fails to annihilate the vacuum. The quantum numbers of the massless boson are those of that generator. These massless bosons couple to the fermions of the theory. This is the cornerstone of our quark model and thus we will go through this idea again later.

Confinement

The property of confinement is a very important feature that QCD needs to contain and that has not yet been rigorously proven. Experimentally no one has ever detected a free quark nor has anyone detected any *colored* particle [4]. That means that, independently of the energy of the particles involved in the collisions, the products of high energy experiments where quarks are playing a mayor role are always uncolored hadrons and leptons. This leads to the idea of confinement: quarks seem to prefer to be confined to form uncolored particles.

Confinement, being such a relevant feature, has been studied from many points of view. One of the most recent ones is using numerical techniques to solve the QCD lagrangian. This is done in *lattice* QCD which is a formulation of the original theory, hopefully preserving its symmetries and properties, in a discrete space-time. In lattice theories confinement seems to emerge naturally from the original lagrangian. Not having a rigorous proof of confinement the first hint showing that QCD probably produces confinement comes from the study of the behavior of the running coupling between quarks and gluons as we let the momentum transfer go to zero. As we see in Fig. 2.2 the coupling constant between quarks and gluons grows as we approach the region of low Q^2. This means that at low momentum transfer, or correspondingly long distances, the strength of the force that binds quarks together grows making it impossible to separate the quarks. The weak point in this argument resides in the fact that it is precisely in that limit where the tools used to calculate the running coupling itself start to blow up [5].

2.1.1   Constituent quarks

Up to now we have devoted our efforts to present QCD and its relevant aspects, now we explain how the constituent quark model emerges from the original theory.

---

vacuum. In this case the spectrum exhibits the symmetries of the lagrangian. A theorem by Coleman [44] asserts that 'the symmetries of the vacuum are the symmetries of the world'. But there is another way, *a la Goldstone*, which corresponds to the case of a vacuum of the theory not been symmetric under the symmetries of the lagrangian. This is what is called spontaneous symmetry breaking, and this is essentially the case for QCD [42, 45].

[4]There are, of course, many evidences of the existence of color as a degree of freedom.

[5]This is similar to what happens when studying the mechanical vibrations on a rope. The simple theory describing the process of small oscillations, e.g. describing the tone of a string guitar, breaks when the oscillations are no longer small and cannot fully describe the resonant processes.

Let us consider the non-strange sector. Therefore, we have quarks u and d, which are almost massless in the original theory and a spectrum of particles that can be understood, in principle only the quantum numbers, from the properties of quarks u and d. The masses of these quarks are so small that the requirements of chiral symmetry, massless quarks, are almost fulfilled. On the other hand the spectrum of low lying hadrons shows no sign of parity doublets providing a clear sign of chiral symmetry being broken not only because of the small quark masses. Thus, we arrive to the conclusion that chiral symmetry needs to be showing up in the spectrum *a la Goldstone*. This, by virtue of the Goldstone theorem, enforces the existence of at least two massless particles and also makes the current quarks get dressed and become constituent quarks. Would the whole process be exact, massless quarks, etc., we would end up with a bunch of massless Goldstone bosons being exchanged between the constituent quarks. In the real world chiral symmetry is only an almost broken symmetry so what we end up with are low mass bosons being exchanged between the constituents.

There are several ways to write an effective chirally invariant lagrangian for the constituent quarks. We consider a linear realization of chiral symmetry [6]:

$$\mathcal{L} = i\,\bar{q}_i\gamma^\mu D_\mu q_j - M_{ij}\,\bar{q}_i q_j - \frac{1}{4}F^{\mu\nu a}F^a_{\mu\nu} \tag{2.4}$$

$$+ \bar{q}_i\,(\sigma\delta_{ij} + i\gamma_5\vec{\pi}\cdot\tau_{ij})q_j + \frac{1}{2}\partial_\mu\,\sigma\partial^\mu\,\sigma + \frac{1}{2}\partial_\mu\vec{\pi}\cdot\partial^\mu\vec{\pi}\,, \tag{2.5}$$

π and σ are the Goldstone modes of the model, a pseudoscalar-isovector (π) and a scalar-isoscalar (σ). At the same time, not being affected by the process of chiral symmetry breaking, the constituent quarks keep exchanging gluons [47]. The scale of chiral symmetry breaking Λ_{ch} is incorporated to the model through a form factor of the form,

$$F(q) = \left(\frac{\Lambda_{ch}^2}{\Lambda_{ch}^2 + \vec{q}^{\,2}}\right)^{1/2}. \tag{2.6}$$

The nature of the physical pion in this framework being both a Goldstone mode exchanged between the quarks and also a bound state of a quark and an antiquark has deserved several discussions [47]. We do not intend to address this problem here but simply quote Ref. [48] where a study of the pion from a Schwinger-Dyson formulation of QCD is performed, arriving to the conclusion that both interpretations of the pion can coexist.

By now we already have most of the ingredients: constituent quarks, whose ~ 300 MeV mass includes the net effect of the quarks moving through the $q\bar{q}$ sea, Goldstone bosons exchanged between the constituent quarks and gluons being a remnant of the perturbative regime of the original theory. We now need to add an ad hoc confinement tool that in our case consists in a two body potential with a suitable color-orbital structure. In Fig. 2.3 we can see the different ingredients of the model.

There are nowadays several constituent quark models which coexist. All of them share most of the main characteristics described above as is the fact that the mass of the quarks

---

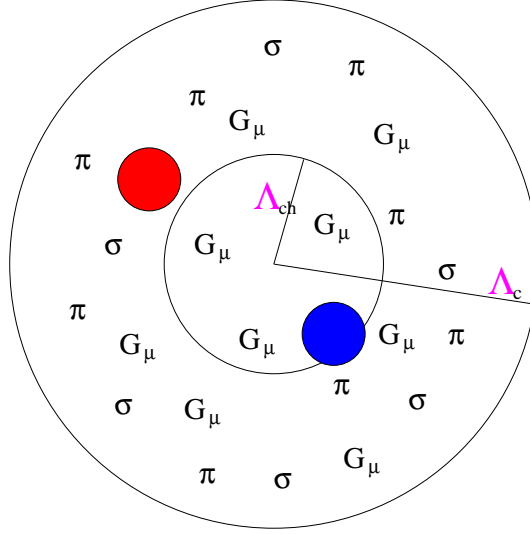[6]Non-linear realizations can also be produced.

Figure 2.3: Different components of the model. We depict two different scales, one which corresponds to the scale of confinement (Λ_c) and the second one which is the scale of chiral symmetry breaking (Λ_{ch}). The figure mimics the 'world' as seen by a quark with green color inside a nucleon.

is a constituent one or that there must be a confinement mechanism and residual interactions. The most crucial differences among them are the residual interactions and confinement mechanisms considered in each case. For instance in the model of Ref. [49] they consider the complete octet of low-lying mesons as the Goldstone bosons, the same case as in Ref. [50] where they give an extension of the model we employ here to the strange sector. In the case of the model of Ref. [51], also employed by [52], the most important difference, that has risen much discussion during the last three years, see for instance Ref. [53], is that they do not include any perturbative one-gluon exchange interaction. Instead of that they claim that they can understand most of the phenomena including only the octet of mesons as Goldstone bosons. Few years ago Nakamoto and Toki [54] emphasized the difficulties encountered to understand both the baryon spectrum and the NN interaction without including some hyperfine interaction similar to the one-gluon exchange and a scalar-isoscalar boson exchange. Very recently Ref. [55] pointed out that when a chiral partner, namely the σ, is included in the model of Ref. [56] and semi-relativistic kinetic energies are considered for the quarks the results for the spectrum of baryons are unstable. Suggesting that the semi-relativistic kinetic energies should be used together with relativized interactions between the quarks.

Particle	Charge (e)	I_3	Mass (MeV)	Composition
u	2/3	1/2	313	u
d	−1/3	−1/2	313	d
proton	1	1/2	939	uud
neutron	0	−1/2	938	udd
Δ^{++}	2	3/2	1232	uuu

Table 2.1: Properties of the constituents. Also some composite particles are shown.

2.2   Ingredients of the model

With the ideas of the previous section in mind we expose the constituent quark model for the non-strange sector which we use in this work.

Constituent quarks

The constituents, quarks u and d, are fermions of spin 1/2 and charge (in units of e) 2/3 and −1/3 respectively carrying also color. These two fermions are considered in an isospin formalism as an isospin doublet with a proper relation between charge and isospin. In this model both non-strange quarks are considered as degenerate in mass. These constituent quarks have a mass of approximately one third of the nucleon mass, 313 MeV. In Table 2.1 we show the main static properties of the constituents. We also present the composition of some non-strange baryons in terms of quarks for a comparison.

Confinement and residual interactions

Confinement is included in an *ad hoc* manner by imposing a two body potential between the constituents so that it does not act on color singlets. A radial structure is also needed and can be taken as linear or quadratic. A quite standard form used in the literature and based on lattice QCD results of Wilson [57] [7] is,

$$V_{CON}(\vec{r}_{ij}) = a_c\, \vec{\lambda}_i \cdot \vec{\lambda}_j r_{ij} \ , \tag{2.7}$$

where $r_{ij} = |\vec{r}_i - \vec{r}_j|$ and λ_i are the $SU(3)$ color matrices.

The confining potential plays a major role for understanding hadronic spectra. There, more sophisticated orbital structures have been considered to take into account the saturation of the confining force at a certain scale. For our study, which mainly refers to two-baryon systems, the precise orbital functional form is not relevant [59]. Due to the arguments explained in Sect. 2.1, we have some residual interactions which have, in principle, two different natures: of perturbative origin and from the spontaneous breaking of chiral symmetry.

---

[7]For a review see Ref. [58].

In the perturbative region, which corresponds to short distances, R<1 fm, we have the one-gluon exchange (OGE) [8]. It was first introduced by de Rujula et al. [60] in a first attempt to understand the spectrum of low-lying baryons. It is a very short ranged force and mainly contributes to the short-range part of the baryon-baryon interaction. The derivation is done from the Feynman diagram for the exchange of one gluon between the quarks and taking the non-relativistic limit. Its spin-color structure is important to understand the mass difference between the N and the $\Delta(1232)$. Here is the usual form for this interaction,

$$V_{OGE}(\vec{r}_{ij}) = \frac{1}{4}\,\alpha_s\,\vec{\lambda}_i \cdot \vec{\lambda}_j \left\{ \frac{1}{r_{ij}} - \frac{\pi}{m_q^2}\left[1 + \frac{2}{3}\vec{\sigma}_i \cdot \vec{\sigma}_j\right]\delta(\vec{r}_{ij}) - \frac{3}{4m_q^2\,r_{ij}^3}\,S_{ij}\right\}, \qquad (2.8)$$

α_s is the strong coupling constant which in the model is to be considered a parameter, $\vec{\sigma}_j$ are the Pauli spin matrices of quark j and S_{ij} is the standard tensor operator defined as,

$$S_{ij} = 3(\vec{\sigma}_i \cdot \vec{r_{ij}})(\vec{\sigma}_j \cdot \vec{r_{ij}}) - (\vec{\sigma}_i \cdot \vec{\sigma}_j)\,. \qquad (2.9)$$

The most important part is the $\vec{\sigma}_i \cdot \vec{\sigma}_j \vec{\lambda}_i \cdot \vec{\lambda}_j$ term of the central part of the potential, called color-magnetic, that gives different behavior for the different S-waves ($^1S_0$ and $^3S_1$) as seen in the NN phase shifts. It also contributes to the $N - \Delta$ mass difference.

As explained in Sect 2.1.1 the spontaneous breaking of chiral symmetry is incorporated in the model arriving to the effective lagrangian of Eq. (2.5). This lagrangian contains a pseudoscalar exchange, the one-pion exchange (OPE), and a scalar one, the one-sigma exchange (OSE). The scale of chiral symmetry breaking is incorporated through the form factor of Eq. (2.6). The second one, OSE, simulates part of the interaction due to the two-pion exchange mechanism which is not explicitly included in our model. Their explicit forms are obtained after a non-relativistic reduction of the corresponding Feynman amplitude for each process and their precise forms are,

$$\begin{aligned} V_{OPE}(\vec{r}_{ij}) &= \frac{1}{3}\,\alpha_{ch}\frac{\Lambda_{ch}^2}{\Lambda_{ch}^2 - m_\pi^2}\,m_\pi\left\{\left[Y(m_\pi\,r_{ij}) - \frac{\Lambda_{ch}^3}{m_\pi^3}Y(\Lambda_{ch}\,r_{ij})\right]\vec{\sigma}_i \cdot \vec{\sigma}_j + \right. \\ &\qquad \left.\left[H(m_\pi\,r_{ij}) - \frac{\Lambda_{ch}^3}{m_\pi^3}\,H(\Lambda_{ch}\,r_{ij})\right]S_{ij}\right\}\vec{\tau}_i \cdot \vec{\tau}_j\,, \qquad (2.10) \end{aligned}$$

$$V_{OSE}(\vec{r}_{ij}) = -\alpha_{ch}\,\frac{4\,m_q^2}{m_\pi^2}\,\frac{\Lambda_{ch}^2}{\Lambda_{ch}^2 - m_\sigma^2}\,m_\sigma\left[Y(m_\sigma\,r_{ij}) - \frac{\Lambda_{ch}}{m_\sigma}\,Y(\Lambda_{ch}\,r_{ij})\right], \qquad (2.11)$$

α_{ch} is the coupling between the Goldstone bosons and the constituent quarks, m_π and m_σ are the masses of the pseudoscalar and the scalar bosons respectively, Λ_{ch} is a cut-off to switch off the interactions below the chiral symmetry breaking scale, and, finally, $Y(x)$ and $H(x)$ are standard Yukawa functions given in Eq. (A.2).

---

[8]In principle we have OGE at all distances, but due to its color structure it only plays a role at very short distances.

The final form of the quark-quark interaction including confinement, one-gluon exchange, and the Goldstone boson exchanges is:

$$V_{qq}(\vec{r}_{ij}) = V_{CON}(\vec{r}_{ij}) + V_{OGE}(\vec{r}_{ij}) + V_{OPE}(\vec{r}_{ij}) + V_{OSE}(\vec{r}_{ij}) \,. \tag{2.12}$$

2.3   Fixing the parameters

The first parameter we consider is the constituent quark mass, which we take as one third of the mass of the nucleon: $m_q = 313$ MeV. The rest of the parameters that have appeared in the description of the model are fixed directly or indirectly from experimental data and/or have some theoretical boundaries.

- **Chiral masses**

  We assimilate the pseudoscalar mode of our model to be the real pion and thus we take its mass from its experimentally measured one $\sim$138 MeV. This ensures that the behavior of the NN potential at long distances is the well-known pionic one. Once the mass of the pion is fixed, PCAC (partial conservation of the axial current) provides a relation for the mass of the scalar partner (sigma meson in our model) [61],

  $$m_\sigma^2 \simeq (2\,m_q)^2 + m_\pi^2 \,. \tag{2.13}$$

- α_{ch}

  It is fixed to reproduce the well known long range tail of the NN interaction. It is not directly measured but can be considered as a very much fixed parameter: α_{ch}=0.027.

- Λ_{ch}

  Λ_{ch} sets the scale at which chiral symmetry is broken. Therefore, at high momentum transfer between the quarks the Goldstone boson exchange interactions vanish. Moreover, this parameter controls the tensor interaction we will have in our model when two-baryon interactions are studied. Once α_{ch} is set to reproduce the long-range tail of the NN interaction, Λ_{ch} determines to a good extent the probability of D-wave on the deuteron. On the other hand a quite narrow range for this parameter was obtained by studying a spin-flip reaction where the relevant part of the quark-quark interaction is the tensor part of the OPE potential. The study was done for $pp \to n\Delta^{++}$ [62]. Combining both the reproduction of the D-wave part of the deuteron and the study of the $pp \to n\Delta^{++}$ reaction we arrive to the value [9] Λ_{ch}=4.2 fm^{-1}.

---

[9]The values of Λ_{ch} are also restricted by the value of $\Lambda_{\pi N}$ according to Ref. [63].

m_q(MeV)	313
b(fm)	0.518
α_s	0.485
a_c(MeV $\cdot$ fm^{-1})	109.7
α_{ch}	0.027
m_σ(fm^{-1})	3.421
m_π(fm^{-1})	0.70
Λ_{ch}(fm^{-1})	4.2

Table 2.2:   Quark model parameters.

- α_s

  With the previous parameters already fixed in the NN interaction we fix the value of α_s to get the correct mass difference between the N and the $\Delta(1232)$. The values for α_s in the literature have ranged between 0.2 and 2.3. In our work we take it as α_s=0.485.

- b

  This parameter was included in the model when the two-nucleon interaction was studied. Its value is roughly fixed to get a reproduction of the nucleon charge radius. In fact the value we use is smaller due to the effect of the pionic cloud. A completely consistent treatment of both the baryon spectrum and the baryon-baryon interactions would require the use of the wave functions obtained studying spectra in the study of for example the NN interaction. The inclusion of the exact wave function would make the baryon-baryon problem much more involved. Moreover Ref. [27] (in Chapter 3 we reproduce their results), showed that the external part of the nucleon wave function can be correctly approximated by using just one gaussian with parameter b=0.518 fm.

- a_c

  This is the parameter appearing in the confining force between the quarks, Eq. (2.7). For the purpose of studying two-baryon forces the value of the parameter is not directly relevant as the contributions from the confinement to the force between two baryons is very small (zero for quadratic confining potential). However, let us simply mention that the value of the parameter is such that it ensures a confining potential and thus that the rest of our interactions make sense (a negative value for a_c would imply a deconfining potential). Its value is fixed through a stability condition for the nucleon mass of the form:

$$\frac{\partial M_N(b)}{\partial b} = 0 \,, \tag{2.14}$$

  giving a value of $a_c = 109.7$ MeV fm^{-1}.

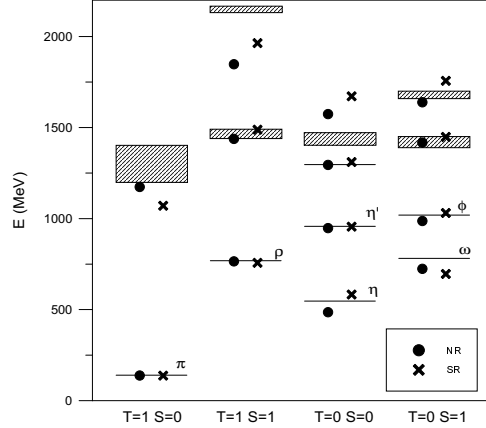We summarize in Table 2.2 the parameters of the model.

Figure 2.4: Spectrum of low lying mesons.

2.4 Previous works

There are many topics that have already been studied in the framework of this constituent quark model. The results obtained are, in general, in good agreement with experimental data or with other theoretical estimates. They can be divided into two type of works: spectra and baryon-baryon interactions.

2.4.1 Spectra

The chiral constituent quark model permits very definite predictions for the spectra of low lying hadrons.

Mesons

For mesons, with the assumptions made in the previous sections, a first approach would be to solve the Schrödinger equation for the quark-antiquark system with the interactions explained above. More refined calculations were also reported in Ref. [64]. In their work they studied, with the wave functions obtained solving the two-body problem, the strong, and, real and virtual, electromagnetic decays of mesons [65].

We show in Fig. 2.4 a spectrum obtained for low-lying mesons taken from the Ph.D. of Blanco [50]. He studied the meson spectrum using a non-relativistic model and also a semirelativistic version of the same model to see if the influence of the kinematics was noticeable.
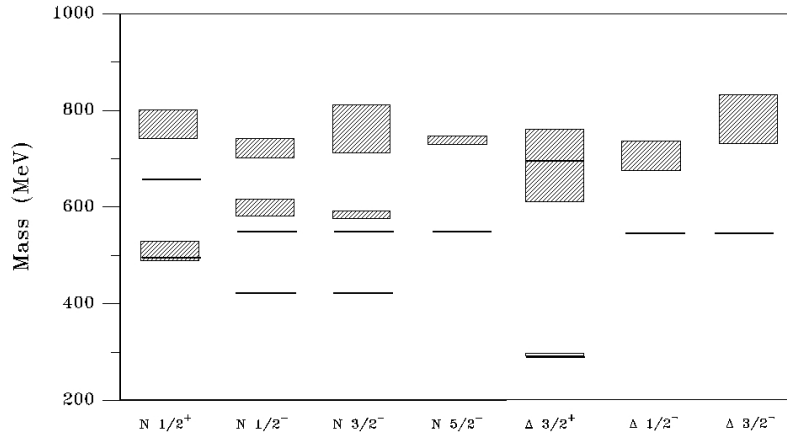
Figure 2.5: Spectrum of non-strange baryons.

Baryons

The problem is considerably more involved for the case of the baryon spectra were a three-body problem with two, and eventually three, body forces needs to be solved. The problem can be formulated in many different ways and solved using various methods [10]. The spectrum which is obtained for baryons has also been the object of extensive study in several works. One of their results is shown in Fig. 2.5. The main difficulty encountered by this model was to reproduce the correct ordering between the first negative, $N^*(1535)$, and first positive parity, $N^*(1440)$, states together with a simultaneous description of the NN interaction [11]. However it is interesting to emphasize that if we consider the two parities independently and allow for a rescaling of the ground state of the negative parity sector we could get a very good reproduction of the complete spectrum. The capability of quark models to give a good reproduction of the spectra of particles is crucial and gives support to any further calculation. Therefore, if a resonance is not well understood in a quark model that may suggest that more components are needed in the Fock space, Eq. (1.2), as we mentioned in the introduction.

2.4.2   Baryon-baryon interactions

Historically the first subject of study of the quark model we make use of in this work was the study of the NN interaction at energies of the order of 300 MeV. It was first studied

---

[10]A description of the various methods can be found in the reviews by Gloeckle [66] and Suzuki and Varga [67].

[11]Ref. [68] shows how the ordering problem could be solved by letting the parameter Λ_{ch} take higher values than the ones that allow an understanding of the NN system, that would be equivalent to including in the model the exchange of η's as in [51].

without the inclusion of the one-sigma exchange [69, 70] and with it a decade later [14]. At the same time all the interactions involving the Δ were obtained using similar tools to those already developed for the calculation of the NN ones but taking into account the fact that the Δ has a different spin-isospin structure [39]. These potentials have been used to make calculations concerning the existence of bound states of nucleons and Δ's [71, 72] recently predicting the existence of a NN dibaryon resonance that has some evidence as seen in experimental analyses [73]. In Chapters 4, 6 and 7 we make use of them.

3 BUILDING BARYONIC INTERACTIONS

In the previous chapter we have explained in some detail the foundations and main points of the chiral constituent quark model which serves as theoretical microscopic framework in this work. Once this has been settled the next step will be the study of the dynamics of compound systems from the dynamics and properties of the constituents. In our case these compound systems are two-baryon systems made of N's, N^*'s and Δ's, which we assume to be made up of 3 constituent quarks.

There are several reasons to study baryon-baryon interactions in the framework of a constituent quark model. The first one is that once we know that quarks are the actual constituents, and that consequently baryons are composite particles, one should be able to understand the interaction between baryons assuming this inner structure and knowing the microscopic laws acting on the components. A particularly relevant case corresponds to the understanding of the NN interaction in terms of quark degrees of freedom. The theoretical scenario is very similar to what happened when the forces that kept atoms bound were understood and the forces between them and also between molecules, clusters of atoms, were derived from them. These forces are the well known Van der Waals forces, which are remnant interactions arising from the electromagnetic force.

The second motivation has to do with the fact that once a cluster nature is postulated for the nucleons this inner composition will in a natural way have some effects on the two-baryon properties. That is because of the fermionic character of the constituents which must obey the Pauli principle. This constrain on the wave function at quark level will first of all have its counterpart on the systems of two identical baryons, as for example the NN system. By imposing the Pauli principle at the microscopic level, we will be able to recover the well known selection rules at the baryonic scale. At the same time we obtain traces of the underlying structure in those systems which are distinguishable at baryonic level, such as the $NN^*(1440)$ system, specially for those partial waves which are forbidden in the NN case as for example the $^1S_0$ (T=0) partial wave. These results are observed without any explicit assumption on the dynamics of the constituents. They are derived from the correct definition of the two-baryon wave function in terms of quark degrees of freedom. At the same time, repulsion at short distances originated by the Pauli principle will be a noticeable feature in some partial waves for some of the interactions derived from constituent quarks, even for those systems where the Pauli principle does not act at the baryonic level due to the non-identity of the baryons.

There are in the literature two well-known methods to study the dynamics of two clusters

of particles (see [59] for a review). They are the RGM [1], which was first used by Oka and Yazaki [22] to study the NN interaction, and the BO employed first by Liberman [75] to study the NN system.

In Sect. 3.1 we study the procedure followed to construct the two-baryon wave function. This wave function already provides a tool to study baryonic effects of the antisymmetry requirement at quark level. In particular the study of the norm of the two-baryon system, which will be defined shortly, gives an explanation to Pauli blocked channels. These two-baryon wave functions are then used in the construction of baryon-baryon interactions.

In Sect. 3.2 we explain briefly the RGM applied to the NN system. We later emphasize the fact that the NN potentials obtained in this way are non-local. This feature is explored in some detail in Chapter 4 where we investigate this source of non-locality as a possible solution to the *missing* [2] energy of the triton bound state. Then we present the BO method and go through the definition of the transition and direct potentials. Both methods are shown to provide similar results when applied to the study of the NN interaction. The implications of the local character of the BO potentials are explored in the chapter devoted to the study of the triton bound state.

3.1   Two-baryon wave functions

Building the wave function of two-baryon systems involves the calculation of the wave function of single baryons. Single baryon wave functions have been calculated using many of the methods available in the literature to solve numerically the quantum mechanical three-body problem (Faddeev, hyperspherical harmonics, etc.). Usually the resulting baryon wave functions obtained with these methods have an involved orbital structure (the spin-isospin structure is the same as the naive one which can be inferred from the quark model). However, Ref. [27] showed that the outer part of the wave functions could be very well approximated by a ground state harmonic oscillator eigenfunction. As an example we show in Fig. 3.1 the wave function obtained for the nucleon together with several gaussians corresponding to different oscillator parameters. It is apparent that the calculated wave function for the nucleon can be approximated by a single gaussian at distances above 1 fm. The best value for the oscillator parameter turns out to be $b = 0.518$ fm. This supports the assumption we make to build the single baryon wave functions: we assume a shell model for the baryons with a harmonic oscillator potential. This simplifies the problem of building baryon-baryon interactions preserving the symmetries of the original problem. Taking into account these considerations the quark wave function of a single baryon contains three different pieces: an orbital part, a spin-isospin part and a color part. Explicitly:

$$|\phi_B\rangle = \phi(\vec{r}_1, \vec{r}_2, \vec{r}_3; R) \otimes \chi_{ST} \otimes \xi_c \,. \tag{3.1}$$

---

[1]The RGM was first employed to study nuclear reactions. It served to find an explanation to the short-range repulsion in the $\alpha\alpha$ reaction [74].

[2]Most standard NN potentials underestimate the triton binding by about 800 MeV.
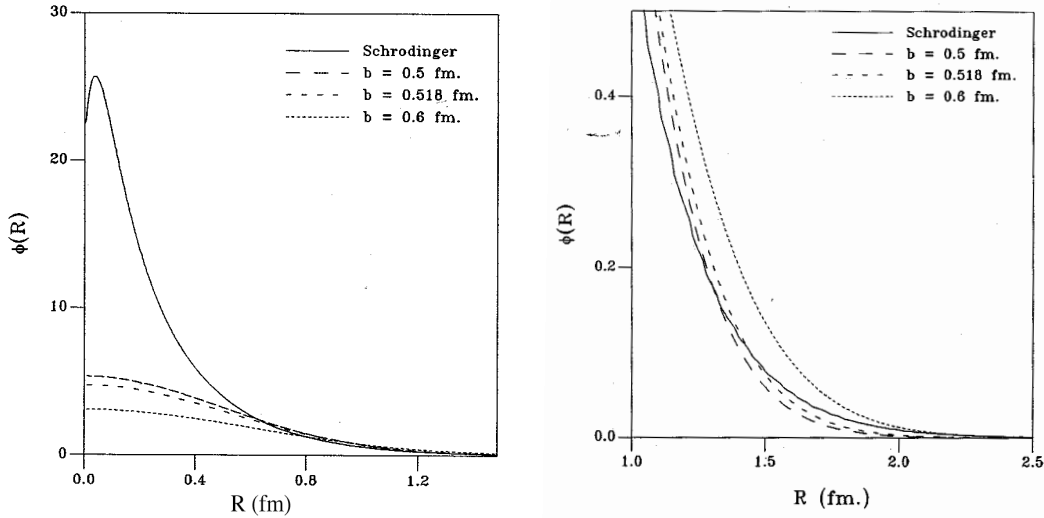
Figure 3.1: Wave functions obtained solving the Scrhödinger equation for the three quark system using a hyperspherical formalism. On the left we show the calculated wave function for the nucleon compared to several gaussians. On the right we show the same figure zooming on the outer part of the wave functions. The pictures are from Ref. [27].

For the baryons we are interested in this work the three components can be treated separately. In other words, for the case of the N, Δ and $N^*(1440)$ the total spin of the baryon has its origin only on the spin of the constituent quarks [3]. These single baryon wave functions are made antisymmetric as demanded by the Pauli principle. The two-baryon wave functions also need to be antisymmetric under the exchange of any two quarks.

3.1.1   The two-baryon antisymmetrizer at the quark level

As already mentioned, one of the key points of working in the framework of constituent quarks is the fact that we retain the proper symmetries of the microscopic problem and thus have the action of the Pauli antisymmetrization principle directly on the constituents. This antisymmetry requirement prevents identical quarks from being close together and may therefore be a source of repulsion at short distances for those partial waves where the available degrees of freedom saturate.

For two-baryon states, with each baryon made up of three particles grouped together, we need an antisymmetrization operator acting on the relevant Hilbert states of the problem. The Hilbert space is constructed as a direct product of spin (S)-isospin (T), color (c) and

---

[3]This is not, for example, the case of the $N^*(1535)$ where the total spin of the particle is the result of coupling the intrinsic spin and relative orbital angular momenta of the quarks.

orbital (o) spaces. A state of the Hilbert space will be of the general form:

$$|\psi\rangle = |\phi_o\rangle \otimes \chi_{ST} \otimes \xi_c \,. \tag{3.2}$$

As we construct our two-baryon wave functions starting from single baryon ones we have an important simplification due to the fact that the single baryon wave functions are already antisymmetric. That is, we need to construct the antisymmetrizer for a system of six particles clustered in two already antisymmetric groups. This has been done for a general two-baryon system. The form of the antisymmetrizer is [76]

$$\mathcal{A} = \frac{1}{N} \left(1 - \sum_{i<j} P_{ij} \right) (1 - \mathcal{P}) \,, \tag{3.3}$$

where P_{ij} is the operator that exchanges particles i and j, and $\mathcal{P}$ is the operator that exchanges particles $(123) \leftrightarrow (456)$. N is a normalization which is not relevant for our purposes as it factors out when defining the potentials as a quotient. The exchange operator can be explicitly written in this way:

$$P_{ij} = P_{ij}^c \ P_{ij}^{ST} \ P_{ij}^o \,, \tag{3.4}$$

where each of them are permutation operators in color, spin-isospin and orbital spaces.

3.1.2   Wave function and Pauli effects

Single Baryon

The wave function of each baryon is constructed to be antisymmetric under the exchange of any two of the three quarks. Each baryon is a color singlet, that is, the color part, ξ_c, is already completely antisymmetric. This impels the rest of the wave function, which corresponds to the orbital and spin-isospin parts, to be completely symmetric.

The single baryon wave functions that we need in this work are the N, $N^*(1440)$ and Δ. Their expressions are the following,

$$N(\vec{r}_1, \vec{r}_2, \vec{r}_3; \vec{R}) = \prod_{n=1}^{3} \left(\frac{1}{\pi b^2} \right)^{3/4} e^{-\frac{(\vec{r}_n - \vec{R})^2}{2b^2}} \otimes [3]_{ST} \otimes [1^3]_c \,, \tag{3.5}$$

$$\Delta(\vec{r}_1, \vec{r}_2, \vec{r}_3; \vec{R}) = \prod_{n=1}^{3} \left(\frac{1}{\pi b^2} \right)^{3/4} e^{-\frac{(\vec{r}_n - \vec{R})^2}{2b^2}} \otimes [3]_{ST} \otimes [1^3]_c \,, \tag{3.6}$$

$$N^*(\vec{r}_1, \vec{r}_2, \vec{r}_3; \vec{R}) = \left(\sqrt{\frac{2}{3}} \phi_1 - \sqrt{\frac{1}{3}} \phi_2 \right) \otimes [3]_{ST} \otimes [1^3]_c \,, \tag{3.7}$$

where $[3]_{ST}$ and $[1^3]_c$ stand for the spin-isospin and color part respectively, $\vec{r}_i$ is the position of quark i, and

$$\phi_1(\vec{r}_1, \vec{r}_2, \vec{r}_3; \vec{R}) = \frac{\sqrt{2}}{3} \left(\frac{1}{\pi b^2} \right)^{9/4} \sum_{k=1}^{3} \left[\frac{3}{2} - \frac{(\vec{r}_k - \vec{R})^2}{b^2} \right] \prod_{i=1}^{3} e^{-\frac{(\vec{r}_i - \vec{R})^2}{2b^2}} \,, \tag{3.8}$$

$$\phi_2(\vec{r}_1, \vec{r}_2, \vec{r}_3; \vec{R}) = -\frac{2}{3}\left(\frac{1}{\pi^{\frac{9}{4}} b^{\frac{13}{2}}}\right) \sum_{j<k=1}^{3} (\vec{r}_j - \vec{R}) \cdot (\vec{r}_k - \vec{R}) \prod_{i=1}^{3} e^{-\frac{(\vec{r}_i - \vec{R})^2}{2b^2}}. \qquad (3.9)$$

We can test for all cases that the center of mass motion of each baryon factors out. That means in practice, that if we write down the above wave functions making use of Jacobi coordinates such as,

$$\begin{aligned}
\vec{S} &= \frac{1}{\sqrt{3}}(\vec{r_1} + \vec{r_2} + \vec{r_3}) \\
\vec{r} &= \frac{1}{\sqrt{2}}(\vec{r_1} - \vec{r_2}) \\
\vec{\rho} &= \sqrt{\frac{2}{3}}\left(\vec{r_3} - \frac{\vec{r_1} + \vec{r_2}}{2}\right),
\end{aligned} \qquad (3.10)$$

the dependence on the center of mass coordinate, $\vec{S}$, factorizes [77].

The same procedure could be applied for any baryon or baryonic resonance with the difference that in each case a different orbital/spin-isospin wave function would have to be constructed. For a complete list of the baryon wave functions on a harmonic oscillator basis see for instance [78].

Two-baryon wave functions

Once we have constructed the single baryon wave functions using a shell model for the baryons we write down the two-baryon wave function with definite spin, isospin and angular momentum of the two-baryon system.

Assuming a two-center shell model the wave function of a two-baryon system, B_1 and B_2, with a definite symmetry under the exchange of the two-baryon quantum numbers is written [39, 79, 80]:

$$\begin{aligned}
\Psi_{B_1 B_2}^{ST}(\vec{R}) &= \frac{\mathcal{A}}{\sqrt{1 + \delta_{B_1 B_2}}}\sqrt{\frac{1}{2}}\Bigg\{ \left[B_1\left(123; -\frac{\vec{R}}{2}\right) B_2\left(456; \frac{\vec{R}}{2}\right)\right]_{ST} \\
&+ (-1)^f \left[B_2\left(123; -\frac{\vec{R}}{2}\right) B_1\left(456; \frac{\vec{R}}{2}\right)\right]_{ST}\Bigg\},
\end{aligned} \qquad (3.11)$$

$S, T(S', T')$ correspond to the spin and isospin of the two-baryon system in the initial (final) state. $\mathcal{A}$ is the six-quark antisymmetrizer described above. A graphical description is given in Fig. 3.2.

One can consider the partial wave decomposition of the wave function of Eq. (3.11):

$$\Psi_{B_1 B_2}^{ST}(\vec{R}) = \sum_{LM} \Psi_{B_1 B_2}^{STLM}(R)\, Y_{LM}(\hat{R}) \equiv \sum_{LM} \Psi_{B_1 B_2}^{STLM}(\vec{R}), \qquad (3.12)$$

the quantities $\Psi_{B_1 B_2}^{STLM}(\vec{R})$ are the projections with definite orbital angular momentum L and third component M. In what follows no dependence on the projection is going to be
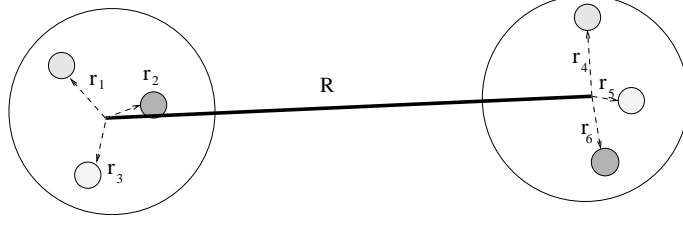
Figure 3.2: Graphical representation of the quarks building a two-baryon wave function where the two clusters are separated a distance R.

needed, so we can ignore this index:

$$\left|\Psi_{B_1 B_2}^{L\,S\,T}(\vec{R})\right\rangle \equiv \Psi_{B_1 B_2}^{STL}(\vec{R}) \equiv \Psi_{B_1 B_2}^{STL0}(\vec{R}) . \tag{3.13}$$

The two terms appearing in Eq. (3.11) differ only in a permutation of the three quarks of each cluster in spin-isospin space. That implies that the second one cannot be reached from the first one only by antisymmetrization.

The action of the $(1 - \mathcal{P})$ operator appearing in the antisymmetrizer on this wave function can be calculated explicitly,

$$\mathcal{P}\left[B_1\left(123; -\frac{\vec{R}}{2}\right) B_2\left(456; \frac{\vec{R}}{2}\right) + (-1)^f B_2\left(123; -\frac{\vec{R}}{2}\right) B_1\left(456; \frac{\vec{R}}{2}\right)\right]_{LST}$$

$$= \left[B_1\left(456; -\frac{\vec{R}}{2}\right) B_2\left(123; \frac{\vec{R}}{2}\right) + (-1)^f B_2\left(456; -\frac{\vec{R}}{2}\right) B_1\left(123; \frac{\vec{R}}{2}\right)\right]_{LST}$$

$$= (-)^{L+S_1+S_2+T_2+T_2-S-T+f}\left[B_1\left(123; -\frac{\vec{R}}{2}\right) B_2\left(456; \frac{\vec{R}}{2}\right)\right.$$

$$\left. + (-1)^f B_2\left(123; -\frac{\vec{R}}{2}\right) B_1\left(456; \frac{\vec{R}}{2}\right)\right]_{LST} . \tag{3.14}$$

So we get that the wave function vanishes unless:

$$L + S_1 + S_2 - S + T_1 + T_2 - T + f = \text{odd} . \tag{3.15}$$

For non-identical baryons this relation fixes the symmetry corresponding to a given set of values (LST). The states, defined by (LST), excluded by Eq. (3.15) are called forbidden states. For identical baryons, $B_1 = B_2$, we recover the well known selection rule (note that f has to be even in order to have a non-vanishing wave function),

$$L + S + T = \text{odd} . \tag{3.16}$$

Pauli antisymmetrization effects

Up to now we have only investigated the antisymmetry effects arising from the $(1 - \mathcal{P})$ operator. The next source comes from the quark permutation operator P_{ij}. The effect of the P_{ij} quark operator on two-baryon systems can be analyzed through the norm of the two-baryon system. This is a measure of the overlapping between the two-baryon wave functions and already shows hints of the consequences of the Pauli principle. The norm of a two-baryon system $B_1 B_2$ is defined as,

$$\mathcal{N}_{B_1 B_2}^{LSTf}(R) = \left\langle \Psi_{B_1 B_2}^{LST}(\vec{R}) \mid \Psi_{B_1 B_2}^{LST}(\vec{R}) \right\rangle . \tag{3.17}$$

The study of the norm has already been shown as a powerful tool to understand the effects of Pauli blocking on two-baryon systems made of nucleons and deltas [80, 81]. For the sake of clarity and completeness we reproduce here the results of their investigations.

Making use of the wave functions of Eqs. (3.5) and (3.6) we can evaluate Eq. (3.17):

$$\mathcal{N}_{B_1 B_2}^{LSTf}(R) = \mathcal{N}_L^{\mathrm{di}}(R) - C(S, T, f; B_1 B_2) \, \mathcal{N}_L^{\mathrm{ex}}(R) , \tag{3.18}$$

where $\mathcal{N}_L^{\mathrm{di}}(R)$ and $\mathcal{N}_L^{\mathrm{ex}}(R)$ refer to the direct and exchange kernel respectively. The direct kernel corresponds to the 1 while the exchange term arises from the P_{36} appearing in the antisymmetrizer. $B_1 B_2$ can be NN, $N\Delta$, $\Delta\Delta$, $NN^*(1440)$ and $N^*(1440)N^*(1440)$ depending on the case we are considering, and LST are the quantum numbers of the two-baryon system. $C(S, T, f; B_1 B_2)$ is a spin-isospin coefficient defined as follows,

$$\begin{aligned} C(S, T, f; B_1 B_2) & = & \frac{3}{1 + \delta_{B_1 B_2}} \left[\langle B_1(123)B_2(456)|P_{36}^{ST}|B_1(123)B_2(456)\rangle_{ST} \right. \\ & + & \left. (-1)^f \langle B_1(123)B_2(456)|P_{36}^{ST}|B_2(123)B_1(456)\rangle_{ST} \right] . \end{aligned} \tag{3.19}$$

The procedure to calculate this kind of coefficients is explicitly shown in Appendix E. This spin-isospin coefficient determines the degree of the Pauli attraction or repulsion as we will see later. Finally the explicit expressions of the direct and exchange kernels are,

$$\begin{aligned} N_L^{\mathrm{di}}(R) & = & 4\pi e^{-\frac{3}{4}\frac{R^2}{b^2}} \, \imath_L \left(\frac{3}{4} \frac{R^2}{b^2} \right) \\ N_L^{\mathrm{ex}}(R) & = & 4\pi e^{-\frac{3}{4}\frac{R^2}{b^2}} \, \imath_L \left(\frac{R^2}{4b^2} \right) , \end{aligned} \tag{3.20}$$

with $\imath_L$ the spherical Bessel functions shown in Appendix A. We summarize in Table 3.1 the spin-isospin coefficients.

Eq. (3.18) can be analyzed in the limit of the distance between the baryons approaching zero. In that limit $(R \to 0)$ we obtain,

$$\mathcal{N}_{B_1 B_2}^{LSTf}(R) \quad \to \quad 4\pi \left(1 - \frac{3}{4} \frac{R^2}{b^2} \right) \frac{1}{1 \cdot 3 \cdots (2L+1)} \left(\frac{R^2}{4b^2} \right)^L$$

NN	
(S,T,f)	$C(S,T,f;NN)$
(0,0,+)	7/9
(0,1,+),(1,0,+)	−1/27
(1,1,+)	31/81
$N\Delta$	
(S,T,f)	$C(S,T,f;N\Delta)$
(1,1,−)	1
(2,2,−)	1
(1,2,+)	1/9
$\Delta\Delta$	
(S,T,f)	$C(S,T,f;\Delta\Delta)$
(0,0,+)	1/3
(0,1,+),(1,0,+)	1/9
(0,2,+),(2,0,+)	−1/3
(0,3,+),(3,0,+)	−1
(1,1,+)	1/27
(1,2,+),(2,1,+)	−1/9
(1,3,+),(3,1,+)	−1/3
(2,2,+)	1/3
(2,3,+),(3,2,+)	1
(3,3,+)	1/3

Table 3.1: Spin, isospin coefficients appearing in the calculation of the norm. "+" ("−") refers to even (odd).

$$\times \quad \left\{ [3^L - C(S,T,f;B_1B_2)] + \frac{1}{2(2L+3)} \left(\frac{R^2}{4b^2} \right)^2 \right.$$

$$\times \quad \left. [3^{L+2} - C(S,T,f;B_1B_2)] + \cdots \right\}. \tag{3.21}$$

This expansion is extremely useful to study the Pauli blocked channels in baryon-baryon systems. The idea is to look into the R dependence of the overlapping at short distances. Of significant interest are those cases where

$$3^L = C(S,T,f;B_1B_2), \tag{3.22}$$

because that implies that the overlapping of the two-cluster wave function behaves as R^{2L+4} instead of the centrifugal barrier behavior R^{2L}, indicating that Pauli blocking occurs.

Table 3.1 shows several of such cases:

- In the NN system there are not such states as can be seen in the table. The repulsion in this system cannot be explained in the absence of dynamics [69].

- In the $N\Delta$ system we find some partial waves with quark Pauli repulsion, those corresponding to $(S,T) = (1,1)$ and $(S,T) = (2,2)$, with angular momentum $L = 0$. In both cases the repulsion can be checked experimentally looking at the πd elastic scattering [82] (these S-wave channels cannot couple to the NN system). There we can infer a hard-core from the phase-shifts changing sign for a pion energy of 219 MeV.

- A similar situation occurs for the $\Delta\Delta$ system. We can check that the spin-isospin coefficient fulfills Eq. (3.22) for the cases $(S,T) = (2,3)$ and $(S,T) = (3,2)$ both with orbital angular momentum $L = 0$. It is also important to mention the existence of Pauli repulsion for a channel with $L \neq 0$ which is a characteristic feature of the $\Delta\Delta$ interaction, this corresponds to $(S,T) = (3,3)$ with orbital angular momentum $L = 1$.

In Sect. 5 we make a similar study for the $NN^*(1440)$ system.

3.2   Two-baryon potentials

The derivation of the dynamics of a two-baryon system from the dynamics of its six constituents is a tough problem. It involves the solution of a quantum many body problem that has not been solved exactly even for the non-relativistic case. An exact solution is not feasible and that compels us to make use of approximation tools.

3.2.1   Resonating group method potential

The RGM has been widely used to derive the dynamics of two-clusters from the dynamics of its constituents. It allows, once the Hilbert space for the six-body problem has been fixed, to treat the inter-cluster dynamics in an exact way.

Its first definition is due to Wheeler [83]. Extensive descriptions of the method applied to the quark/baryon case can be found in Refs. [59, 84]. Here we refer to the non-local NN potential derived through a Lippmann-Schwinger formulation of the RGM equations in momentum space [40, 85].

The formulation of the RGM for a system of two baryons, B_1 and B_2, needs the wave function of the two-baryon system constructed as explained in the previous section but keeping the wave function of the relative motion between the two clusters:

$$\Psi_{B_1 B_2} = \mathcal{A}[\chi(\vec{P})\, \Psi_{B_1 B_2}^{ST}] = \mathcal{A}\,[\chi(\vec{P})\, \phi_{B_1}(\vec{p}_{\xi_{B_1}})\, \phi_{B_2}(\vec{p}_{\xi_{B_2}})\, \chi_{B_1 B_2}^{ST}\xi_c[2^3]\,], \qquad (3.23)$$

where $\mathcal{A}$ is the antisymmetrizer of the six-quark system, $\chi(\vec{P})$ is the relative motion wave-function of the two clusters, $\phi_{B_1}(\vec{p}_{\xi_{B_1}})$ is the internal spatial wave function of the baryon

B_1, ξ_{B_1} are the Jacobi coordinates of the three quarks of baryon B_1. $\chi_{B_1 B_2}^{ST}$ denotes the spin-isospin wave function of the two-baryon system coupled to spin (S) and isospin (T), and, finally, $\xi_c[2^3]$ is the product of two color singlets. The same conclusions obtained in the previous section could be obtained using more involved techniques [21] .

The dynamics of the system is governed by the Schrödinger equation:

$$(\mathcal{H} - E_T)|\Psi>= 0 \quad \Rightarrow \quad < \delta\Psi|(\mathcal{H} - E_T)|\Psi >= 0, \tag{3.24}$$

where

$$\mathcal{H} = \sum_{i=1}^{N} \frac{\vec{p_i}^2}{2m_q} + \sum_{i<j} V_{ij} - T_{c.m.}\,, \tag{3.25}$$

with $T_{c.m.}$ being the center of mass kinetic energy, V_{ij} the quark-quark interaction described above, and m_q the constituent quark mass.

Assuming the same functional form, $0s$ harmonic oscillator wave functions, as before we get that Eq. (3.24) can be written in the following way, after the integration of the internal degrees of freedom of both clusters,

$$\left(\frac{\vec{P}^2}{2\mu} - E\right)\chi(\vec{P}) + \int \left(V_D(\vec{P}, \vec{P_i}) + W_L(\vec{P}, \vec{P_i})\right)\chi(\vec{P})d\vec{P_i} = 0\,, \tag{3.26}$$

$V_D(\vec{P}, \vec{P_i})$ is the direct RGM kernel and $W_L(\vec{P}, \vec{P_i})$ is the exchange RGM kernel, composed of three different terms

$$W_L(\vec{P}, \vec{P_i}) = T_L(\vec{P}, \vec{P_i}) + V_L(\vec{P}, \vec{P_i}) + (E + E_{in})K_L(\vec{P}, \vec{P_i})\,. \tag{3.27}$$

E_{in} is the internal energy of the two-body system, $T_L(\vec{P}, \vec{P_i})$ is the kinetic energy exchange kernel, $V_L(\vec{P}, \vec{P_i})$ is the potential energy exchange kernel and $K_L(\vec{P}, \vec{P_i})$ is the exchange norm kernel. Note that if we do not mind how $V_D(\vec{P}, \vec{P_i})$ and $W_L(\vec{P}, \vec{P_i})$ were derived microscopically, Eq. (3.26) can be regarded as a general single channel equation of motion including energy-dependent non-local potential. $V_D(\vec{P}, \vec{P_i})$, which contains the direct RGM potential, and $W_L(\vec{P'}, \vec{P_i})$, which contains the exchange RGM potential coming from quark antisymmetry, constitute our energy-dependent non-local potential.

3.2.2   Born-Oppenheimer potential

Among the methods available in the literature the BO scheme is one of the most commonly used to derive effective potentials from the microscopic degrees of freedom. Initially it was used to derive potentials between two nucleons [75, 86, 87]. The idea of the BO method, also known as *adiabatic approximation*, is that we can differentiate two momentum scales in the problem. One is the scale at which quarks are moving and the other one is the scale at which the compound particles are moving. The essential part is to integrate out the fast degrees of freedom assuming a fixed position for the center of each cluster obtaining in this way a local potential depending on the distance between the center of mass of the clusters. The method can be summarized graphically in Fig. 3.3.

Figure 3.3: The BO transition potential. We sandwich the two-baryon wave functions with the Hamiltonian at the quark level to obtain the effective transition potential between the two two-baryon states.

Now we already have the ingredients needed to calculate the Born-Oppenheimer potential, that are, on the one hand the microscopic Hamiltonian of the particles that form the system described in detail in Chapter 2, and on the second hand, the wave functions of the two-baryon system. We define the BO potential in the following way [86, 87],

$$V_{B_1 B_2 (L\,S\,T)\to B_3 B_4 (L'\,S'\,T')}(R) = \xi_{L\,S\,T}^{L'\,S'\,T}(R) \, - \, \xi_{L\,S\,T}^{L'\,S'\,T}(\infty)\,, \tag{3.28}$$

where

$$\xi_{L\,S\,T}^{L'\,S'\,T}(R) \; = \; \frac{\left\langle \Psi_{B_1 B_2}^{L'\,S'\,T}(\vec{R}) \mid \sum_{i<j=1}^{6} V_{qq}(\vec{r}_{ij}) \mid \Psi_{B_3 B_4}^{L\,S\,T}(\vec{R}) \right\rangle}{\sqrt{\left\langle \Psi_{B_1 B_2}^{L'\,S'\,T}(\vec{R}) \mid \Psi_{B_1 B_2}^{L'\,S'\,T}(\vec{R}) \right\rangle}\sqrt{\left\langle \Psi_{B_3 B_4}^{L\,S\,T}(\vec{R}) \mid \Psi_{B_3 B_4}^{L\,S\,T}(\vec{R}) \right\rangle}} \;. \tag{3.29}$$

Eq. (3.28) is written in a way that it can represent the most general transition between two two-baryon systems:

$$B_1 \, B_2 \; \to \; B_3 \, B_4 \,, \tag{3.30}$$

with definite L, S, T of the two-baryon initial state and L', S', T' of the final state.

We call direct potentials to the cases where the initial and final baryons are the same, for instance the direct NN potential or the direct $NN^*(1440)$ potential correspond to, $V_{NN\to NN}$ and $V_{NN^*(1440)\to NN^*(1440)}$ respectively. The cases where the two initial baryons are not the same as the two final ones are called transition potentials, as for example the $NN \to N\Delta$ or $NN \to \Delta\Delta$ transition potentials.

3.2.3   Comments on the methods

We have presented the most utilized methods to derive the interaction of clusters of particles in terms of the dynamics of the constituents. There are not many works in the literature where the results obtained with both methods are compared. Both of them permit the evaluation of the influence that the Pauli principle has at the quark level on the properties of the baryon-baryon interactions. Toki [21] pointed out a difficulty arising when the RGM is to be used to study the NN system. He explains how the Pauli blocked states should be removed by hand from the RGM norm so that the physical states are orthogonal to the redundant solutions of the problem.

In this thesis we make use of both kind of baryon-baryon potentials. In Chapter 4, dedicated to the study of the triton bound state, we seize the opportunity to study the

implications of using any of them in the calculation of the triton binding energy. In Chapter 6 we make use of the RGM potentials for the NN and $N\Delta$ transitions and include a BO derived transition to the $NN^*(1440)$ system to look for non-nucleonic components on the deuteron. In Chapter 7 we utilize both methods again and calculate the NN phase-shifts above the Δ region. There we see how at low energies both descriptions are quantitatively similar giving different behaviors when the energy goes above 600 MeV.

The main conceptual difference between the resulting baryon-baryon potentials obtained using BO and RGM, is that in the first case the potential between the baryons is local in space while it is non-local for the RGM:

$$
\begin{aligned}
V^{RGM}_{B_1 B_2 \to B_3 B_4} &\equiv V^{RGM}_{B_1 B_2 \to B_3 B_4}(R, R') \\
V^{BO}_{B_1 B_2 \to B_3 B_4} &\equiv V^{BO}_{B_1 B_2 \to B_3 B_4}(R) \,,
\end{aligned}
\tag{3.31}
$$

this means that the T matrix calculated solving a Lippmann-Schwinger equation has a different off-shell behavior [4] and thus will give different results when applied to the study of few body physics. These differences will be larger the more we let the particles explore the off-shell region. With these ideas in mind let us go to the study of the triton bound state with potentials derived using the tools described above.

---

[4] The on-shell behavior is very similar, in fact as we will see in Chapter 4 we can almost achieve on-shell equivalence by fine tuning the quark model parameters.

4 STUDYING FEW BODY SYSTEMS: TRITON

4.1 Quark models and few-body systems

During the last decade the development of quark-model based interactions for the hadronic force has led to NN potentials that provide a fairly reliable description of the on-shell data. Several models including quark-degrees of freedom have been used to study the NN interaction [59] and also the baryon spectra [13, 88]. As has been discussed the chiral quark model described in Chapter 2 was the only one that pursued a simultaneous understanding of different low-energy phenomena based on a unique quark-quark interaction.

Nevertheless, quark-model based NN interactions have not been often used to study few-body systems. One could argue two different reasons for that. First of all, as has been explained in Chapter 1, most of the quark-model based interactions for the two-nucleon system needed to be supplemented with meson-exchange potentials between the baryons to obtain a reasonable description of the experimental data [89, 90], loosing in this way their quark-based character. Secondly, other quark-model based interactions were designed to describe the baryon spectra [51], presenting severe problems when they are applied to the two-nucleon system [52, 54].

In this chapter we want to perform, for the first time, a study of the triton bound state making use of a NN potential fully derived from quark-quark interactions. The quark model has been previously used to make investigations of three-body systems (NNN, $NN\Delta$, $N\Delta\Delta$, and $\Delta\Delta\Delta$) [72, 91] by means of baryon-baryon potentials constructed as explained in Chapter 3.

An important consequence of deriving the NN potential from the quark-model, is the presence of non-localities arising due to the internal structure of the nucleon. These non-localities, that emerge form the underlying dynamics in a natural way, are reflected in the off-shell properties. The relevance and/or necessity of considering the non-local parts of NN potentials in realistic interactions is still under debate. Indeed, over the past few years several studies have appeared in the literature which stress the potential importance of the non-local effects for the quantitative understanding of few-body observables and, specifically, for the triton binding energy [29, 92, 93, 94, 95, 96]. However, the majority of these investigations [92, 93, 94, 95, 96] explore only non-localities arising from the meson-exchange picture of the NN interaction.

Therefore, as a second objective, we want to make an estimation of the importance of the non-localities generated in a quark-model derivation of baryonic potentials for the

case of the three-nucleon bound state. It has been argued that the assumptions associated with the meson-exchange models sharply limit the nature of the off-shell behavior of those potentials, when the on-shell matrix elements are adjusted to fit the two-nucleon data [97]. Therefore, it is very interesting to investigate the off-shell properties of potentials derived from a quark-model. Some preliminary investigations have been done by Takeuchi et al. [29], where the short-range part of the interaction, obtained by means of quark-model techniques, was supplemented by an intermediate and long-range part based on baryonic potentials, and therefore depriving of import any possible conclusion with respect to the effects of the quark substructure. As a consequence, more systematic studies are lacking altogether.

We choose the triton as the place to test our quark-model based two-body interaction, because it is known that three-body systems are sensitive to the off-shell behavior of the nuclear force. To have an estimation of the non-local effects generated by the quark-model we compare the results for the three-body system calculated with two different quark-model based potentials derived from the same basic quark-quark Hamiltonian. The first potential is the RGM one. In order to isolate the non-local effects we compare our results to those obtained by means of a local BO interaction derived as explained in Sect. 3.2.2. The potentials will be made nearly phase-equivalent by a fine tuning of the model parameters.

4.2   Triton binding energy

The triton binding energy is obtained by means of a Faddeev calculation using the NN interaction calculated as described in Chapter 3. We perform a so-called five-channel calculation, i.e., we use only the $^1S_0$ and $^3S_1 - {}^3D_1$ NN partial waves as input. Note that since in our model there is a coupling to the $N\Delta$ system, a fully consistent calculation would require the inclusion of two more three-body channels. However, their contribution to the $3N$ binding energy is known to be rather small [98] and therefore we neglect them for simplicity reasons.

To solve the three-body Faddeev equations in momentum space we first perform a separable finite-rank expansion of the $NN(-N\Delta)$ sector utilizing the EST method [99]. In Appendix B we explain in some detail the procedure to obtain the expansions and also the interest in building separable versions of two-body potentials. Such a technique has been extensively studied for various realistic NN potentials [100, 101] and specifically for a model that also includes a coupling to the $N\Delta$ system [102]. In these works it was shown that with a separable expansion of sufficiently high rank, reliable and accurate results on the three-body level can be achieved. In the present case it turned out that separable representations of rank 6-8 for $^1S_0 - ({}^5D_0)$ and rank 6 for $^3S_1 - {}^3D_1$, are sufficient to get converged results. The set of energies used for the EST separable representations are listed in Table 4.1.

The quality of the separable expansion on the NN sector can be seen in Figs. 4.1 and 4.2, where we show for our non-local potential phase shift results obtained with the original

RGM(Non-Local)							
Partial wave	(E_μ, l_μ)						
$^1S_0^{NN} - {}^5D_0^{N\Delta}$	(0,0)	(50,0)	(300,0)	(−20,0)	(−20,2)	(−50,0)	
$^3S_1 - {}^3D_1$	ϵ_d	(100,0)	(175,2)	(300,2)	(−50,0)	(−50,2)	

BO (Local)								
Partial wave	(E_μ, l_μ)							
$^1S_0^{NN} - {}^5D_0^{N\Delta}$	(0,0)	(5,2)	(50,0)	(50,2)	(300,0)	(−50,0)	(−50,2)	(−20,2)
$^3S_1 - {}^3D_1$	ϵ_d	(200,0)	(100,2)	(300,2)	(−50,0)	(−50,2)		

Table 4.1: Expansion (lab) energies E_μ (in MeV) used in the EST representations of the non-local and local potentials. ϵ_d refers to the deuteron binding energy. l_μ is the boundary condition chosen for the angular momentum l_μ of the initial state [100, 102].

	QM RGM (Non-Local)	Bonn B	Paris	Nijm II	QM BO (Local)
E_B (MeV)	−7.715	−8.17	−7.30	−7.65	−7.572
P_S (%)	91.49	91.35	90.22	90.33	91.41
$P_{S'}$ (%)	1.430	1.368	1.450	1.339	1.597
P_P (%)	0.044	0.049	0.064	0.064	0.044
P_D (%)	7.033	7.235	8.265	8.267	6.946

Table 4.2: Properties of the three-nucleon bound state.

potential and with its separable expansion, being almost impossible to distinguish between them. The results obtained for the triton[1] are summarized in Table 4.2.

First of all, let us emphasize that the predicted triton binding energy is comparable to those obtained from conventional NN potentials, such as Paris or Nijmegen [100, 101, 102]. We have used exactly the same constrain, the fit of the NN scattering data in the range 0-300 MeV, and our results give support to the use of quark model based interactions for few-body calculations. One should not forget at this point that the number of free parameters is greatly reduced in our model. Besides, they are strongly correlated in order to obtain a reasonable description of the baryon spectrum. The similarity of our results to other non-local potentials could be accidental in the case of the Nijm-I (see Table 4.2). This potential keeps non-local the central component, while the tensor force is local. Non-localities in the central force have only a very moderate influence on the binding energy as compared to non-localities in the tensor force.

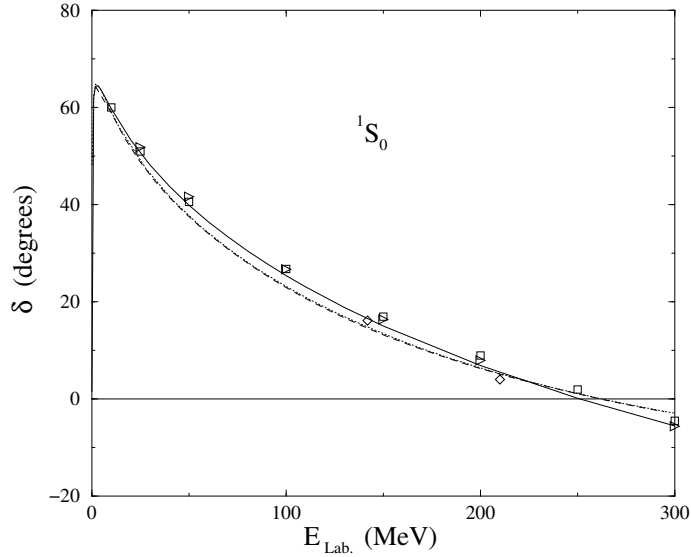[1]Some months after this work was finished another quark-model calculation of the triton was reported [105].

Figure 4.1: $^1S_0$ NN phase shift. The solid line stands for the RGM (non-local) potential while the dashed line correspond to the BO (local) potential. The squares, diamonds and triangles are the experimental data taken from [28], [103], and [104], respectively. The dotted line shows the result of the EST separable representation of the BO model.

4.3   Estimation of non-local effects

In order to obtain a rough estimation of the contribution to the triton binding energy provided by the non-local effects generated by the quark-model potential we will proceed in the following way. We will consider a local potential based on the same quark-quark Hamiltonian. The local potential will be the one obtained by means of the BO method in Chapter 3.

This local NN potential has been widely used in the literature providing results of a comparable quality for the scattering and bound state problems in the two-nucleon sector to the non-local ones [72, 91]. The BO approximation provides a clear-cut prescription for removing the non-localities while preserving the general properties of the interaction for lower partial waves. Though both potentials yield a fairly good reproduction of the experimental phase shifts, they do not provide precisely the same on-shell results. However, on-shell equivalence is desirable for the present investigation, because then one can reliably judge the influence of the non-localities as reflected in different off-shell properties. Thus, in order to isolate the non-local effects, we will try to achieve phase equivalence between the local and non-local interaction models by fine tuning the quark model parameters. We have listed in Table 4.3 the parameters used for the local model. In Table 4.4 we compile the low-energy scattering parameters and deuteron properties as compared to the non-local model and the experimental data. In Figs. 4.1 and 4.2 we also show the phase shifts obtained with the local model.
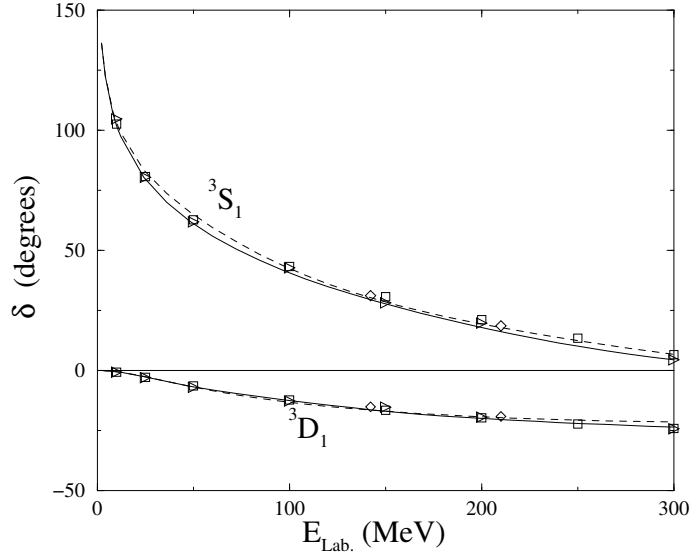
Figure 4.2: Same as Fig. 4.1 for the $^3S_1$ and $^3D_1$ partial waves.

The three-body calculation is done in the same way as for the non-local case. We perform separable expansions EST with the set of energies listed in Table 4.1. The results for the triton binding energies are summarized in Table 4.2, compared to the non-local model and the experimental data. The results can be considered of the same quality as standard local potentials, and as could be a priori expected, the binding energy within our local model gets decreased with respect to the non-local potential. It is also interesting to observe the similarity between our results and the Nijmegen potential, where we have found results for local and non-local versions of the potential. We see how in both cases the non-local result increases the binding in the order of 100-150 keV. In particular, for our local and non-local models one observes that there is about 150 keV more binding for the non-local potential. Is this the enhancement we can expect from the non-localities due to the quark substructure of the nucleon? In order to answer this question we need to go back again to the NN results and scrutinize the on-shell properties carefully. For the $^1S_0$ partial wave the differences in the low-energy scattering parameters and in the phase shift are indeed very small, see Table 4.4. Actually, one can get an estimation of the uncertainty in the predicted triton binding energy due to deviations from phase equivalence from a work by Gibson and Stephenson [106], who studied the dependence of the triton binding on variations of the effective range parameters. The scale set by their investigations implies that the smaller effective range r_s of the non-local potential (by about 0.01 fm) might be responsible for about 20 keV of the additional binding. There is much less sensitivity to the scattering length a_s [92]. However, here our models are in perfect agreement anyway. Unfortunately, for the $^3S_1 - ^3D_1$ partial wave the situation is much more complicated. While the deuteron binding energy and also the $^3S_1$ and $^3D_1$
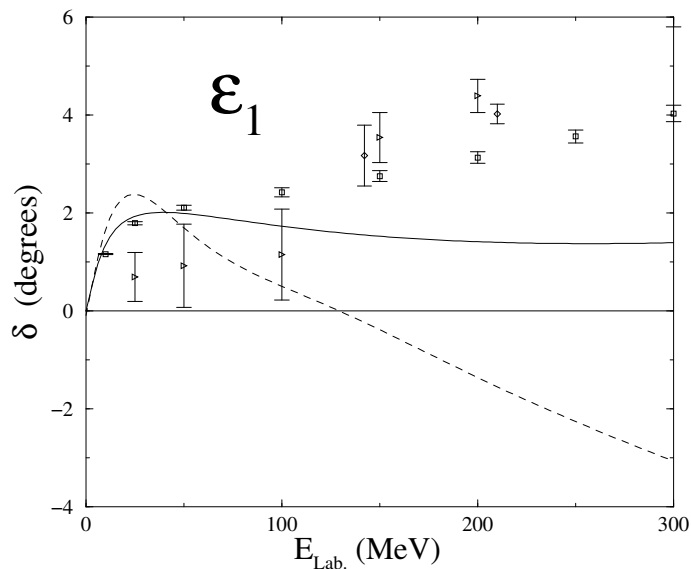
Figure 4.3: Mixing parameter ε_1. Same description as in Fig. 4.2.

phase shifts are in excellent agreement, this cannot be said about the mixing parameter ε_1, see Fig. 4.3. In this case, it is difficult to estimate reliably the effect from the obvious deviation from phase equivalence on the triton binding energy.

However, one can clearly separate the effects from the two involved partial waves. For this purpose, we carried out additional $3N$ calculations where we combined the $^1S_0$ of the local model with the $^3S_1 - {}^3D_1$ of the non-local model and vice versa. Corresponding results are compiled in Table 4.5. They strongly suggest that the non-localities present in the $^1S_0$ alone are already responsible for the enhancement of around 150 keV in the triton binding energy. The shift in the binding energy is independent of whether we use the local or non-local version model for the $^3S_1 - {}^3D_1$ partial wave. On the other hand, the non-localities present in the $^3S_1 - {}^3D_1$ partial wave seem to even decrease the binding energy. However, we suspect that here the effect of the non-localities is obscured by the fact that the two models are not strictly phase equivalent. Indeed, the discrepancies in ε_1 present in our models are qualitatively comparable to those existing between the Bonn NN models A and B presented in Ref. [94] (see Fig. 4.4 of this reference). Thus, we can use the $3N$ results for those models in order to get at least a rough estimation for the effects caused by the deviation from phase equivalence. The triton binding energy (for the five-channel configuration) for Bonn A is -8.371 MeV and for Bonn B is -8.161 MeV [101]. This means that the weaker tensor force present in model Bonn A, which causes the mixing parameter ε_1 to be smaller and even to become negative at higher energies, yields additional binding of about 200 keV as compared to Bonn B. If we now transfer this result to our situation we would expect that the binding energy for our local model (where ε_1 becomes negative as well) is likewise enhanced by about such an amount as compared

	RGM	BO
m_q(MeV)	313	313
b(fm)	0.518	0.518
α_s	0.4977	0.4850
g_{ch}^2	6.60(6.86)	6.96
$m_S(\text{fm}^{-1})$	3.400	3.422 (3.280)
$m_{PS}(\text{fm}^{-1})$	0.70	0.70
$\Lambda_{ch}(\text{fm}^{-1})$	4.20	4.47

Table 4.3: Quark model parameters for the RGM (non-local) and BO (local) models. The values in brackets are used for a correct description of the deuteron.

		RGM	BO	Nijm II	Bonn	Paris	Exp
		Low-energy scattering parameters					
$^1S_0$	a_s (fm)	-23.759	-23.758		-23.750	-17.612	-23.749
	r_s (fm)	2.682	2.694		2.71	2.88	2.766
$^3S_1$	a_t (fm)	5.461	5.464	5.420	5.427	5.427	5.427
	r_t (fm)	1.820	1.779	1.753	1.763	1.766	1.755
		Deuteron properties					
ϵ_d (MeV)		-2.2242	-2.2245	-2.2246	-2.2245	-2.2249	-2.22465
P_D (%)		4.85	4.79	5.635	4.38	5.77	-
Q_d (fm^2)		0.276	0.280	0.271	0.274	0.279	0.286
A_S (fm$^{-1/2}$)		0.891	0.900	0.8845	0.8867	0.8860	0.8846
A_D/A_S		0.0257	0.0243	0.0252	0.0263	0.0261	0.0271

Table 4.4: NN properties. Nijm II, Bonn and Paris refer to [16, 17, 18]. Experimental values are taken from [16].

with a potential that would be phase equivalent to the non-local model. Then the "true" effect of the non-localities from the $^3S_1 - {}^3D_1$ partial wave would be also an increase of the binding energy by about 150 keV. Indeed, this is a plausible result because we would expect intuitively that the effect of non-localities should go into the same direction for either partial wave, and they should be of comparable magnitude because both partial waves contribute about the same amount to the total triton binding energy. The total enhancement of the triton binding energy due to the non-localities coming from the quark substructure of the nucleon would then amount to about 300 keV, similar to the result obtained in [94] for the non-local effects of the CD-Bonn model.

Recently, Doleschall and Borbely [96] have published a systematic study on the influence of non-local NN interactions on the triton data. In particular, they have shown that non-localities can, in principle, even provide for an additional binding of about 1 MeV as it is required for conventional (local) NN potential in order to achieve agreement

		$^3S_1 - {}^3D_1$	
		BO	RGM
$^1S_0$	BO	-7.572	-7.544
	RGM	-7.745	-7.715

Table 4.5: Three-nucleon binding energy (in MeV) for different combinations of the BO (local) and RGM (non-local) models.
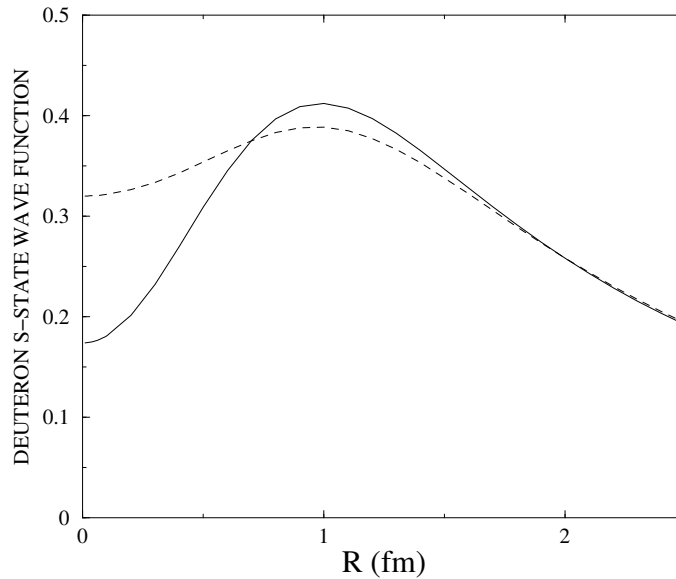

Figure 4.4: Deuteron S-state wave function. The solid line corresponds to the non-local NN interaction while the dashed line is the result for the local interaction.

with the experimental triton binding energy. Our results show the same trend, however, quantitatively the effect of the non-localities on the $3N$ binding energy turned out to be smaller. This is not too surprising, because in our case the extent of non-localities is fixed by the dynamics, i.e., by the quark model from which the NN interaction models are derived. On the other hand, in [96] the non-localities are introduced phenomenologically into the NN interaction and their magnitude and range are not constrained a priori.

In order to facilitate a comparison with their work we present here the deuteron S-state wave function, Fig. 4.4, and the zero-energy wave function of the $^1S_0$ partial wave, Fig. 4.5, for our local and non-local models. [2] It can be clearly seen that the non-localities in the NN interaction lead to a modification of those wave functions at short distances. However, it is interesting to note that the non-localities resulting from the quark substructure of the nucleon generate changes in the wave functions that go into the opposite direction as

---

[2]Note that our codes do not allow to calculate exactly at $E_{\text{lab}} = 0$ MeV, therefore we choose a small finite energy.
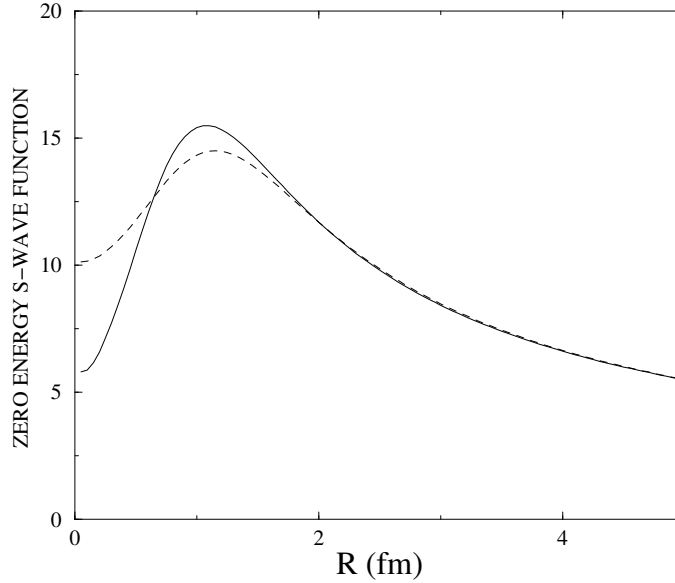
Figure 4.5: Scattering wave function for the $^1S_0$ partial wave at E_{Lab}=0.1 MeV. The solid line corresponds to the non-local NN interaction while the dashed line is the result for the local interaction.

the ones introduced phenomenologically in Ref. [96]. We observe a suppression of both wave functions at very short distances, whereas an (in part significant) enhancement of the wave function occurs for all cases postulated by Doleschall and Borbély. We should point out, however, that for our models there is an enhancement for inter-nucleonic distances around $R \approx 1$ fm. These modifications of the wave function at intermediate distances will certainly have an impact on the $3N$ results and we believe that they are primarily responsible for the increase in the triton binding energy that we obtain for our non-local NN potential.

Let us also mention that there are sources of non-localities of a completely different origin. For example, the CD-Bonn model takes into account non-localities coming from the square root factor $M/\sqrt{EE'}$ appearing in the relativistic Blankenbecler-Sugar formulation [94], known as minimal relativity. Clearly, these non-localities have a relativistic origin because the approximation $E = E' = M$ gives rise to the non-relativistic local version of the Bonn potential. Therefore these effects, quark substructure and minimal relativity, could complement each other as to obtain the correct triton binding energy.

Finally it is important to state that we have also shown that the description of the few-body observables making use of the BO scheme for the derivation of the NN potentials is completely justified if one is not interested in accurate quantitative results. As found for the triton binding energy, the differences encountered in the calculated bindings are lower than 5%.

5 THE $NN^*(1440)$ SYSTEM

It has become clear in the last years the major role played by baryonic resonances, in particular the low-lying nucleonic resonances $\Delta(1232)$ and $N^*(1440)$, in many electromagnetic and strong reactions that take place in nucleons and nuclei. This justifies the current experimental effort along this line in several facilities : TJNAF with a specific experimental program of electroexcitation of resonances, WASA in Uppsala to study $NN \rightarrow NN\pi\pi$ reactions, etc.

The $\Delta(1232)$ appears as the most important P-wave resonance in the πN system. The $N^*(1440)$ appears as a peak in the (α, α') reaction on a proton target [107] interpreted as an excitation of the target mediated by an isoscalar exchange between the α and the proton [36]. From the point of view of their quark structure the Δ corresponds to a spin-flavor flip of one of the quarks of the nucleon. The quark structure of the $N^*(1440)$ seems more elusive. Descriptions as a radial excitation of the nucleon, as assumed in most spectroscopic quark models and that we shall adopt hereforth, are the simplest ones. Alternatively, the $N^*(1440)$ has been considered a breathing bag model mode [108] or a hybrid state containing quarks and gluons [109]. Even recently, it has been pointed out a possible explanation of the $N^*(1440)$ as a dynamical effect in πN scattering without resorting to any quark structure [110].

At the baryonic level, the role played by the Δ in many nucleonic and nuclear reactions has been extensively studied within the framework of the intermediate energy Δ isobar model [111]. Regarding the $N^*(1440)$ its role in the NN interaction, as much in the scattering problem [112] as in the deuteron structure [113], has been considered in the past. Also the contribution of intermediate $N^*(1440)$ resonances to the three-nucleon interaction has been estimated [114]. More recently, its relevance in $NN \rightarrow NN\pi\pi$ reactions has been emphasized [115].

In this context the transition, $NN \rightarrow NR$ (R: resonance), and direct $NR \rightarrow NR$ and $RR \rightarrow RR$ interactions should be understood. Usually these interactions have been written as straightforward extensions of some pieces of the $NN \rightarrow NN$ potential with the modification of the values of the coupling constants, extracted from their decay widths. Though this procedure can be appropriate for the very long-range part of the interaction, it is under suspicion at least for the short-range part for which the detailed structure of the baryons may determine to some extent the form of the interaction. This turns out to be the case for the $NN \rightarrow N\Delta$ and $N\Delta \rightarrow N\Delta$ potentials previously analyzed elsewhere [39]. It seems therefore convenient to proceed to a derivation of these potentials based on the more elementary quark-quark interaction. This is the purpose of this chapter: starting from the

(S,T)	$(1,0)$	$(0,1)$	$(0,0)$	$(1,1)$
$C(S,T)$	$-1/27$	$-1/27$	$7/9$	$31/81$

Table 5.1: $C(S,T)$ spin-isospin coefficients as defined in Eq. (5.2).

quark-quark non-relativistic potential explained in Chapter 2, we implement the baryon structure through technically simple variational gaussian wave functions and we calculate the potential at the baryonic level in the static BO approach explained in Chapter 3. The $N^*(1440)$ is taken as a stable particle. For dynamical applications, such as the study of the NN interaction of Chapter 7, its width should be implemented through the coupling to the continuum.

This chapter is organized as follows. In Sect. 5.1 we obtain the norm of the the $NN^*(1440)$ system. The direct $NN^*(1440) \rightarrow NN^*(1440)$ potential is obtained in Sect. 5.2 while in Sect. 5.3 we present the $NN \rightarrow NN^*(1440)$ transition potential.

5.1   Norm of the $NN^*(1440)$ system

The effects of quark substructure on two-baryon systems can be seen just by studying the overlapping between the two two-baryon wave functions. The precise definition of the norm of a two-baryon system was given in Chapter 3, here we give the expression for the $NN^*(1440)$ system:

$$\mathcal{N}_{NN^*(1440)}^{LSTf}(R) = \mathcal{N}_L^{\text{di}}(R) - C(S,T)\mathcal{N}_L^{\text{ex}}(R).$$ (5.1)

Their explicit expressions are given in Appendix C. $C(S,T)$ is a factor depending on the total spin (S) and the total isospin (T) of the $NN^*(1440)$ system and given by

$$C(S,T) = \frac{1}{4}\sum_{\chi_i=\eta_i=0}^{1}\left\langle\left(\chi_1,\frac{1}{2}\right),\frac{1}{2};\left(\chi_2,\frac{1}{2}\right),\frac{1}{2};S,M_S\left|P_{36}^S\right|\left(\chi_3,\frac{1}{2}\right),\frac{1}{2};\left(\chi_4,\frac{1}{2}\right),\frac{1}{2};S,M_S\right\rangle$$

$$\left\langle\left(\eta_1,\frac{1}{2}\right),\frac{1}{2};\left(\eta_2,\frac{1}{2}\right),\frac{1}{2};T,M_T\left|P_{36}^T\right|\left(\eta_3,\frac{1}{2}\right),\frac{1}{2};\left(\eta_4,\frac{1}{2}\right),\frac{1}{2};T,M_T\right\rangle,$$ (5.2)

χ_i (η_i) stands for the coupled spin (isospin) of two quarks. For $L=0$ and $R\rightarrow 0$ one obtains:

$$\mathcal{N}_{NN^*(1440)}^{L=0,STf}(R\rightarrow 0) \sim \left\{1-\frac{1}{3}\left[5+2(-)^f\right]C(S,T)\right\} + \mathcal{O}(R^4),$$ (5.3)

the values of $C(S,T)$ are given in Table 5.1.

Pauli blocked channels correspond to f=odd and $C(S,T)$=1, or f=even and $C(S,T)$=3/7. From the values given in Table 5.1 it is clear that although there are no Pauli blocked channels there is a Pauli repulsion for those S-wave channels without NN counterpart, (S,T)=(0,0),(1,1), i.e., forbidden in the NN case. This is illustrated in Fig. 5.1, where we show the norm of the $NN^*(1440)$ wave function for $L=0$. As can be seen, the norm
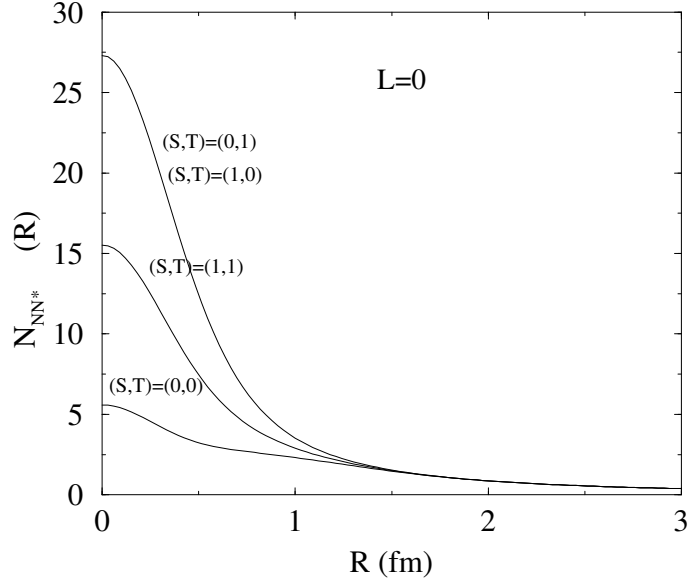
Figure 5.1: $NN^*(1440)$ overlapping as a function of the interbaryon distance for $L = 0$ partial waves.

gets suppressed in those cases where the channel is forbidden for the NN case. This is a remnant of the near to identity similarity of N and $N^*(1440)$.

5.2 Direct $NN^*(1440) \to NN^*(1440)$ potential

We center our attention in the $NN^*(1440) \to NN^*(1440)$ potential where a complete parallelism with the $NN \to NN$ case can be easily established. Notice that the quark-quark interaction parameters are fixed (from the $NN \to NN$ case) and are kept independent of the baryons involved in the interaction. This eliminates the bias introduced in models at the baryonic level by a different choice of effective parameters according to the baryon-baryon interaction considered (this effectiveness of the parameters may hide distinct physical effects).

5.2.1 Derivation of the $NN^*(1440) \to NN^*(1440)$ Potential

To derive the $NN^*(1440) \to NN^*(1440)$ potential from a quark-quark interaction we follow the BO method.

From Eq. (3.28) and from the structure of the antisymmetrizer the potential contains direct terms, not involving quark exchanges, and quark-exchange pieces. We have illustrated in Figs. 5.2 and 5.3 the most important diagrams contributing to the potential. We have separated them regarding to the part of the radial wave function that contributes to this
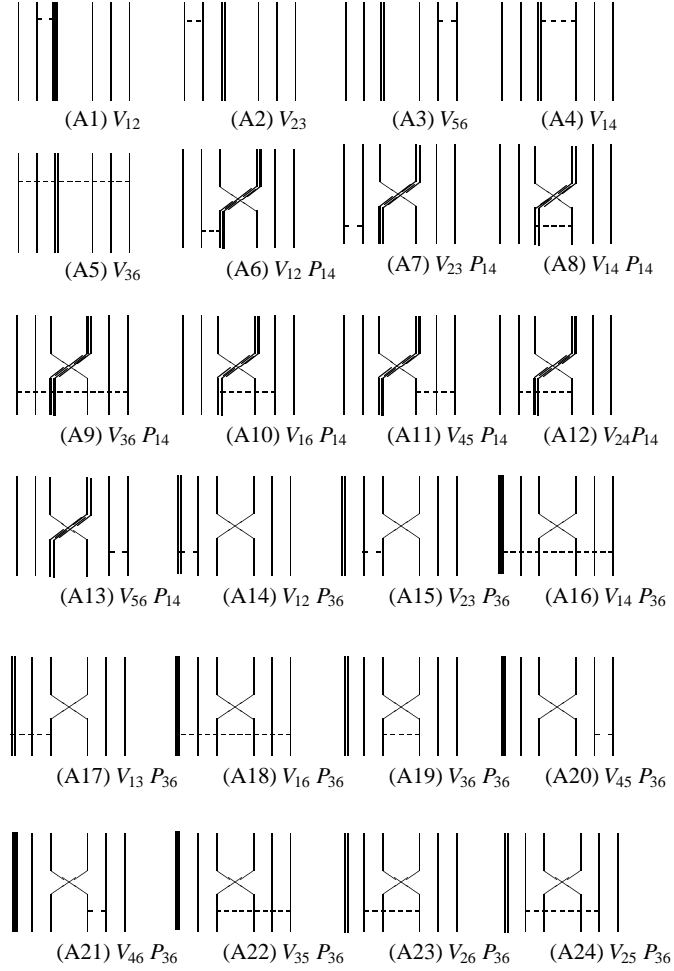
Figure 5.2: Different diagrams contributing to the $NN^*(1440)$ interaction. The double line denotes an excited quark on the 1s shell and the dotted line stands for an excited quark on the 0p shell. Diagrams (A1), (A2), (A3), (B1), (B2) and (B3) are topologically equivalent although involving interactions between excited or non-excited quarks. In the next figures and for simplicity they will be denoted by V_{12}. The remaining diagrams can be also grouped in topologically equivalent classes. The simplified notation in next figures corresponds to such a grouping.

(B1) V_{12} (B2) V_{23} (B3) V_{56} (B4) V_{14}

(B5) V_{36} (B6) $V_{13}\, P_{36}$ (B7) $V_{23}\, P_{14}$ (B8) $V_{14}\, P_{14}$

(B9) $V_{36}\, P_{14}$ (B10) $V_{16}\, P_{14}$ (B11) $V_{45}\, P_{14}$ (B12) $V_{24}P_{14}$

(B13) $V_{25}\, P_{36}$ (B14) $V_{36}\, P_{36}$

(C1) $V_{23}\, P_{14}$ (C2) $V_{16}\, P_{36}$ (C3) $V_{16}\, P_{36}$
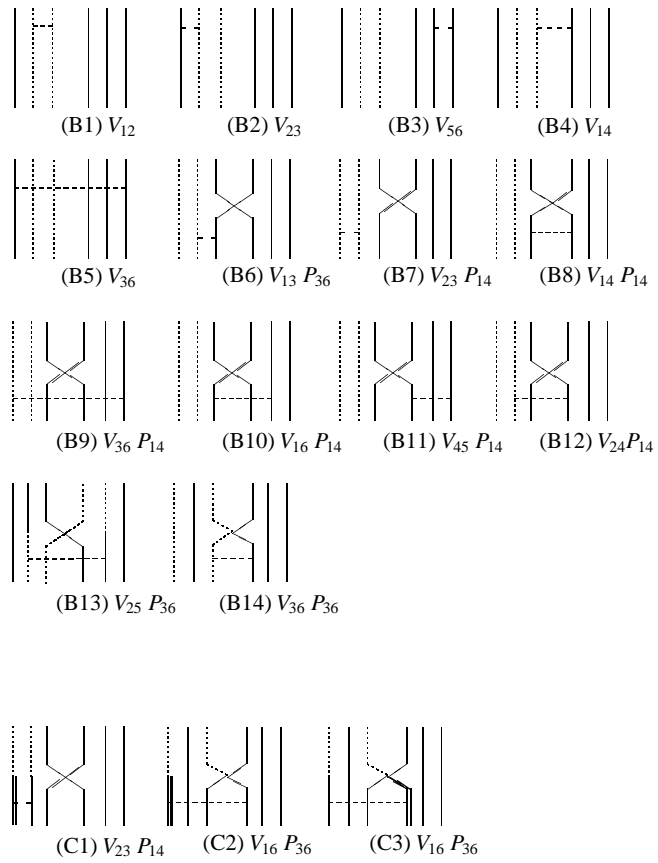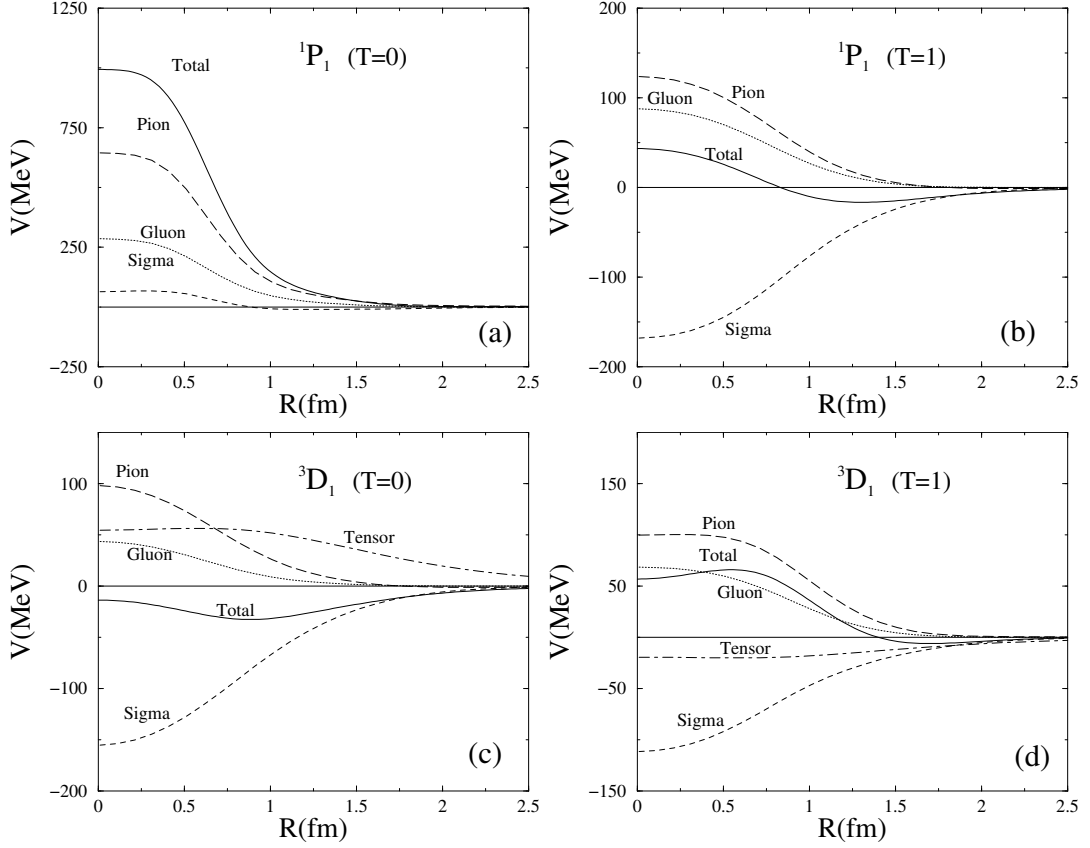
Figure 5.3: Continuation of Fig. 5.2.
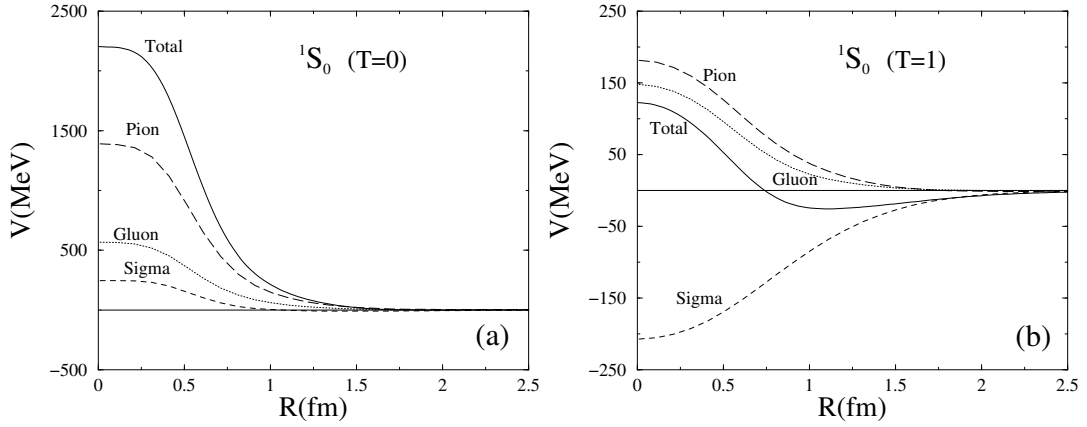
Figure 5.4: $NN^*(1440)$ potential for different $L = 0$ partial waves. The contribution of the different terms of the potential has been depicted.

diagram. Most of them, from diagrams (A1) to (A24), are generated by ϕ_1, Eq. (3.8), diagrams (B1) to (B14) are due to ϕ_2, Eq. (3.9), and the only relevant diagrams coming from the mixing of both terms, ϕ_1 and ϕ_2, are (C1) to (C3). Diagrams (A1) to (A3) and (B1) to (B3) correspond to self-energy, and are therefore subtracted in Eq. (3.28). Diagrams (A4), (A5), (B4) and (B5) give the direct contribution, and they generate the asymptotic behavior of the $NN^*(1440)$ interaction. The remaining diagrams are of quark-exchange type and their relevance depends on the degree of overlap of the baryon wave functions. Within these ones, from (A6) to (A13), (B13) and (C3), correspond to baryon exchange, i.e., $NN^*(1440) \rightarrow N^*(1440)N$ terms, while the remaining diagrams are associated to $NN^*(1440) \rightarrow NN^*(1440)$ terms.

Spin-isospin-color matrix elements are the same than in the NN case and can be taken from [15].

5.2.2   Analysis of the direct potentials

In Figs. 5.4, 5.5 and 5.6 we show the potentials obtained for all the $L = 0$ partial waves and some representative $L = 1$ and $L = 2$ partial waves (T=0 and T=1) as a function of the interbaryon distance. Contributions from the different terms of the potential are also depicted. In Fig. 5.7 contributions from the different diagrams (for simplicity we have grouped the diagrams attending to their topology, see caption of Fig. 5.2) are separated for some partial waves.

There are general features of the results for all the partial waves that can be enumerated:

i) For very-long distances ($R > 4$ fm) the interaction comes determined by the OPE potential, since this corresponds to the longest-range piece. The OPE is also responsible altogether with the OSE for the long-range part behavior (1.5 fm $< R < 4$ fm), due to the combined effect of shorter range and a bigger strength for the OSE as compared to
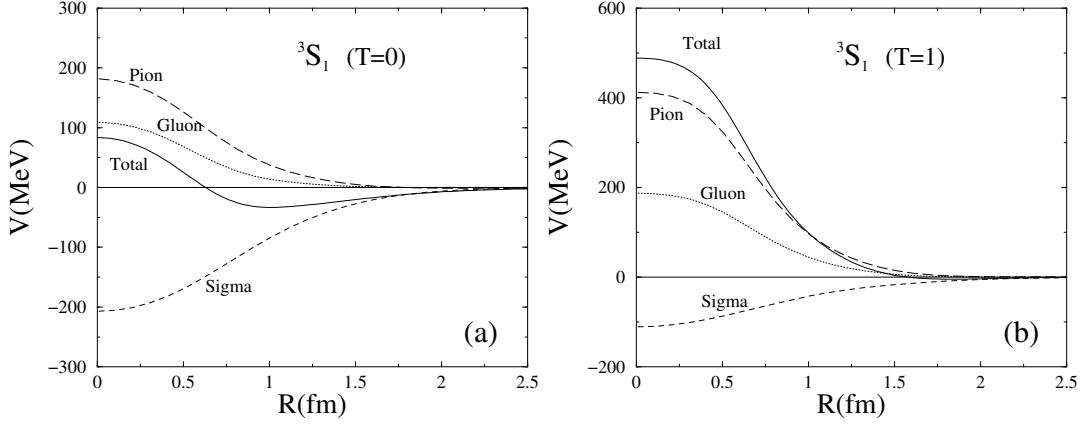
Figure 5.5: Same as Fig. 5.4.

the OPE.

ii) For $L =$ even and isospin channels with a correspondence in the NN case, f even, that we shall call *allowed* channels hereforth, the OSE gives the dominant contribution in the intermediate range (0.8 fm $< R <$ 1.5 fm), determining the attractive character of the potential in this region. Analogously for $L =$ odd and *forbidden* channels (those without correspondence in the NN case). In other cases, the OSE reduces its relative contribution or becomes even repulsive. This can be explained by the combined effect of the spatial parity, defined by L, and the spin-isospin parity defined by f. When L and f have the same signature, i.e., they are both even or odd, the contributions from combinations of the two terms on the right hand side of Eq. (3.11) add attractively while for different signature they can alternatively add or subtract.

iii) For S (L=0) and P (L=1) waves the short-range ($R <$ 0.5 fm) potential is repulsive. This repulsion comes determined by the OGE and the OPE through quark-exchange diagrams. For D (L=2) waves, where these quark-exchange contributions are weakened by the presence of a stronger centrifugal barrier that prevents a large overlapping of the baryons, the short-range potential may become even attractive (see Figs. 5.4, 5.6 (c)).

iv) The *forbidden (allowed)* channels in S and D waves (P waves) are much more repulsive than the *allowed (forbidden)* channels. Moreover the potential for the *forbidden* $^1S_0(T = 0)$ channel is very much the same than the potential for the *allowed* $^1P_1(T = 0)$ and similarly for $^3S_1(T = 1)$ and $^3P_J(T = 1)$ (in this last case with small dependences on J due to the tensor interaction). This can be understood in terms of the Pauli and the centrifugal barrier repulsions. The Pauli correlations and the centrifugal barrier in the P waves prevent all the quarks to be in the same spatial state, much the same effect one has due to Pauli correlations in the S *forbidden* waves added to the presence of the radially excited quark in the $N^*(1440)$.

v) For the *allowed (forbidden)* channels in S or D waves (P waves), the dominant

Figure 5.6: $NN^*(1440)$ potential for different $L = 1, 2$ partial waves. The contribution of the different terms of the potential has been depicted.

repulsion comes from $V_{36}P_{36}$. This corresponds to the interaction taking place between the same two-exchanged quarks. In the other cases, the $V_{13}P_{36}$ or $V_{16}P_{36}$ terms, where an exchanged quark interacts with a non-exchanged one, provide the dominant repulsion. As above, these dominances come out from the combined effect, through the P_{36} operator, of the spatial and spin-isospin parities.

vi) The dynamical effect of quark antisymmetrization can be estimated by comparing the total potential with the one arising from diagram V_{36} which is the only significant one that does not include quark exchanges. The V_{36} potential turns out to be attractive everywhere. Let us note however that Pauli correlations are still present in the V_{36} potential, through the norm, in the denominator of Eq. (3.28). To eliminate the whole effect of quark antisymmetrization one should eliminate quark-Pauli correlations from the norm as well. By proceeding in this way one gets a genuine baryonic potential, that we call direct potential. The comparison of the total and direct potentials reflects the quark antisymmetrization effect beyond the one-baryon structure. As V_{36}, the direct potential is
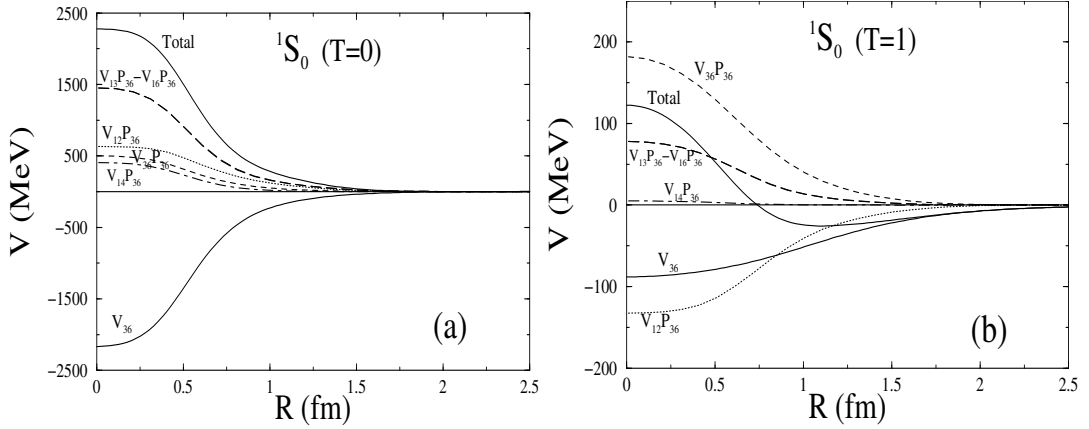
Figure 5.7: Depicting the contribution of the different diagrams drawn in Fig. 5.2, with the convention explained in the caption.

attractive everywhere (see Fig. 5.9). It becomes then clear that the repulsive character of the interaction at S and P waves at short distances is due to dynamical quark-exchange effects. For distances $R \geq 2$ fm the direct, V_{36}, and total potentials are equal since then the overlap of the N and the $N^*(1440)$ wave functions is negligible and no exchange diagrams contribute appreciably.

vii) Phase shifts for the two $^1S_0$ isospin channels are shown in Fig. 5.10. The correlation between *allowed* and *forbidden* states established above translates into the values of the corresponding phase shifts. NN phase shifts are also drawn for comparison. The quite similar behavior observed has to do again with the close to identity character of the $NN^*(1440)$ and NN wave functions in the *allowed* channels commented before.

5.2.3 Phenomenological $NN^*(1440) \to NN^*(1440)$ potentials

It is interesting to compare our results for $NN^*(1440)$ with the ones obtained for NN derived in the same manner. This will allow to emphasize the differences derived from the non-identity of the baryons in the $NN^*(1440)$ case and to analyze phenomenological approaches at the baryonic level which take the same form for the $NN^*(1440) \to NN^*(1440)$ and the $NN \to NN$ potentials and proceed to a fit of the strength of the different pieces of the potential from data.

We should first realize that strictly speaking baryonic potentials, for the $NN^*(1440)$ case as much as for the NN one, are only justified beyond distances $R \sim 2$ fm, where no quark-exchange effects are present. For $R < 2$ fm the direct potential, which represents a genuine baryonic potential since no quark-exchanges are included, differs very much from the total potential (see Fig. 5.9). However we all know the usefulness of effective baryonic potentials where through the parametrization of the form of the interaction and the effective values of the parameters, quark-exchange effects are mostly incorporated.
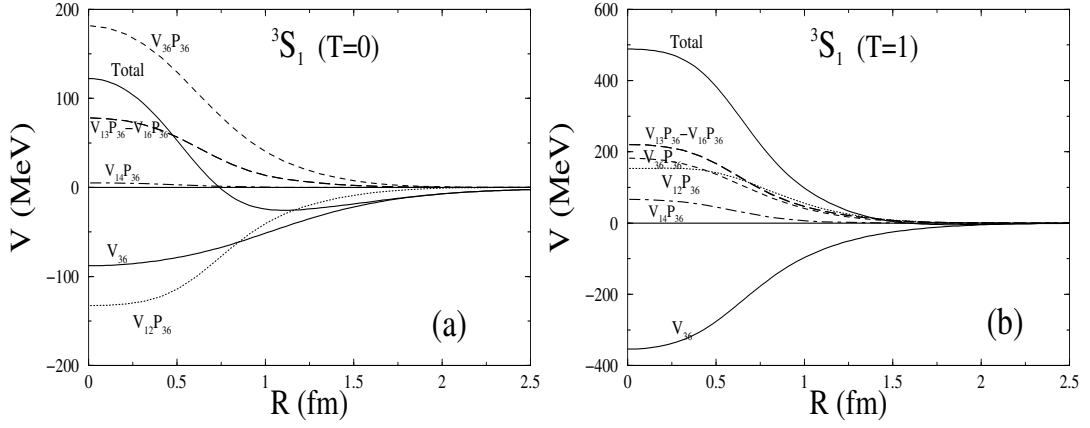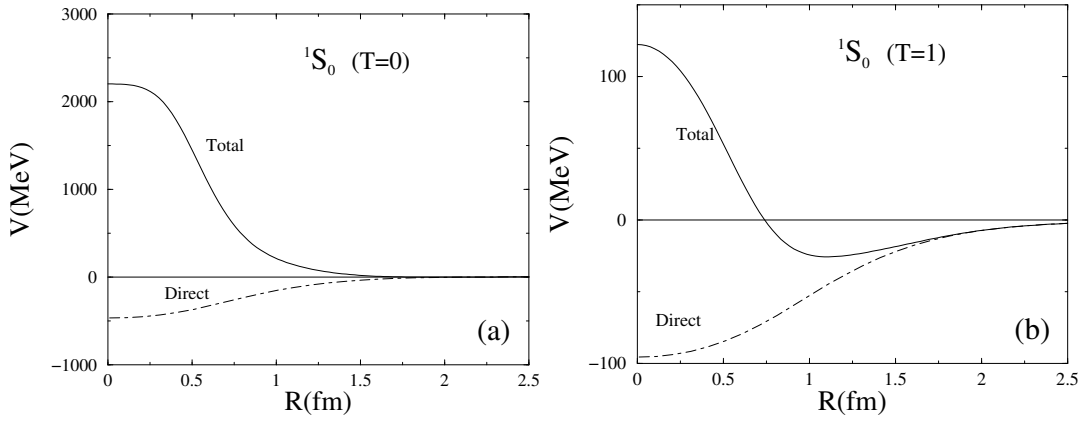
Figure 5.8: Same as Fig. 5.7.

Figure 5.9: Comparison between the total and direct (as defined in the text) potential for different $NN^*(1440)$ partial waves.

The same seems to be true for *allowed* channels in the $NN^*(1440)$ case, since potentials are at most 15% percent different than NN ones (see Fig. 5.10).

For *forbidden* states the task of constructing a reliable baryonic potential appears a priori more complicated since there is no NN guide. Nevertheless remembering the discussion in the former section, from the correspondence that can be established between *allowed* and *forbidden* states in different partial waves, one can imagine that a baryonic phenomenological description would also be available.

By proceeding in this way it is important to notice a main formal difference with the quark treatment related to the fact that quark interaction coupling constants are fixed from NN data once for all keeping their values independently of the baryons involved. On
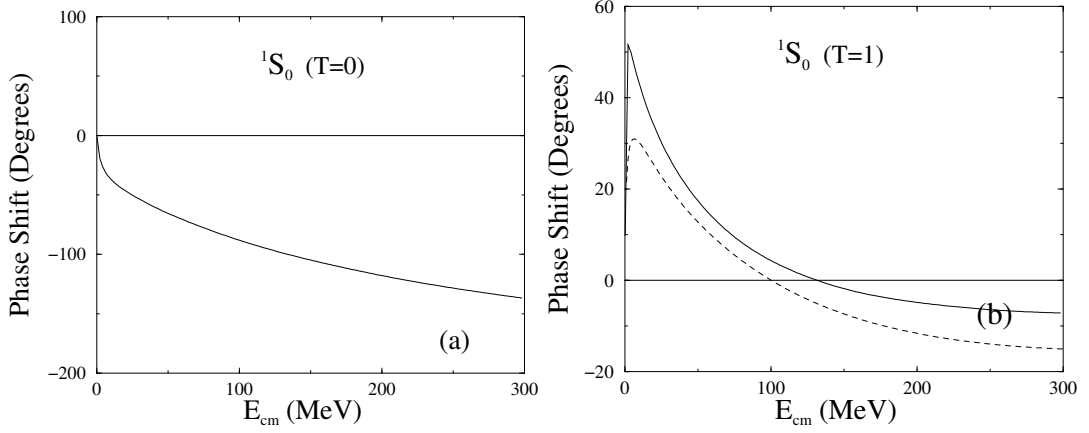
Figure 5.10: Phase shifts for $L = 0$ $NN^*(1440)$ partial waves (solid line) compared to the corresponding NN phase shifts (dashed line).
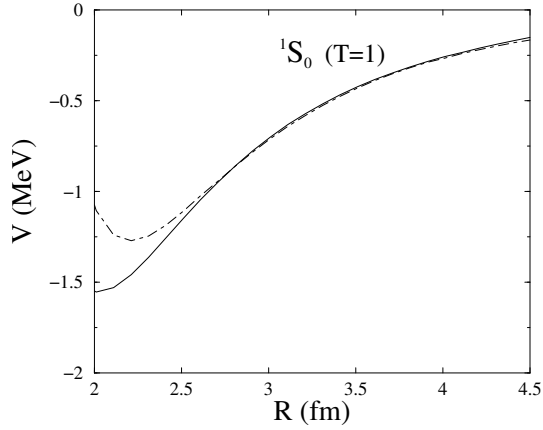
Figure 5.11: Asymptotic behavior of the $^1S_0(T = 1)$ OPE potential in configuration space for NN (solid line) and $NN^*(1440)$ (dashed line) systems.

the contrary baryon coupling constants are fixed phenomenologically case by case. The same is true for the cut-off masses for the vertices. This makes possible, at least for some forms of the interaction, to give, from quark coupling values, predictions for the unknown baryonic couplings. Obviously this prediction could be altered in the $NN^*(1440)$ case through the inclusion of the $N^*(1440)$ width. Let us take for example the OPE potential. Since the pion-baryon-baryon coupling constant is calculated at zero momentum transfer we have to examine the asymptotic behavior of the OPE in configuration space. In the NN case this comparison between the baryonic OPE and the quark OPE potential fixes

the πqq coupling constant. For $NN^*(1440)$ the form of the interaction does not change with respect to NN. Furthermore as can be checked from Fig. 5.11 there is no significant difference beyond $R > 2.5$ fm between the NN and $NN^*(1440)$ cases. One should realize however that for $NN^*(1440)$, due to the presence of $NN^*(1440) \rightarrow NN^*(1440)$ as well as $NN^*(1440) \rightarrow N^*(1440)N$ there are two different couplings involved, $g_{\pi N^* N^*}$ and $g_{\pi NN^*}$, apart from $g_{\pi NN}$. It turns out that the dominant contribution comes from $NN^* \rightarrow NN^*$ from what one concludes that $g_{\pi N^* N^*} \sim g_{\pi NN}$.

Concerning the use of OPE $NN^*(1440) \rightarrow NN^*(1440)$ potentials, for example in the fitting of the NN scattering at intermediate energies (see for example [116]), some caution is necessary. Let us remind that the OPE is the dominant piece only at very long distances, $R > 4$ fm. One should be aware that for distances 1.5 fm $< R < 4$ fm, the OSE contribution is as important as the OPE. Therefore the use of only the OPE for energies involving long-distances might induce an error of the same size as the contribution considered. Certainly this OSE contribution could be to some extent included through a renormalization of the pion-baryon-baryon or of other couplings, but this renormalization depends not only on the particular partial wave but also on the energy. Therefore it seems more reliable, when long-range $NN^*(1440) \rightarrow NN^*(1440)$ potentials are taken into account, for example in NN phase shift analysis for Lab energies $T_N \sim 1000$ MeV ($N^*(1440)$ threshold), to consider altogether the effects of OPE plus OSE potentials.

For the short- and medium-distance part of the interaction, the modeling of simple baryonic potentials becomes much more difficult, since quark Pauli effects have non-trivial consequences on the form of the baryonic potential arising from a given form of the quark-quark interaction. This is reflected in phenomenological baryon treatments where quite different forms of repulsive cores are employed to parametrize the interaction. To this respect our results, though obtained in a simple approximation, can serve as a guide for a sensible choice of the parametrization.

5.3 Transition $NN \rightarrow NN^*(1440)$ potential

Graphs involving the excitation of $N^*(1440)$ appear in different systems, as for example the neutral pion production in proton-proton reactions [117] or the three nucleon interaction mediated by π and σ exchange contributing to the triton binding energy [114]. The excitation of the $N^*(1440)$ resonance has also been advocated to explain the missing energy spectra at small angles in the $\alpha + p \rightarrow \alpha + X$ reaction [36], and the coupling of the $N^*(1440)$ to the πN and σN channels could also be important in heavy ion collisions at relativistic energies [118]. Therefore it appears of great interest to evaluate the $NN \rightarrow NN^*(1440)$ transition potential and the $\pi NN^*(1440)$ and $\sigma NN^*(1440)$ coupling strengths. This has been recognized for a long time motivating the proposal of transition potentials written as simple generalizations of some pieces of the $NN \rightarrow NN$ potential and incorporating resonance width effects [116, 119, 120]. Nonetheless this procedure may have serious shortcomings specially concerning the short-range part of the interaction due to the important role played by the Pauli principle at the quark level, as has been shown for

the $NN \to N\Delta$ [121] and $N\Delta \to N\Delta$ [122] cases in previous analyses carried out within a quark model framework, that has been also used for the study of $NN \to NN$ [14, 85], $\Delta\Delta \to \Delta\Delta$ [71], and $NN^*(1440) \to NN^*(1440)$ potentials in previous section.

In this Section we shall adopt the same quark model approach and center our attention in the derivation of a $NN \to NN^*(1440)$ transition potential from a quark-quark (qq) basic interaction incorporating gluon, pion and sigma exchanges. For the sake of simplicity we follow a BO method with harmonic oscillator baryon wave functions written in terms of quarks. The $N^*(1440)$ is considered as a stable particle.

5.3.1 Calculation of the $NN \to NN^*$ potential

Forbidden channels play a relevant role in the $NN^*(1440) \to NN^*(1440)$ case as we saw previously in Sect. 5.2.1. However for the $NN \to NN^*(1440)$ transition we are considering here, the situation simplifies considerably. In fact, as the strong interaction preserves isospin, $T_{NN^*} = T_{NN}$, and the structure of the interaction given by Eq. (2.12) allows only to connect NN and $NN^*(1440)$ channels verifying $L' - L = 0$ or $2 = S' - S$, hence the initial state selection rule translates to the final state, i. e. only $f =$ even $NN^*(1440)$ channels are allowed.
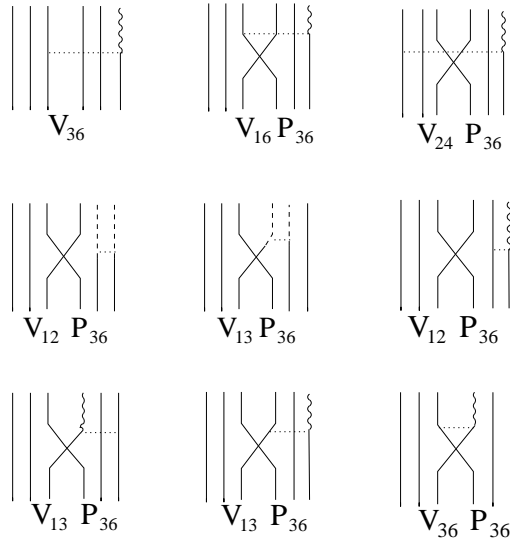
Figure 5.12: Different diagrams contributing to the $NN \to NN^*(1440)$ interaction. The wavy line denotes an excited quark on the $1s$ shell and the dashed line stands for an excited quark on the $0p$ shell. We have labeled the diagrams attending to their topological equivalence, although they involve interactions between excited or non-excited quarks. This simplified notation will be used in the next figures to separate the different contributions to the interaction.

The most important diagrams contributing to the $NN \to NN^*(1440)$ potential, as calculated from Eq. (3.28) are drawn in Fig. 5.12. We distinguish between the direct diagrams (labeled as V_{36} in Fig. 5.12), not involving quark exchanges, and the rest of diagrams including exchange of quarks (labeled as $V_{ij}P_{36}$ in Fig. 5.12). Most part of the diagrams contributing to the interaction are due to the first term of the $N^*(1440)$ wave function ($|[3](0s)^2(1s)\rangle$), only a few of them, those with two vertical dashed lines, correspond to the second term of the $N^*(1440)$ wave function ($|[3](0s)(0p)^2\rangle$). The spin-isospin matrix elements necessary to evaluate the different contributions of each diagram are taken from the $NN \to NN$ case.

5.3.2 Analysis of the transition potential

In Figs. 5.13, 5.14, and 5.15, we show the potentials obtained for $L = 0$: $^1S_0$, $^3S_1$; $L = 1$: $^1P_1$, $^3P_0$, and $L = 2$: $^1D_2$, $^3D_1$ partial waves. Contributions from the different terms of the potential as separated in Eq. (2.12) have been made explicit. For some selected partial waves, we separate in Fig. 5.16 the contribution of the different diagrams depicted in Fig. 5.12. As in the case of the direct $NN^*(1440) \to NN^*(1440)$ there are a number of general features that we detail:

(i) The very long-range part of the interaction ($R > 4$ fm) comes dominated, as for $NN \to NN$ and $NN^*(1440) \to NN^*(1440)$, by the one-pion exchange, the longest-range piece of the potential. However the asymptotic potential reverses sign respect to both $NN \to NN$ and $NN^*(1440) \to NN^*(1440)$. Thus for S and D waves the $NN \to NN^*(1440)$ interaction is asymptotically repulsive. This sign reversal is a direct consequence of the presence of a node in the $N^*(1440)$ wave function what implies a change of sign with respect to the N wave function at long distances (for $NN^*(1440) \to NN^*(1440)$ there are two compensating changes of sign coming from the two $N^*(1440)$'s). This is also corroborated by the study of the one-sigma exchange interaction that it is always asymptotically repulsive at difference with the $NN \to NN$ and $NN^*(1440) \to NN^*(1440)$ cases. The reversal of the sign represents a clear signal of the relevance of quark substructure of baryons and it contradicts the usual procedure of obtaining NN^* potentials by a simple scaling of the coupling constants of the NN potential.

It is worth to remark that no quark-antisymmetrization effects survive either in the numerator or in the denominator (norm) of Eq. (3.28) at these distances. In other words, the potential corresponds to a direct baryon-baryon interaction.

(ii) For the long-range $2 < R < 4$ fm part, the one-pion and one-sigma exchange potentials altogether determine the character of the interaction, since the one-gluon exchange gives a negligible contribution for $R \geq 2$ fm. One should also notice that although quark-exchange diagrams are not dominant for $R \geq 2$ fm, some quark antisymmetrization effects may still be present through the norm (see Fig. 5.1).

(iii) At the intermediate range $0.6 < R < 2$ fm a complex interplay among all pieces of the potential (gluon, pion and sigma) generates the final form of the interaction. When decreasing R from 2 fm to 0.6 fm two effects take place: on the one hand, quark exchange diagrams are increasingly important becoming dominant below $R = 1.5$ fm, on the other
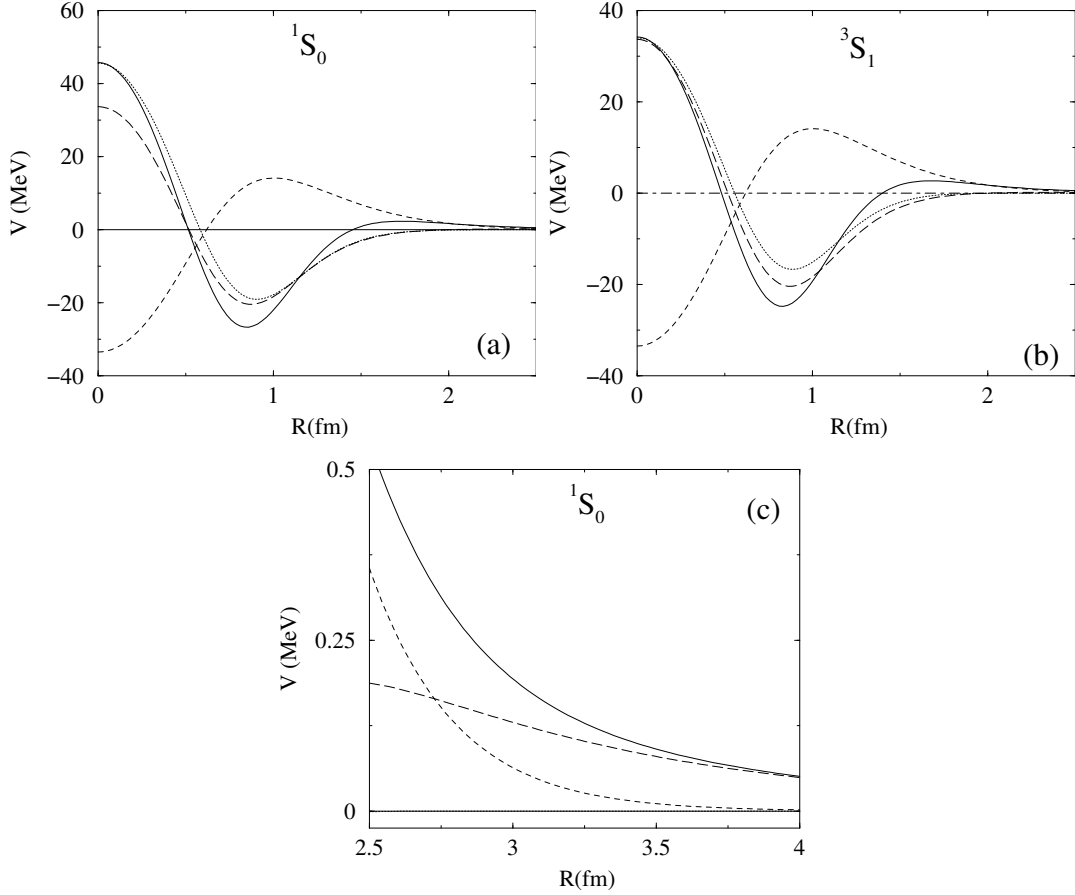
Figure 5.13: $NN \rightarrow NN^*(1440)$ potential for (a) the $^1S_0$ partial wave, (b) the $^3S_1$ partial wave, and (c) the long-range part of the $^1S_0$ partial wave. We have denoted by the long-dashed, dashed, dotted, and dot-dashed lines, the central OPE, OSE, OGE, and the tensor contributions, respectively. By the solid line we plot the total potential.

hand the different pieces of the potential are changing sign: from attractive to repulsive for the gluon in all partial waves, from repulsion to attraction for the sigma in S and D waves and from repulsion to attraction and again to repulsion for the pion in S and D waves. As a combined result of these effects the total potential turns out to be attractive from $R = 1.5$ fm down to a lower value of R different for each partial wave. This behavior, related again to the node in the $N^*(1440)$ wave function, contrasts with the $NN \rightarrow NN$ and $NN^*(1440) \rightarrow NN^*(1440)$ cases, where for instance for S and D waves the scalar (sigma) part keeps always the same sign and gives the dominant contribution for $R > 0.8$ fm.

(iv) The choice of 0.6 fm as a lower limit for the intermediate range comes motivated
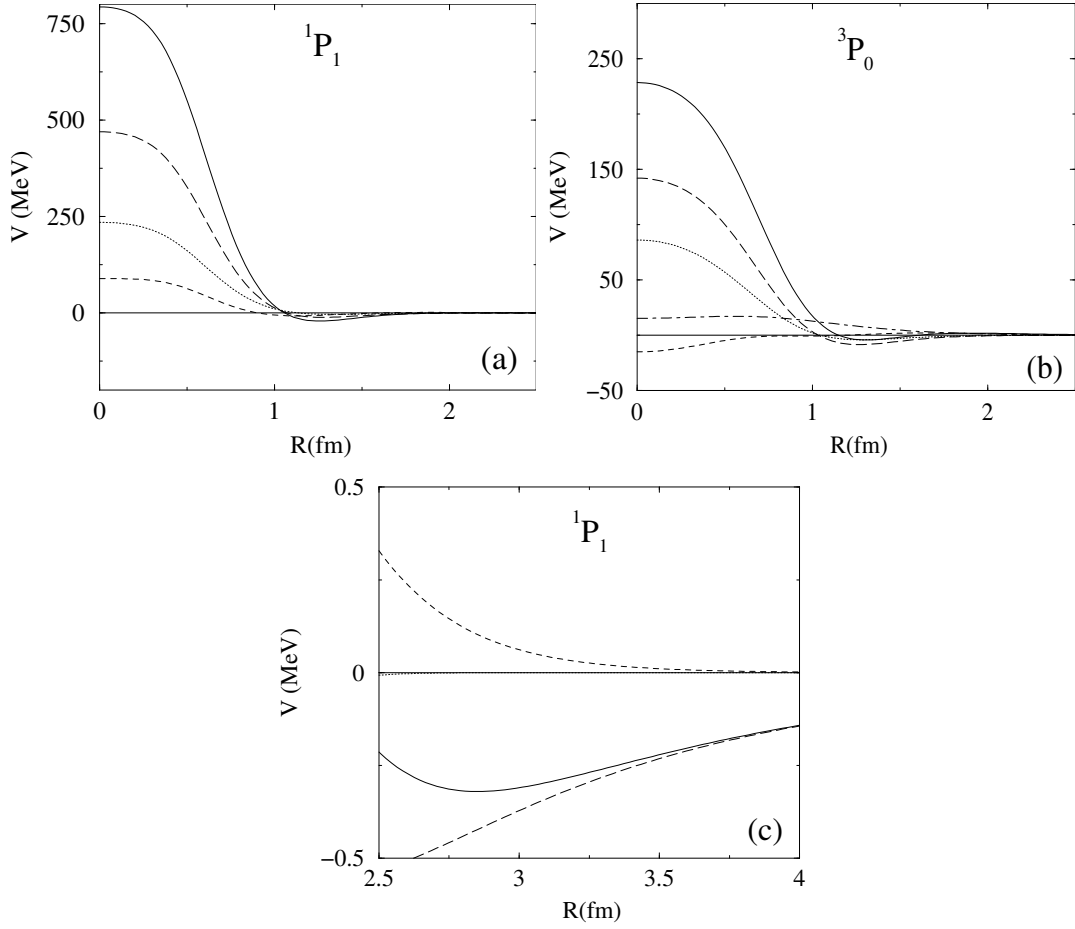
Figure 5.14: Same as Fig. 5.13 but for (a) the $^1P_1$ partial wave, (b) the $^3P_0$ partial wave, and (c) the long-range part of the $^1P_1$ partial wave.

by the repulsive character of the potential in all partial waves for shorter distances. The one-gluon and one-pion quark exchange parts are mainly responsible for such a repulsion as it turns out to be the case for $NN \to NN$ and $NN^*(1440) \to NN^*(1440)$. Nevertheless there are two distinctive features with respect to these cases: in $NN \to NN^*(1440)$ the intensity of the repulsion at $R = 0$ and the value of R at which the interaction becomes repulsive are significantly lower than in $NN \to NN$ and $NN^*(1440) \to NN^*(1440)$. This is a clear effect of the more similarity (higher overlap) in these cases between initial and final states.
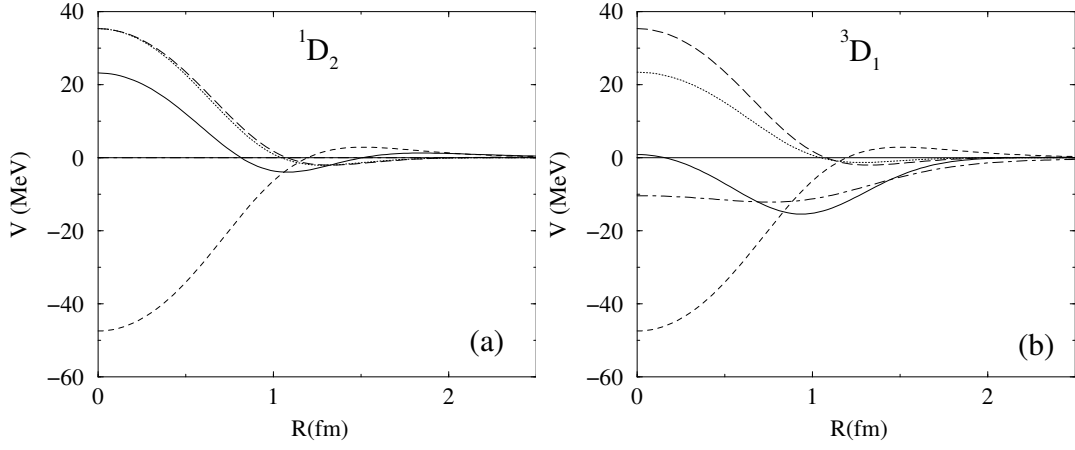
Figure 5.15: Same as Fig. 5.13 but for (a) the $^1D_2$ partial wave and (b) the $^3D_1$ partial wave.
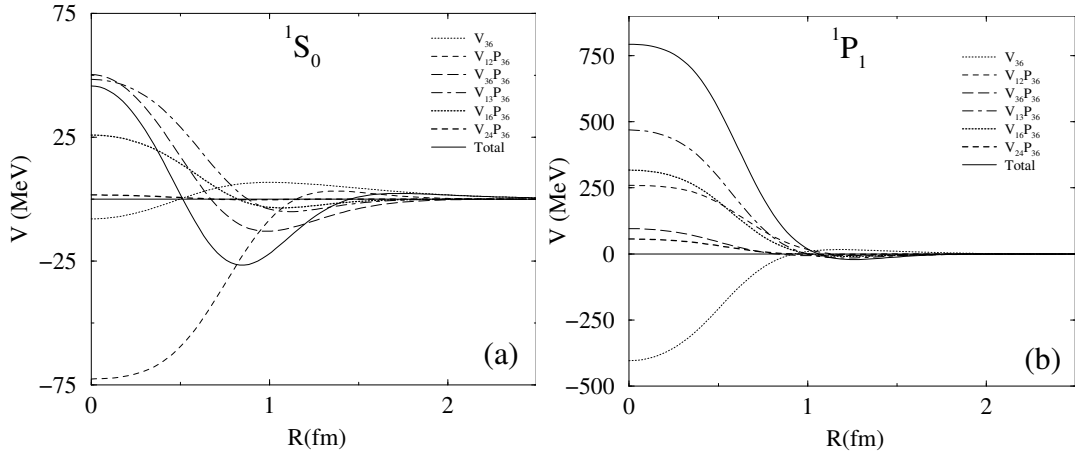
Figure 5.16: $NN \rightarrow NN^*(1440)$ potential for (a) the $^1S_0$ partial wave and (b) the $^1P_1$ partial wave. We have made explicit the contribution of the different diagrams shown in Fig. 5.12, with the convention explained in the caption.

6 APPLICATIONS OF BARYONIC POTENTIALS

In this chapter we present three applications of the calculated baryonic potentials. First in Sect. 6.1 we study the presence of non-nucleonic components in the deuteron. Then in Sect. 6.2 we describe the way baryonic coupling constants between nucleons, resonances and the Goldstone modes of the model can be extracted from the transition potential. Finally in Sect. 6.3 we explore the mechanism of *Roper excitation in the target* proposed in Ref. [37] making use of the $NN \to NN^*(1440)$ transition potential derived in Chapter 5.

Each of the aforementioned sections is briefly introduced.

6.1 N^* and Δ components on the deuteron

Since the discovery of nucleon structure, nucleon resonances have attracted considerable attention from theorists and experimentalists. An important effort was made to choose and design experiments that could probe the presence of resonance configurations in different nuclear systems. The basic idea lies in the observation that a small fraction of the nucleons will be internally excited and therefore present as virtual resonances in every nucleus. This may happen even at low energies due to the possibility of exciting internal nucleon degrees of freedom according to the process $NN \to NN^*$ or $NN \to N^*N^*$ involving intermediate N^*'s. As a consequence, the many nucleon wave function should be supplemented by configurations involving one or several nucleons in an excited baryon resonance state.

If the virtual N^*'s exist in bound nuclear states, one expects them to play an important role already in the bound two-nucleon system, the deuteron [123]. The most prominent low-lying even-parity nucleon resonances are the P_{33}, the $\Delta(1232)$, and the P_{11}, the $N^*(1440)$ resonance.

The N^*'s contribute predominantly to the nucleon short-range correlations and enhance the high momentum components of the nuclear two-particle density. Being the deuteron isoscalar, the energetically lowest state $N\Delta$ is forbidden, and therefore the $\Delta\Delta$ and $NN^*(1440)$ components would be the relevant non-nucleonic configurations. The admixture probabilities of these *exotic* states are small due to the low nuclear density and the rather high resonance-nucleon mass difference. Nonetheless, they have been advocated long ago to understand elastic proton-deuteron backward scattering at energies above pion threshold [124] or the angular distribution of deuteron photo-disintegration at energies above $E_\gamma = 100$ MeV [125]. Recent calculations have renewed the interest on these non-nucleonic components as they could be indirectly observed in several reactions as for

example antiproton-deuteron annihilation [126], subthreshold antiproton production [127] or $pd \rightarrow dp$ processes [128, 129]. Although the evidence for resonance configurations in the deuteron from such processes is indirect, is suggestive and encouraging.

The treatment of nucleon resonances in the nuclear wave function can be done in several ways. One possibility has consisted in keeping only nucleons (and no resonances) in the nuclear wave function and using effective operators. However, it would be surprising if such an *ad hoc* procedure would phenomenologically account for any detailed internal dynamics, because in the hard-core region two nucleons are likely to excite each other and thus mutually probe their internal degrees of freedom. If one wants to turn the attention to the virtual contribution from these nucleon excited states, one has to include explicitly N^* transition potentials in a coupled channel calculation.

When performing a coupled channel calculation for the deuteron based on effective baryon-baryon potentials, a problem immediately arises. If one uses for the nucleon-nucleon (NN) channel an effective potential which is fitted to the NN scattering data, it will already include contributions from intermediate N^*'s, and thus one would obtain too much attraction at medium range. Therefore one has to modify the normal nucleon-nucleon potential and weaken the intermediate range attraction in order to account for the additional attraction from the explicit dispersion contribution to the potential with intermediate N^*'s. Such a procedure usually introduces an unwanted model dependence on the results obtained.

There are multiple examples in the literature of these type of calculations. Haapakoski and Saarela [130] studied $\Delta\Delta$ components on the deuteron changing in an *ad hoc* manner the intermediate range attraction of the central Reid soft-core potential until the deuteron binding energy was fit to the experimental value. The tensor force was not changed. Arenhovel et al. [131] studied $NN^*(1440)$ configurations using perturbation theory with the one-pion-exchange potential and Hulthén NN deuteron wave functions. The singular nature of the potentials required a cutoff factor and the results were found to be rather sensitive to the cutoff chosen. Weber [132] and Nath and Weber [133] calculated NN^* components by means of an OPE potential in momentum space. The resulting probabilities were again found to be rather dependent on the high momentum suppression factor. Finally, Rost [134] performed a calculation where the existence of resonance components is taken into account by a modification of the intermediate attraction of the Reid hard-core potential. As a consequence, the study of non-nucleonic configurations in the deuteron based on standard meson-exchange NN potentials depends on two basic assumptions: on one hand, the hypothesis done to modify the intermediate range attraction of the NN interaction, on the other hand, the specific transition potential to the resonance configurations used.

The two-baryon problem based on quark-quark interactions is solved by means of the RGM in a coupled-channel scheme considering usually NN, $\Delta\Delta$ and hidden color-hidden color components. The importance of particular configurations, like $N\Delta$, to describe the low orbital angular momentum partial waves has been recently demonstrated [121]. Such calculations present the great advantage that any baryon-baryon interaction can be determined, once the NN potential has been fixed, in a completely parameter-free way. There-

fore, the quark-model framework provides an adequate scheme to study non-nucleonic configurations on the deuteron without the aforementioned uncertainties appearing in meson-exchange models.

In this section we want to focus on the influence of the most important non-nucleonic channels on the deuteron properties. In order to have a consistent calculation we will make use of baryonic potentials constructed as explained in Chapter 3. This implies that no parameters are fitted independently for the different channels. The quark-model parameters have been previously determined to describe the deuteron binding energy and S-wave NN phase shifts with enough accuracy so that conclusions on the role played by the different channels, and thus, by the $N^*(1440)$ resonance or Δ can be inferred.

Within the quark model framework, this problem has already been partially undertaken using different approximations. The possible effects of a bigger Hilbert space were considered in Ref. [90] through the formation of six-quark bags at short-distances. Kusainov et al. [135] proposed an alternative formulation in terms of quark-shell configurations, later on projected onto physical channels. Glozman and Kuchina [136] proposed an indirect calculation where the non-nucleonic configurations were not explicitly considered for the calculation of the two-body system. As a consequence, these methods rely again on several hypothesis that could hide physical conclusions. In Ref. [137] the influence of N and Δ resonances on the NN interaction has been studied. The most significant contribution was obtained from channels involving N and Δ ground states, although a quantitative calculation of the non-nucleonic configurations was not performed.

6.1.1 NN, $NN^*(1440)$, $N\Delta$, and $\Delta\Delta$ potentials

In this section we will make use of the baryon-baryon potentials which have already been derived. For the NN, $N\Delta$ and $\Delta\Delta$ pieces we consider the RGM derived ones [85], while for the $N^*(1440)$ pieces we consider the potential described in detail in Chapter 5. As already mentioned in Chapter 4 the NN potential yields a fairly good reproduction of the experimental data up to laboratory energies of 250 MeV. For a correct description of the $^1S_0$ phase shift it is necessary to take into account the coupling to the $^5D_0$ $N\Delta$ channel that provides an isospin-dependent mechanism generating the additional attraction in this channel.

6.1.2   Probability of $N^*(1440)$ and Δ configurations

We have calculated the deuteron binding energy and wave function making emphasis in a simultaneous description of the NN scattering phase shifts. For the bound state problem, Eq. (3.26) can be discretized in momentum space and written as

$$\sum_j (H_{ij} - E\delta_{ij})\Psi_j = 0 \,, \tag{6.1}$$

where we have used a simplified notation and the indices i and j run not only for all the discretization points but also for the channels included in the calculation. The non-trivial

solutions are given by the zeroes of the Fredholm determinant

$$|H_{ij} - E\delta_{ij}| = 0\,, \tag{6.2}$$

being the values of E that satisfy the previous equation the energy of the bound states. Once the energies have been found the wave function can be easily calculated solving the linear problem of Eq. (6.1).

We show in Table 6.1 the different configurations and partial waves included in our calculation. In Tables 6.2 and 6.3 we present the results obtained for the non-nucleonic probabilities and the static properties of the deuteron. In all cases the deuteron binding energy is correctly reproduced, being $E_d = -2.2246$ MeV. We have shown the results of a calculation including only NN components, including NN and $\Delta\Delta$ configurations and finally the full calculation including also $NN^*(1440)$ configurations. Among the allowed configurations, the $NN^*(1440)$ has not been usually included in the deuteron calculations due to the great uncertainty associated to the coupling constant and cutoff parameters [131, 134]. The first result we would like to emphasize is the fact that the probability of $NN^*(1440)$ channels are smaller than the $\Delta\Delta$ ones. They do not show much influence on the static properties of the deuteron as it seems to be case for the deuteron form factors [138]. However, these small components find support in the explanation given in the literature to some deuteron reactions [126, 127, 128, 129]. Subthreshold antiproton production in $d-p$ and $d-d$ reactions [127], $pd \rightarrow dp$ reactions [128, 129], or antiproton-deuteron annihilation at rest [126] are compatible with small percentage of $NN^*(1440)$ in the deuteron wave function.

B_1B_2	Partial waves	Mass difference (MeV)
NN	$^3S_1$ - $^3D_1$	0.0
$NN^*(1440)$	$^3S_1$ - $^3D_1$	501.0
$\Delta\Delta$	$^3S_1$ - $^3D_1$ - $^7D_1$ - $^7G_1$	586.0

Table 6.1: Channels and partial waves considered in our calculation.

The prediction we obtain for the $NN^*(1440)$ probabilities, a larger component of the $^3D_1(NN^*(1440))$ partial wave than the $^3S_1(NN^*(1440))$ partial wave, agrees with the ordering obtained by other calculations available in the literature [134, 137]. This can be understood if one takes into account that the tensor coupling, which is the main responsible for the presence of non-nucleonic components on the deuteron wave function, is much stronger for the $^3S_1(NN) \rightarrow {}^3D_1(NN^*(1440))$ transition than for the $^3D_1(NN) \rightarrow {}^3S_1(NN^*(1440))$ one, enhancing in this way the D-wave influence with respect to the S-wave component. Regarding the absolute value of the probabilities, our results are a factor ten smaller than those reported on Ref. [134], where an estimation of 0.17% for the $NN^*(1440)$ configuration was obtained (0.06% for the $^3S_1$ and 0.11 % for the $^3D_1$ partial wave). The dependence of this result on the hypothesis made and the deviation from the results we obtain could be understood in the following way. The

	NN		$NN^*(1440)$		$\Delta\Delta$			
	$^3S_1$	$^3D_1$	$^3S_1$	$^3D_1$	$^3S_1$	$^3D_1$	$^7D_1$	$^7G_1$
(A)	95.3780	4.6220	-	-	-	-	-	-
(B)	95.1989	4.5606	-	-	0.1064	0.0035	0.1243	0.0063
(C)	95.1885	4.5377	0.0022	0.0148	0.1224	0.0036	0.1245	0.0063

Table 6.2: Deuteron wave function (%).

	$r_m(\text{fm})$	$A_S(\text{fm}^{-1/2})$	η
(A)	1.976	0.8895	0.0251
(B)	1.985	0.8941	0.0250
(C)	1.985	0.8941	0.0250

Table 6.3: Deuteron properties.

deuteron is calculated using the Reid hard-core potential. When including $NN^*(1440)$ components, the channel coupling induces an attractive interaction on the NN system, that needs to be subtracted out. Such a subtraction was done by reducing the intermediate range attraction of the central part of the Reid hard-core potential without modifying the tensor part, as was done in Ref. [130] to calculate the probability of $\Delta\Delta$ components. As a consequence, in these type of calculations the strength of the tensor coupling to the $NN^*(1440)$ state can be enhanced by decreasing the intermediate range attraction in the NN channel. The balance between these two sources of attraction cannot be disentangled in a clearcut way. This is a similar problem to the one arising in the $^1S_0(NN)$ partial wave when the coupling to the $N\Delta$ system was included [139]. The same attractive effect could be obtained by a central potential or a tensor coupling to a state with higher mass, being necessary other observables to discriminate between the two processes [139]. This seems to be the reason of the much bigger probability for the $NN^*(1440)$ components in Ref. [134], that on the other hand showed a great dependence on the choice of the NN phenomenological potential. In Ref. [137], although the contribution of resonance configurations has been included to study the NN system, there are no numerical predictions to compare with.

There are other estimations in the literature. The results of Ref. [131] are only of qualitative interest. The pathological behavior of the transition potential to resonance states was regularized by a cutoff factor that made the potential too weak at small distances. In Ref. [136] they study the effective numbers for different resonance configurations on the deuteron making use of baryon wave functions obtained from the diagonalization of a quark-quark interaction containing gluon and pion exchange in a harmonic oscillator basis including up to $2\hbar\omega$ excitations, and deuteron wave functions obtained from the Paris potential or a different quark model approach. They obtain an upper limit of 1% for $\Delta\Delta$ components and 0.1% for $NN^*(1440)$ in agreement with the order of magnitude and ordering of our results.

6.2   Baryonic coupling constants

A main feature of our quark treatment is its universality in the sense that all the baryon-baryon interactions can be treated on the same foot. This allows a microscopic understanding and connection of the different baryon-baryon interactions that is beyond the scope of any analysis based only on distinguishable hadronic degrees of freedom. This is important not only in the short-range regime, where it does not exist a definite prescription when resonances are involved, but also at all distances. In particular, the asymptotic behavior of the derived potentials allows both, the prediction of the values of the πNR and σNR coupling constants, and the calculation of their ratios to the πNN and σNN coupling constants respectively, where R stands for any resonance. The values of these coupling constants are free parameters that need to be fixed by specific reactions when working at baryonic level. For example, the value of the $\sigma NN^*(1400)$ coupling constant is fitted indirectly in Ref. [36] using the $p\,(\alpha, \alpha')$ reaction [1]. In the next section, Sect. 6.3, we consider a similar reaction, $p(d,\ d')$, and explore to which extent we can understand the peak attributed to the $N^*(1440)$ with our quark-model derived potentials.

In Chapter 5 we have derived the $NN \rightarrow NN^*(1440)$ potential, now we exemplify how the $\pi NN^*(1440)$ and $\sigma NN^*(1440)$ coupling constants can be extracted.

6.2.1 $\pi NN^*(1440)$ and $\sigma NN^*(1440)$ coupling constants

The potential obtained can be written at all distances in terms of baryonic degrees of freedom [76]. One should realize that a quark-quark (qq) spin and isospin independent potential as the scalar one-sigma exchange, gives rise at the baryon level apart from a spin and isospin independent potential, to a spin-spin, a isospin-isospin and a spin-isospin dependent interaction [14]. Nevertheless for distances $R \geq 4$ fm, where quark antisymmetrization interbaryon effects vanish, we are left with the direct part of the one-sigma and one-pion exchange potentials whose functional forms are the same than for the corresponding qq potentials. From these baryonic functional forms we can extract the $\pi NN^*(1440)$ and $\sigma NN^*(1440)$ coupling constants. To get such a prediction we write the asymptotic baryonic transition potentials for the $^1S_0$ partial wave (such an analysis could be performed for any partial wave obtaining the same result). As the Λ depending exponential term is negligible asymptotically as compared to the Yukawa term, we write the asymptotic interaction as:

$$V^{OPE}_{NN\rightarrow NN^*(1440)}(R) = \frac{1}{3}\frac{g_{\pi NN}}{\sqrt{4\pi}}\frac{g_{\pi NN^*(1440)}}{\sqrt{4\pi}}\frac{m_\pi^2}{8M_N M_r}\frac{\Lambda^2}{\Lambda^2 - m_\pi^2}[(\vec{\sigma}_N.\vec{\sigma}_N)(\vec{\tau}_N.\vec{\tau}_N)]\frac{e^{-m_\pi R}}{R}\,,$$
(6.3)

and

$$V^{OSE}_{NN\rightarrow NN^*(1440)}(R) = -\frac{g_{\sigma NN}}{\sqrt{4\pi}}\frac{g_{\sigma NN^*(1440)}}{\sqrt{4\pi}}\frac{\Lambda^2}{\Lambda^2 - m_\sigma^2}\frac{e^{-m_\sigma R}}{R}\,,$$
(6.4)

---

[1]In Ref. [36] they first consider the contribution to the cross section of the process which comes from the Δ resonance, the remaining part is attributed to both an interference term and the $N^*(1400)$ excitation.

where g_i stands for the coupling constants and M_r is the reduced mass of the $NN^*(1440)$ system

$$\frac{1}{M_r} = \frac{1}{M_N} + \frac{1}{M_{N^*(1440)}} \ . \tag{6.5}$$

By comparing these baryonic potentials with the asymptotic behavior of the OPE and OSE previously obtained from the quark calculation we can extract the $\pi NN^*(1440)$ and $\sigma NN^*(1440)$ coupling constants. As the parameters at the quark level are fixed once for all from the NN interaction our results allow a prediction of these constants in terms of the elementary πqq coupling constant and the one-baryon model dependent structure. The sign obtained for the meson-$NN^*(1440)$ coupling constants and for their ratios to the meson-NN coupling constants is ambiguous since it comes determined by the arbitrarily chosen relative sign between the N and $N^*(1440)$ wave functions. Only the ratios between the $\pi NN^*(1440)$ and $\sigma NN^*(1440)$ would be free of this uncertainty. This is why we will quote absolute values except for these cases where the sign is a clear prediction of the model. To get such a prediction we can use any partial wave. We shall use for simplicity the $^1S_0$ wave, this is why we only wrote the central interaction in Eq. (6.3).

The $[\Lambda^2/(\Lambda^2 - m_i^2)]$ vertex factor comes from the vertex form factor chosen at momentum space as a square root of monopole $[\Lambda^2/(\Lambda^2 + \vec{q}\,^2)]^{1/2}$, the same choice taken at the quark level, where chiral symmetry requires the same form for pion and sigma. A different choice for the form factor at the baryon level, regarding its functional form as well as the value of Λ, would give rise to a different vertex factor and eventually to a different functional form for the asymptotic behavior. For instance, for a modified monopole form, $[(\Lambda^2 - m^2)/(\Lambda^2 - \vec{q}\,^2)]^{1/2}$, where m is the meson mass (m_π or m_σ), the vertex factor would be 1, i.e. $[(\Lambda^2 - m^2)/(\Lambda^2 - m^2)]$, keeping the potential the same exponentially decreasing asymptotic form. Then it is clear that the extraction from any model of the meson-baryon-baryon coupling constants depends on this choice. We shall say they depend on the coupling scheme.

For the one-pion exchange and for our value of $\Lambda = 4.2$ fm^{-1}, $[\Lambda^2/(\Lambda^2 - m_\pi^2)] = 1.03$, pretty close to 1. As a consequence, in this case the use of our form factor or the modified monopole form at baryonic level makes little difference in the determination of the coupling constant. This fact is used when fixing $g_{\pi qq}^2/4\pi$ from the experimental value of $g_{\pi NN}^2/4\pi$ extracted from NN data. The value we use for

$$\alpha_{ch} = \frac{m_\pi^2}{4m_q^2}\frac{g_{\pi qq}^2}{4\pi} = \left(\frac{3}{5}\right)^2 \frac{g_{\pi NN}^2}{4\pi}\frac{m_\pi^2}{4m_N^2}e^{-\frac{m_\pi^2 b^2}{2}} = 0.027 \tag{6.6}$$

corresponds to

$$g_{\pi NN}^2/4\pi = 14.83\,. \tag{6.7}$$

To get $g_{\pi NN^*(1440)}/\sqrt{4\pi}$ we turn to our results for the $^1S_0$ OPE potential, Figs. 5.13 and 6.1, and fit its asymptotic behavior (in the range $R : 5 \rightarrow 9$ fm) to Eq. (6.3). We obtain

$$\frac{g_{\pi NN}}{\sqrt{4\pi}}\frac{g_{\pi NN^*(1440)}}{\sqrt{4\pi}}\frac{\Lambda^2}{\Lambda^2 - m_\pi^2} = -3.73\,, \tag{6.8}$$
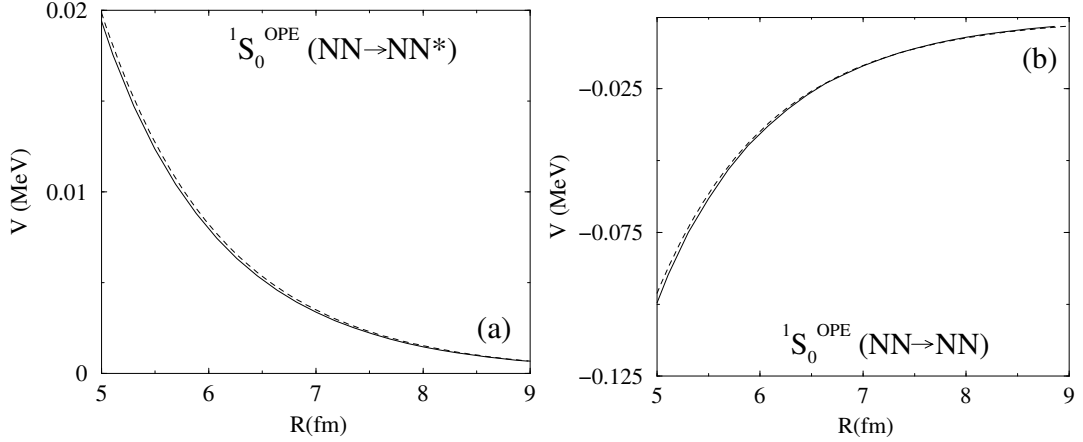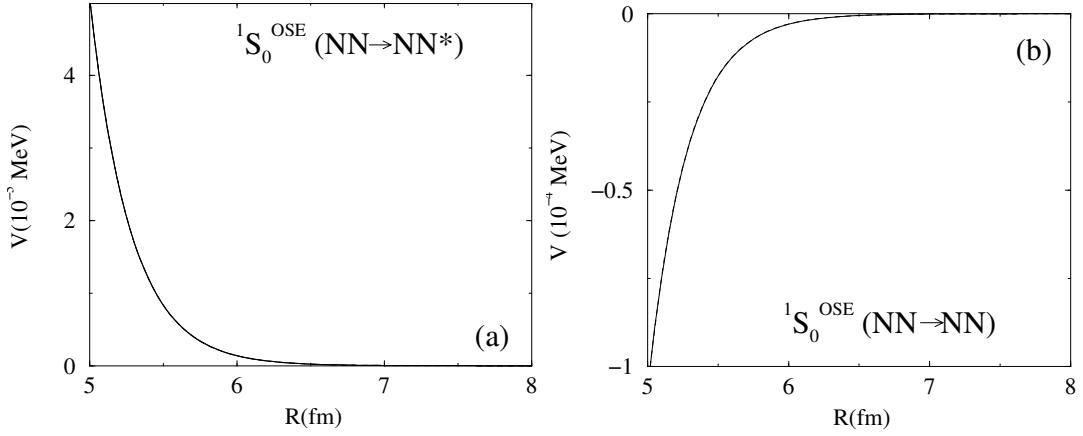
Figure 6.1: (a) Asymptotic behavior of the one-pion exchange $^1S_0$ $NN \rightarrow NN^*(1440)$ potential (solid line). The dashed line denotes the fitted curve according to Eq. (6.3). (b) Same as (a) but for the one-pion exchange $^1S_0$ $NN \rightarrow NN$ potential.

i.e. $g_{\pi NN^*(1440)}/\sqrt{4\pi} = -0.94$. As explained above only the absolute value of this coupling constant is well defined. Let us note that in Ref. [140] a different sign with respect to our coupling constant is obtained what is a direct consequence of the different global sign chosen for the $N^*(1440)$ wave function. The coupling scheme dependence can be explicitly eliminated if we compare $g_{\pi NN^*(1440)}$ with $g_{\pi NN}$ extracted from the $NN \rightarrow NN$ potential within the same quark model approximation, Fig. 6.1. Thus we get

$$\left| \frac{g_{\pi NN^*(1440)}}{g_{\pi NN}} \right| = 0.25 \,. \tag{6.9}$$

By proceeding in the same way for the OSE potential, i.e. by fitting the potential given in Fig. 6.2 (a) to Eq. (6.4), and following an analogous procedure for the NN case, Fig 6.2 (b), we can write

$$\left| \frac{g_{\sigma NN^*(1440)}}{g_{\sigma NN}} \right| = 0.47 \,. \tag{6.10}$$

The relative phase chosen for the $N^*(1440)$ wave function with respect to the N wave function is not experimentally relevant in any two step process comprising $N^*(1440)$ production and its subsequent decay. However it will play a relevant role in those reactions where the same field (π or σ) couples simultaneously to both systems, NN and $NN^*(1440)$. In these cases the interference term between both diagrams would determine the magnitude of the cross section [36].

The ratio given in Eq. (6.9) is similar to that obtained in Ref. [140] and a factor 1.5 smaller than the one obtained from the analysis of the partial decay width [140]. Nonetheless one can find in the literature values for $f_{\pi NN^*(1440)}$ ranging between $0.27 - 0.47$ coming

Figure 6.2: (a) Asymptotic behavior of the one-sigma exchange $^1S_0$ $NN \rightarrow NN^*(1440)$ potential (solid line). The dashed line denotes the fitted curve according to Eq. (6.4). (b) Same as (a) but for the one-sigma exchange $^1S_0$ $NN \rightarrow NN$ potential.

from different experimental analyses with uncertainties associated to the fitting of parameters [38, 115, 141].

Regarding the ratio obtained in Eq. (6.10), our result agrees quite well with the only experimental available result, obtained in Ref. [36] from the fit of the cross section of the isoscalar Roper excitation in $p(\alpha, \alpha')$ in the $10-15$ GeV region, where a value of 0.48 is given. Furthermore, we can give a very definitive prediction of the magnitude and sign of the ratio of the two ratios,

$$\frac{g_{\pi NN^*(1440)}}{g_{\pi NN}} = 0.53 \, \frac{g_{\sigma NN^*(1440)}}{g_{\sigma NN}} \, , \tag{6.11}$$

which is an exportable prediction of our model.

For the sake of completeness we give the values of $g_{\sigma NN^*(1440)}$ and $g_{\sigma NN}$, though one should realize that the corresponding form factor $\Lambda^2/(\Lambda^2 - m_\sigma^2) = 2.97$ differs quite much from 1. Moreover, the quark model dependence is quite strong what can make nonsense any comparison to other values obtained in the literature within a different framework. We get

$$\frac{g_{\sigma NN}^2}{4\pi} \frac{\Lambda^2}{\Lambda^2 - m_\sigma^2} = 72.4 \, , \tag{6.12}$$

i.e. $g_{\sigma NN}^2/4\pi = 24.4$, and

$$\frac{g_{\sigma NN}}{\sqrt{4\pi}} \frac{g_{\sigma NN^*(1440)}}{\sqrt{4\pi}} \frac{\Lambda^2}{\Lambda^2 - m_\sigma^2} = 34.3 \, , \tag{6.13}$$

i.e. $g_{\sigma NN^*(1440)}^2/4\pi = 5.5$.

Concerning the absolute value of $g_{\sigma NN^*}$ some caveats are in order. Our value is scheme and quark-model dependent and should only be sensibly compared with a value obtained in the same framework. As a matter of fact, if we had extracted the quark model factor dependence from the coupling constant ($e^{m_\sigma^2 b^2/2}$) the result would have been $g^2_{\sigma NN^*(1440)}/4\pi$ =1.14 that compares quite well with the value given in Ref. [36], $g^2_{\sigma NN^*(1440)}/4\pi = 1.33$. With respect to the results given in Ref. [142] they are very sensitive to both the decay width of the sigma meson into two pions and the mass of the sigma as reflected in the large error bars given. Both quantities are highly undetermined in the Particle Data Book [43], the mass of the sigma being constrained between $400-1200$ MeV and the width between $600-1000$ MeV. These values have been fixed arbitrarily in Ref. [142] to m_σ =500 MeV and Γ_σ =250 MeV. Varying the mass of the sigma between 400 and 700 MeV for a fixed width of 250 MeV, the coupling constant according to Eq. (9) of Ref. [142] varies between $0.18-2.54$. Taking a width of 450 MeV the resulting coupling is $0.27-1.64$. In both cases, our value lies in the interval given above what makes it compatible with the $N^*(1440)$ decay and production phenomenology.

Let us finally mention that at short distances, the interaction could be fitted in terms of two different Yukawa functions, one depending on the meson mass, m, the other with a shorter range depending on $\sqrt{(M_{N(1440)} - M_N + m)m}$. These two Yukawa functions could be associated to the two diagrams with different intermediate states (mNN and $mNN^*(1440)$) appearing in time ordered perturbation theory when an effective calculation at the baryonic level is carried out (let us realize that in a quark calculation the intermediate state is always mqq, the $N - N^*(1440)$ mass difference being taken into account through the N and $N^*(1440)$ wave functions).

6.3   Roper excitation in *pd* scattering

As already stated, the role played by N^*'s and Δ's in several nuclear reactions has been the object of many discussions during the last years. Among them there are two experiments where the contribution from the $N^*(1440)$ resonance was *isolated* by means of model-dependent theoretical methods. The first one is the $p(\alpha, \alpha')$ reaction carried out in Saclay [143] already ten years ago. The data showed two peaks in the cross section that were not understood for some years. The most prominent one was attributed to a *Delta excitation in the projectile* (DEP) [144]. The second peak was explained when a *Roper excitation in the target* (RET) [36] was considered [2] giving a plausible explanation to the measured differential cross section. These two mechanisms were investigated from a phenomenological point of view making use of effective lagrangians.

The second experiment is the $p(d, d')$ reaction. It was considered and studied making use of the same mechanisms [37]. In Fig. 6.3 we show the two diagrams which give the bulk contribution to the cross section of the processes. These two reactions are particularly
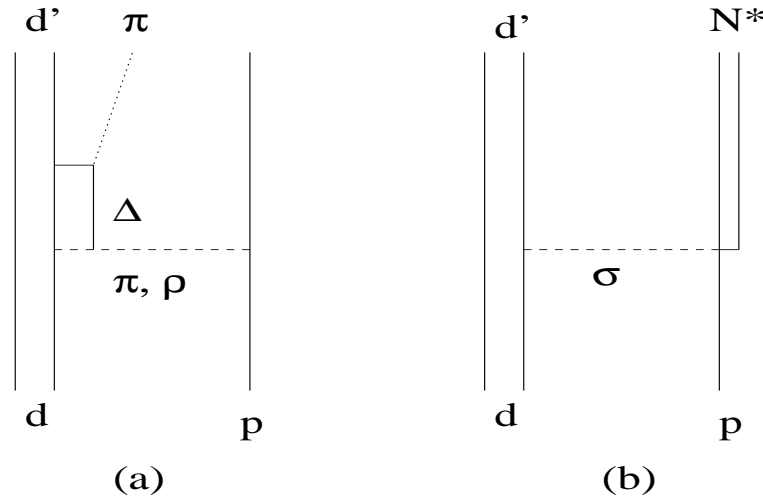
Figure 6.3: Mechanisms considered by Hirenzaki et al. [37].

interesting because in both cases the projectile (d or α) has $T = 0$. This ensures that the $N^*(1440)$ reaction mechanism, (Fig. 6.3 (b)), can only be driven by a scalar interaction, σ. Therefore these reactions could provide a method to determine the baryonic coupling constant between the N, $N^*(1440)$ and the σ meson if the interference term between the two mechanisms is proved to be small, as has been the case for $p(d, d')$, and the Δ contribution has been fixed.

We have devoted Chapter 5 to the derivation and study of the transition and direct potentials involving NN and $NN^*(1440)$ systems. These potentials are obtained in a

---

[2]Other mechanisms were also explored and found to be much weaker than these ones.

parameter-free way once the quark Hamiltonian was fixed in previous works. Our purpose in this section is to study the $p(d, d')$ process making use of our transition potential, $V_{NN \to NN^*(1440)}$, to explore the mechanism proposed in Ref. [37].

In Sect. 6.3.1 we explain in detail the calculation of the cross section for the RET and then proceed to its evaluation with our quark-model derived potential in Sect. 6.3.2. In Sect. 6.3.3 we analyze the results obtained comparing to the ones reported in Ref. [37].

6.3.1 Target Roper excitation

The experimental data were measured for an incident energy of the deuteron $E_d = 2.3$ GeV (in the frame where the proton is at rest (L)) and for a laboratory angle between the initial and final deuterons $\theta_L = 1.1$ deg. For a detailed description of the experimental setup see Ref. [37]. Our purpose is to concentrate on the $N^*(1440)$ excitation mechanism (RET), Fig. 6.3 (b). This mechanism together with the DEP allows for an understanding of the experimental data. The interference term between the two mechanisms is proven to be small.

We detail the evaluation of the cross section for the $N^*(1440)$ process. The differential cross section for the process is given by:

$$\frac{d^2\sigma}{dE_{d'}d\Omega_{d'}^L} = \frac{p_{d'}}{(2\pi)^5} \frac{M_d^2 M^2}{\lambda^{1/2}(s, M^2, M_d^2)} \int \frac{d^3 p_\pi}{E_{N'}\omega_\pi} \bar{\Sigma}\Sigma|T|^2 \delta(E_d + E_N - E_{d'} - E_{N'} - \omega_\pi), \quad (6.14)$$

with $\lambda(x, y, z) = x^2 + y^2 + z^2 - 2xy - 2yz - 2xz$ and $\bar{\Sigma}\Sigma|T|^2$ is the amplitude for the elementary process of $N^*(1440)$ production. We evaluate the cross section in the center of mass system and then relate the result to the one which is shown by the experimentalists making use of:

$$\frac{d^2\sigma}{dE_{d'}d\Omega_{d'}^L} = \frac{d^2\sigma}{dE_{d'}d\Omega_{d'}^{cm}} \frac{d\Omega_{d'}^{cm}}{d\Omega_{d'}^L} . \quad (6.15)$$

For the kinematics considered it can be shown that,

$$\frac{d\Omega_{d'}^{cm}}{d\Omega_{d'}^L} = \frac{p_d^L p_{d'}^L}{p_d^{cm} p_{d'}^{cm}} \left(1 - \frac{E_d^{cm}}{\sqrt{s}}\right) + \frac{\cos(\theta^{cm})}{p_{d'}^{cm\,2}} \frac{E_{d'}^{cm}}{\sqrt{s}} p_d^L p_{d'}^L . \quad (6.16)$$

Phenomenological baryonic result

We rederive the results of Ref. [37]. There they write down the amplitude in the following way,

$$\bar{\Sigma}\Sigma|T|^2 = 12F_d^2 \left(\frac{f'}{m_\pi}\right)^2 g_{\sigma NN}^2 g_{\sigma NN^*}^2 |G^*|^2 |D_\sigma F_\sigma^2|^2 q_{cm}^2 . \quad (6.17)$$

This expresses the fact that the net effect of the deuteron can, as usual, be factored out from the excitation of the $N^*(1440)$ through the process $N(N, N^*)N$. The deuteron form factor is defined as:

$$F_d(\vec{k}) = \int d\vec{r} \, \phi^*(\vec{r}) \, e^{i\frac{\vec{k}\cdot\vec{r}}{2}} \, \phi(\vec{r}) \quad (6.18)$$

M^* (MeV)	1440
$\Gamma^*(s = M^{*2})$ (MeV)	300
M (MeV)	939
M_d (MeV)	$2M - 2.2245$
$P_{\pi\pi}$	0.35
f'	0.472
$f_{\pi\Delta N^*}$	2.45

Table 6.4: Parameters used in the calculation of Ref. [37].

where $\phi(\vec{r})$ is the deuteron S-wave function, and the momentum $\vec{k} = \vec{p}_d - \vec{p}_{d'}$ is taken in the initial deuteron rest frame. The propagator of the $N^*(1440)$ is written:

$$G^*(s) = \frac{1}{\sqrt{s} - M^* + \frac{i}{2}\Gamma^*(s)} \, . \tag{6.19}$$

The width takes the form,

$$
\begin{aligned}
\Gamma^*(s) &= \Gamma^*(s = M^{*2})(1 - P_{\pi\pi})\frac{q_{cm}^3(s)}{q_{cm}^3(M^{*2})} \\
&+ \Gamma^*(s = M^{*2}) \, P_{\pi\pi}\Gamma_{\pi\pi}(s) \, ,
\end{aligned}
\tag{6.20}
$$

where s is the invariant mass of the πN system, $q_{cm}(s)$ is the pion momentum in the πN center of mass system and $P_{\pi\pi}$ is the $\pi\pi N$ branching ratio. The functional form of $\Gamma_{\pi\pi}(s)$ is [36]:

$$\Gamma_{\pi\pi}(s) = \frac{1}{3\pi^2}\left(\frac{f_{\pi\Delta N^*}}{m_\pi}\right)^2 \int dp_\pi \, \frac{p_\pi^4}{\omega_\pi}|G_\Delta(s_\Delta)|^2 \, \Gamma_\Delta(s_\Delta) \, , \tag{6.21}$$

G_Δ is the Δ propagator, and the process $N^* \to N\pi\pi$ is assumed to go through $N^* \to \Delta\pi \to N\pi\pi$. The values used for the calculation are listed in Table 6.4.

The scalar interaction appearing in Eq. (6.17), responsible for the $N^*(1440)$ excitation, has the following propagator and form factor:

$$
\begin{aligned}
D_\sigma(q) &= \frac{1}{(q^0)^2 - \vec{q}^{\,2} - m_\sigma^2} \\
F_\sigma(q) &= \left(\frac{\Lambda_\sigma^2 - m_\sigma^2}{\Lambda_\sigma^2 - q^2}\right)^2 \, ,
\end{aligned}
\tag{6.22}
$$

$m_\sigma = 550$ MeV and $\Lambda_\sigma = 1700$ MeV. Also $g_{\sigma NN}^2/4\pi = 5.69$ and $g_{\sigma NN^*}^2/4\pi = 1.33$. Both $N^*(1440)$ coupling constants, $f' = f_{\pi NN^*}$ and $g_{\sigma NN^*}$, are fitted in their original paper to get the best reproduction of the data. In Fig. 6.4 we show the results obtained as explained above which reproduce the results of Ref. [37].

The uncertainty in the experimental properties of the scalar exchanged meson [3], σ, may have some influence on the predicted contribution of the $N^*(1440)$ mechanism to

---

[3]The traditional σ meson appears as $f_0(600)$ in the last Particle Data Booklet [43]. Its mass is in the range [600 - 1200] MeV and its width $\Gamma = [400 - 1200]$ MeV.
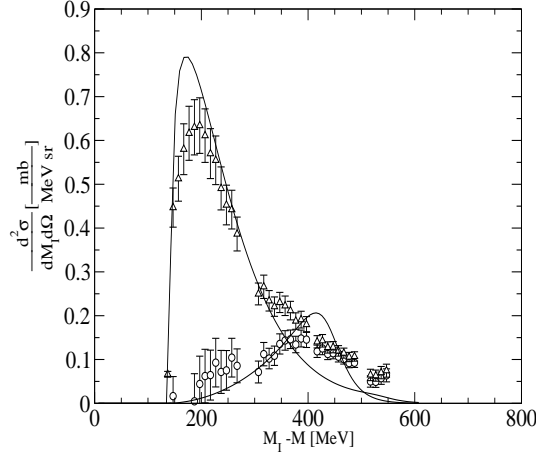
Figure 6.4: Results obtained for $T_d = 2.3$ GeV and $\theta^L = 1.1$ deg. Triangles are the experimental data, rhomboids correspond to the experimental data once the theoretical Δ contribution has been removed, both taken form Ref. [37].

the $p(d, d')$ process. To illustrate this point we depict in Fig. 6.5 the obtained $N^*(1440)$ contribution to the total cross section of the process depending on the mass of the σ meson and also on the cut-off chosen. As can be seen, the smaller the cut-off, the smaller the cross section, and the smaller m_σ the bigger the cross section. Let us also emphasize the use of a dipole form-factor, Eq. (6.22), what makes the potentials stronger at short distances [145].

6.3.2   Quark-model calculation

We have at our disposal the quark model derived $NN \rightarrow NN^*(1440)$ potential expanded in partial waves and depending on the distance between the baryons. In order to perform a similar calculation we will need to define our transition amplitude. In the baryonic case the transition potential is defined as,

$$V_{NN \rightarrow NN^*} = g_{\sigma NN} g_{\sigma NN^*} D_\sigma F_\sigma^2 \,. \tag{6.23}$$

In our case we need to extract the genuine scalar potential at all distances from our $NN \rightarrow NN^*(1440)$ transition potential. At short distances, $R < 2$ fm, the quark model based potential has a non-trivial structure. Due to the presence of the antisymmetrizer we have that, for instance, a scalar coupling at quark level gives rise to a scalar, spin-spin, pseudoscalar and pseudovector couplings [146]. The extraction of the scalar part can be done once the potential has been added up to have an unprojected potential:

$$V^{(S,T)}_{NN \rightarrow NN^*(1440)}(R) \,, \tag{6.24}$$
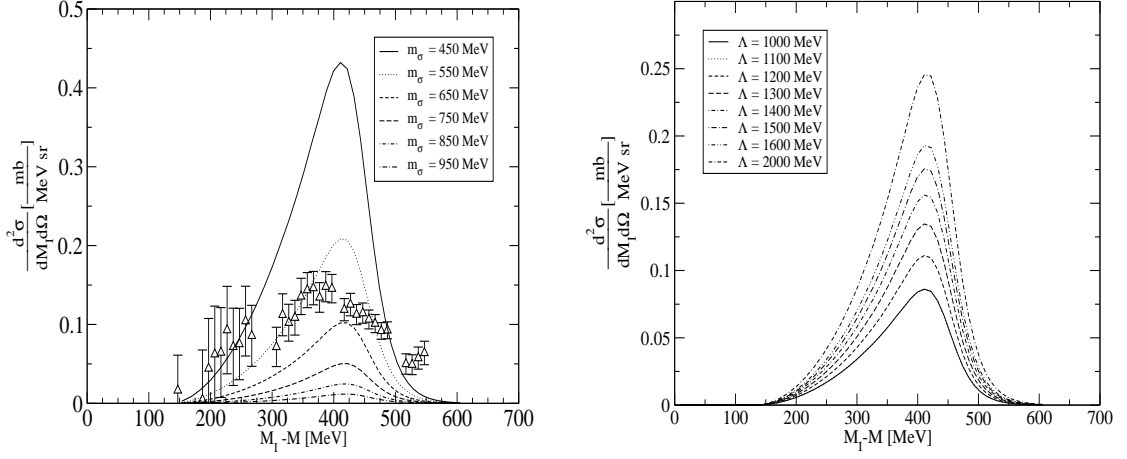
Figure 6.5: Results obtained for $T_d = 2.3$ GeV and $\theta^L = 1.1$ deg. Left: Dependence of the cross section on the mass of the σ. Right: Dependence of the cross section on the baryonic cut-off.

we can then write down the most general form for our interaction:

$$V_{NN \to NN^*}^{(S,T)} = V_0(R) + V_1(R)\, \vec{\sigma_1} \cdot \vec{\sigma_2} + V_2(R)\, \vec{\tau_1} \cdot \vec{\tau_2} + V_3(R)\, \vec{\sigma_1} \cdot \vec{\sigma_2}\, \vec{\tau_1} \cdot \vec{\tau_2}. \quad (6.25)$$

$V_i(R)$ are functions of the interbaryon distance R, $\vec{\sigma_i}$ and $\vec{\tau_i}$ are spin and isospin matrices of the baryons. $V_0(R)$ is the scalar part of the total potential which is the only part that can be included in our process of $N^*(1440)$ excitation in $p(d, d')$ reactions.

We obtain the following system of equations:

$$
\begin{aligned}
V_{NN \to NN^*}^{(0,0)}(R) &= V_0(R) - 3V_1(R) - 3V_2(R) + 9V_3(R) \\
V_{NN \to NN^*}^{(1,0)}(R) &= V_0(R) + V_1(R) - 3V_2(R) - 3V_3(R) \\
V_{NN \to NN^*}^{(0,1)}(R) &= V_0(R) - 3V_1(R) + V_2(R) - 3V_3(R) \\
V_{NN \to NN^*}^{(1,1)}(R) &= V_0(R) + V_1(R) + V_2(R) + V_3(R) \,,
\end{aligned}
\quad (6.26)
$$

and solve for the scalar part,

$$V_0(R) = \frac{1}{16}\left[V_{NN \to NN^*}^{(0,0)}(R) + 3V_{NN \to NN^*}^{(0,1)}(R) + 3V_{NN \to NN^*}^{(1,0)}(R) + 9V_{NN \to NN^*}^{(1,1)}(R) \right]. \quad (6.27)$$

The unprojected potential is obtained from the projected one calculated in Chapter 5 adding the partial-wave decomposed one in the following way [4],

$$V(\vec{q}; ST) = \frac{4\pi}{\mathcal{N}^{ST}} \sum_{JM_J}^{J_{MAX}} \sum_{LM_L} \sum_{M_S} C_{JM_J}^{LSM_LM_S} Y_{LM_L}(\hat{q}) \int_0^\infty r^2\, dr\, j_L(qr)\, \hat{V}^{L,S;JT}(r), \quad (6.28)$$

---

[4]We do not consider the tensor parts as they will not contribute to the scalar potential.
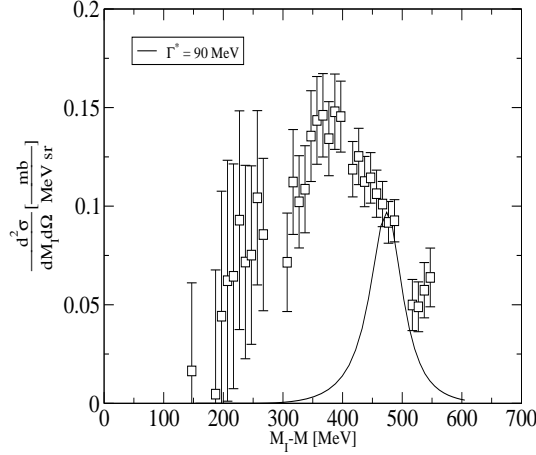
Figure 6.6: Result obtained with our quark model potential as explained in the text.

where we are adding up the partial waves up to a certain J_{MAX}. $\mathcal{N}^{ST}$ is the unprojected norm of the $NN^*(1440)$ system and $\hat{V}^{L,S;JT}$ is the potential defined in Chapter 5 multiplied by the norm of the corresponding partial wave.

6.3.3 Quark-model results

We have focused our attention on the target Roper excitation process as we are mainly interested in exploring the mechanism from the point of view of quark-model derived baryon-baryon potentials. The parameters of the Δ excitation on the projectile used in the phenomenological model were settled in the (α, α') reaction. We assume this process to be correctly described. Therefore we consider the data where the Δ contribution has already been subtracted (see Fig. 6.4) as our experimental data.

In Fig. 6.6 we show the result obtained using the quark-model derived $NN \to NN^*(1440)$ potential compared to the data. As can be seen, the predicted cross section is smaller that the model-dependent experimental data. If we choose a small value for the width of the $N^*(1440)$, the results come closer to the experimental data. Let us notice that the bigger disagreement with the extracted data corresponds to the region where the errorbars are larger, in other words, to the region where the uncertainties related to the theoretical method used to subtract the Δ contribution and interference term are important. For the sake of clarity, let us note that the subtraction of the Δ contribution is proportional to the square of the $\pi N\Delta$ coupling constant. This coupling constant is different as used in baryonic processes, $f^2_{\pi N\Delta}/4\pi = 0.35$, as the one used in our quark model, $f^2_{\pi N\Delta}/4\pi = 0.22$ [121]. This value is crucial when trying to reproduce the $^1S_0$ NN phase shift through the tensor coupling to the $^5D_0$ $N\Delta$. Using the baryonic coupling one would obtain much bigger attraction than observed experimentally. As a consequence, the bary-
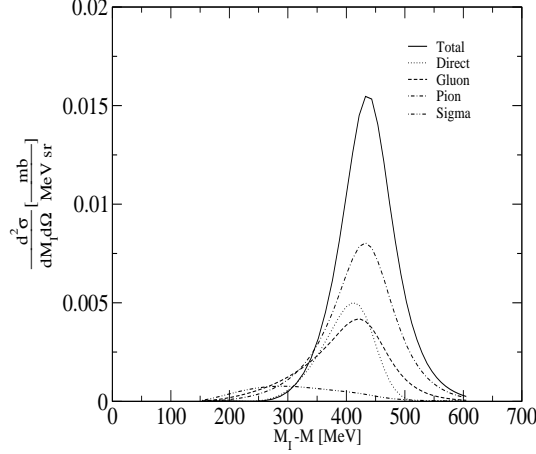
Figure 6.7: Detailed contributions to the cross section coming from the different interactions at the quark level, neglecting the interference terms.

onic calculation of the Δ contribution could be underestimating the region above the peak overestimating in this way the $N^*(1440)$ contribution. The way to wipe out those uncertainties would be to calculate the Δ contribution together with the interference term making use of quark-model baryonic potentials.

A second source of uncertainty on the baryonic result is its sensitivity to variations in the mass of the σ meson (that is quite uncertain according to the PDG [43]), see Fig. 6.5. This sensitivity would show up in a broad band for their predicted cross section attributed to the $N^*(1440)$ mechanism and also in the value of their scalar coupling constant.

In spite of our previous discussion we find a relevant result. In the previous section we found that the long-range part of our quark-model derived baryon-baryon interactions could be fitted with a Yukawa. This allowed us to extract the coupling constant between the Goldstone modes, N and $N^*(1440)$. In the process we are considering now the short-range part of the interaction plays an important role as can be inferred from the fact that there are the scalar contributions of the OPE and OGE the ones that give most of the cross section, see Fig. 6.7 (Left). As previously discussed, these scalar contributions arise due to the presence of the quark antisymmetrizer and are therefore related to the short-range structure. In fact, the relevance of the short-range is closely related to the strong dependence observed in the baryonic result on the cut-off chosen as seen in Fig. 6.5.

The results obtained with the quark-model derived interactions are qualitatively quite different to the ones reported using baryonic degrees of freedom. In fact, the baryonic form-factor could be hiding effects of the substructure that we find in our quark-model treatment through the contributions to the scalar channel from every term in the quark-quark Hamiltonian. If these results are confirmed by means of the full calculation within the quark model, this could open a new way to search for effects of the microscopic

structure.

7 NN SYSTEM ABOVE THE Δ REGION

Many different theoretical approaches have successfully described the NN interaction, phase shifts and deuteron properties, at energies below 300 MeV [14, 16, 17, 18, 49, 85, 147]. Above this energy the NN experimental data present several structures which are not well described within these theoretical models. This is due to the completely different problem we are facing when trying to describe the interaction above the thresholds for producing other particles, in this case the pion. In order to correctly treat the problem we need to incorporate to our theoretical framework the description of the produced particles, in the energy range considered this translates into the inclusion of πNN states.

One way of incorporating the effects of pion production and subsequent decay is through the explicit inclusion of nucleon-resonance channels in the model. The first two resonances which can be produced giving structure to the NN elastic data are the $\Delta(1232)$ and the $N^*(1440)$. There exist in the literature some works where the influence of these channels is explored in some detail using parametrizations of the potentials entering in the calculation.

The early works of Lomon [116] present a calculation of the NN interaction up to 900 MeV. Ref. [116] uses as NN potential the Feshbach-Lomon interaction [148], which gives similar results to the Paris potential [18] together with phenomenological transition potentials to the $N\Delta$, $NN^*(1440)$ and $\Delta\Delta$ systems. This model was improved later on by González and Lomon [112] with the inclusion of the widths of the resonances and some transitions omitted in the previous work. At the same time Lee [120] explored the NN interaction using a subtraction scheme to correctly remove the non-nucleonic components from the Paris potential together with phenomenological couplings to the $N\Delta$ and $NN^*(1440)$ channels [1]. These non-nucleonic components, that for instance in our quark-model derived potentials provide most of the attraction to the $^1S_0$ partial wave [121], need to be removed from potentials fitted to the phase shift data or some double counting effects would occur.

The use of phenomenological potentials for the transition pieces to the resonance channels introduces free parameters in the model. This is not the case when the NN system is studied together with baryon-baryon potentials obtained within a constituent quark model. Once the quark-model parameters are fixed, any baryon-baryon transition or direct potential can be obtained using the tools described in Chapter 3. Here we present the first calculation of the NN interaction where we include explicitly couplings to $N\Delta$

---

[1] Of special interest are also the works of the Hannover group, they developed a model to study the influence of pions and Δ's [149].

and $NN^*(1440)$ channels with all the potentials derived consistently. Previous works explored the influence of the coupling to Δ channels extending the energies up to 900 MeV [122, 150].

The formalism we employ is the *Coupled Channel Method*. We first explain the formalism in detail in Sect. 7.1. Then in Sect. 7.2 we show results for the phase shifts and inelasticities up to 2 GeV.

7.1   Coupled channel method

We consider a coupled-channel Lippmann-Schwinger formalism defined by the following set of integral equations[2]:

$$
\begin{aligned}
T_{NN} &= V_{NN} + V_{NN}G_N T_{NN} + V_{N\Delta}G_\Delta T_{\Delta N} + V_{NN^*}G_{N^*}T_{N^*N} \\
T_{\Delta N} &= V_{\Delta N} + V_{\Delta N}G_N T_{NN} + V_{\Delta\Delta}G_\Delta T_{\Delta N} + V_{\Delta N^*}G_{N^*}T_{N^*N} \\
T_{N^*N} &= V_{N^*N} + V_{N^*N}G_N T_{NN} + V_{N^*\Delta}G_\Delta T_{\Delta N} + V_{N^*N^*}G_{N^*}T_{N^*N} \,,
\end{aligned}
\tag{7.1}
$$

where each symbol, N, Δ and $N^*(1440)$ denotes a two-body channel according to:

$$
\begin{aligned}
N &\equiv NN \\
\Delta &\equiv N\Delta \\
N^* &\equiv NN^*(1440) \,.
\end{aligned}
\tag{7.2}
$$

G_A is the propagator of the two-body system, A, (in Sect. 7.1.1 the precise form used is discussed in detail).

In our approach we neglect the transitions between two-baryon states containing resonances, $V_{\Delta N^*} = V_{N^*\Delta} = 0$, assuming that little flow does indeed go through them. Therefore the system of coupled equations that we will solve is,

$$
\begin{aligned}
T_{NN} &= V_{NN} + V_{NN}G_N T_{NN} + V_{N\Delta}G_\Delta T_{\Delta N} + V_{NN^*}G_{N^*}T_{N^*N} \\
T_{\Delta N} &= V_{\Delta N} + V_{\Delta N}G_N T_{NN} + V_{\Delta\Delta}G_\Delta T_{\Delta N} \\
T_{N^*N} &= V_{N^*N} + V_{N^*N}G_N T_{NN} + V_{N^*N^*}G_{N^*}T_{N^*N} \,.
\end{aligned}
\tag{7.3}
$$

In Fig. 7.1 a diagrammatic representation of the model is given.

All the interactions V_{AB} appearing in Eq. (7.3) are derived from the quark model presented in Chapter 2 using the tools explained in Chapter 3. In particular the calculation of the pieces involving the $N^*(1440)$ resonance were explained in detail in Chapter 5. The NN and the transition to the $N\Delta$ system are taken from Ref. [85], similarly to what we did to study the non-nucleonic components in the deuteron in Sect. 6.1.

No parameters are fitted for specific channels and thus the results are genuine predictions of the quark-model and the above presented formalism.

---

[2]The assumptions made to arrive to the coupled channel method are detailed in, for example, Ref. [151].
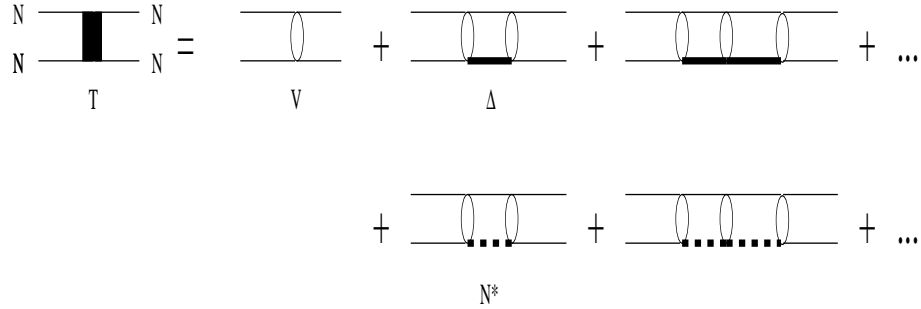
Figure 7.1: Graphical representation of the coupled channel formalism for the NN system of Eq. (7.4). The black box corresponds to the NN t-matrix. Ellipses correspond to the two-baryon direct and transition potentials. The solid thin lines are the nucleons while the thick lines are the resonances, Δ's (straight) and $N^*(1440)$ (dashed). See Eqs. (7.4) and (7.5).

Eqs. (7.3) can be conveniently rewritten so that the final form is a one-channel Lippmann-Schwinger equation for the NN system, but with a redefined effective NN potential which already includes the effect of the resonances:

$$T_{NN} = \bar{V}_{NN} + \bar{V}_{NN} G_N T_{NN} \,, \tag{7.4}$$

where it can be easily checked that,

$$
\begin{aligned}
\bar{V}_{NN} &= V_{NN} \\
&+ V_{N\Delta} G_\Delta \left[1 - V_{\Delta\Delta} G_\Delta\right]^{-1} V_{\Delta N} \\
&+ V_{NN^*} G_{N^*} \left[1 - V_{N^*N^*} G_{N^*}\right]^{-1} V_{N^*N} \,.
\end{aligned} \tag{7.5}
$$

This way of writing the system of equations [3] strongly simplifies the calculation procedure as now it can be solved numerically using any of the techniques already available in the literature. We use the method described in Ref. [152]. Thus we make the problem discreet in momentum space by defining the integral equation, Eq. (7.4), on a mesh of Gauss-Legendre points. Once this is done the resulting algebraic system of equations is solved using matrix inversion. The method can be tested and is stable once the number of mesh points is above 32.

We restrict our study to partial waves with $J \leq 2$ (J being the total angular momentum of the two-baryon system). In Table 7.1 the explicit channels included in the calculation are listed.

---

[3]Let us note that the inclusion of any other two-baryon channel just needs the addition of the corresponding *box-term* in Eq. (7.5). No changes are needed in the numerical method because the dimension of the *matrix* $\bar{V}_{NN}$ is not altered. Some authors neglect the direct potentials for the resonance terms, e.g. $V_{\Delta\Delta} = 0$.

NN	$N\Delta$	$NN^*(1440)$
Isospin 0		
$^3S_1-^3D_1$	$-$	$^3S_1-^3D_1$
$^1P_1$	$-$	$^1P_1$
Isospin 1		
$^1S_0$	$^5D_0$	$^1S_0$
$^3P_0$	$^3P_0$	$^3P_0$
$^3P_1$	$^3P_1-^5P_1-^5F_1$	$^3P_1$
$^1D_2$	$^5S_2-^3D_2-^5D_2-^5G_2$	$^1D_2$
$^3P_2-^3F_2$	$^3P_2-^5P_2-^3F_2-^5F_2$	$^3P_2-^3F_2$

Table 7.1: NN, $N\Delta$ and $NN^*(1440)$ channels included in the calculation.

7.1.1 Propagator of the two-baryon system

The propagators G_A of the two-baryon systems appearing in the Lippmann-Schwinger formulation are taken as follows,

$$
G_\Delta = \frac{1}{E - \Delta M_\Delta - \Gamma_\Delta(E)}
$$
$$
G_{N^*} = \frac{1}{E - \Delta M_{N^*} - \Gamma_{N^*}(E)} .
$$
(7.6)

ΔM_B is the mass difference, $M_B - M_N$, and $\Gamma_B(E)$ is the width of resonance B. We take the width of the resonance from previous calculations made in the framework of constituent quark models [40, 140]. Their explicit expressions are the following:

$$
\Gamma_\Delta = \frac{2}{3} \frac{f_{\pi N\Delta}^2(k_0)}{4\pi m_\pi^2} \frac{m_N}{E_\pi(k_0) + m_N} k_0^3
$$
$$
\Gamma_{N^*(1440)} = 6 \frac{f_{\pi NN^*}^2(k_0)}{4\pi m_\pi^2} \frac{m_N}{E_\pi(k_0) + m_N} k_0^3
$$
(7.7)

where,

$$
f_{\pi N\Delta}(k) = 2\sqrt{2} f_{\pi qq} \left(1 + \frac{E_\pi(k)}{6m_q}\right) e^{-\frac{b^2 k^2}{6}} ,
$$
$$
f_{\pi NN^*(1440)}(k) = \frac{\sqrt{3}}{18} \left(k^2 b^2 + \frac{3}{2} \frac{E_\pi(k)}{m_q}\right) e^{-\frac{b^2 k^2}{6}} f_{\pi NN}
$$
(7.8)

and k_0 is the pion momentum in the resonance rest frame, E_π is its energy, $f_{\pi qq}^2 = g_{ch}^2 m_\pi^2/4m_q^2$ and $f_{\pi NN} \sim 1$.

7.2 Results

The influence of $N\Delta$ channels has already been proved to be relevant to understand the NN interaction above the pion production threshold. Due to isospin conservation the NN system can only couple to $N\Delta$ channels in those partial waves with $T = 1$. For $T = 0$ channels there is no influence from Δ excitations and thus the $N^*(1440)$ is expected to account for most part of the observed inelasticity.

In the next section we present our results for $T = 1$ channels, which include NN, $NN^*(1440)$ and $N\Delta$. The role played by the Δ resonance is shown to be much more relevant than that of the $N^*(1440)$. This could be *a priori* inferred just by looking at the masses of the resonances. Results for $T = 0$ channels are presented in Sect. 7.2.2.

7.2.1 Isospin 1 Channels

We first consider the case where both $N\Delta$ and $NN^*(1440)$ channels can be excited. In this case the effect of channels containing Δ's, which are opened (not considering the width) at 632 MeV in the laboratory frame, can be expected to be more relevant than the effect of the coupling to the $NN^*(1440)$ system. However, the inclusion of $N^*(1440)$ channels has sometimes been addressed as a possible way to improve the quality of the description of the NN phase shifts. First we isolate the effects of the Δ. This means we neglect the $N^*(1440)$ pieces $V_{NN \to NN^*} = 0$ and $V_{NN^* \to NN^*} = 0$. Secondly, we perform a full calculation and find that the effect of including the $N^*(1440)$ is small for these channels.

$^1S_0$ Partial wave: NN and $N\Delta$ only

In Fig. 7.2 we depict the phase shift and inelasticity obtained for the $^1S_0$ partial wave. The first relevant feature that can be outlined is the agreement obtained at low energies, $E_L < 300$ MeV. This low-energy regime was the one considered earlier when the triton binding energy was studied in Chapter 4.

We also find that the energy dependence of the phase shift at energies above 500 MeV is not well described. Our quark model result lacks repulsion at high energies not being able to describe the data. Regarding the inelasticity, η, our result understimates, by a factor 3, the experimental[4] one.

^3P_J Partial waves: NN and $N\Delta$ only

The correct reproduction of the ^3P_J partial waves even at low energies cannot be achieved in the absence of spin-orbit terms [154]. There are in our model three sources of spin-orbit, the OGE, the OSE, and the confining potential. The non-relativistic reduction of the OGE diagram between quarks provides two different types of spin-orbit terms. The Galilei-invariant one was already used in Ref. [155], where they demonstrate that this

---

[4]For now on we refer as experimental results to the analysis of Ref. [153].

term allows to understand the observed spin-orbit splitting in the NN interaction with a strong coupling $\alpha_s \sim 1.6$. However, they had to include an effective meson force between the nucleons. Ref. [154] explores the Galilei-invariant term arising from both the OSE and OGE at the quark level. They obtain that both terms add up together in the ^3P_J partial waves allowing a qualitative understanding of the energy dependence of the phase shifts (to get quantitative results the parameters needed to be forced). The uncertainties associated to the antisymmetric spin-orbit terms [156] and the nature of the confinement interaction are the reasons why we have not included any source of spin-orbit, and thus we do not intend to reproduce these partial waves.

For the sake of completeness we give our results for one of the partial waves. In Fig. 7.2 we depict the phase shift and inelasticiy obtained for the $^3P_1$ partial wave. The energy dependence of the phase shift is not well described at high energies, our result saturates at earlier energies, $\sim 500\text{MeV}$, lacking repulsion at higher energies as already occurred in the $^1S_0$ partial wave. The inelasticity is described reasonably well.

$^1D_2$ partial wave: NN and $N\Delta$ only

The experimental data for the $^1D_2$ partial wave show a quite prominent peak in the phase shifts at around 500 MeV. This can be seen, together with our results, in Fig. 7.3. This peak is very well described in our model and is an important consequence, already noticed by González and Lomon [112], of considering the coupling to the $N\Delta$ system. Above the peak, the soft energy dependence of the phase shifts is reasonably described by our model. The structure present in the inelasticity is overall reproduced by our model. The observed behavior, with the phase shift being described while the inelasticity is 10% below the data is a common feature to other calculations [157].

$^3F_2$, and ε_2: NN and $N\Delta$ only

This partial wave is coupled to the $^3P_2$ one and therefore the discussion regarding the importance of spin-orbit terms should be kept in mind. We show in Fig. 7.3 the results for the $^3F_2$, and ε_2. The energy dependence of the phase shift is not described for the $^3F_2$ partial wave in the whole energy domain shown. The results for the mixing parameter, ε_2, are however qualitatively correct at low energies. The inelasticity parameter is in reasonable agreement.

$N^*(1440)$ influence in T=1 channels

Up to now we have only shown results including Δ channels. As explained above, the $N\Delta$ channel is opened at $E_L \sim 640$ MeV. Thus the $N\Delta$ transition will mainly drive the NN interaction in the energy range we are considering. The effect of the coupling to the $NN^*(1440)$ system in those channels with $T = 1$ was found to be very small already by Lee [158]. Here we show some results including the coupling to both $N\Delta$ and $NN^*(1440)$ channels with isospin 1. In Fig. 7.4 the phase shifts obtained for the $^1S_0$ and

$^3P_1$ partial waves are shown. We depict the results including all the transitions (solid) and including only $N\Delta$ ones (dot-dashed).

The results agree with the previous ones of Lee [158] and thus we do not find any important influence of the $NN^*(1440)$ channels in partial waves with $T = 1$. Actually, the two lines in Fig. 7.4 are almost indistinguishable in all cases up to 1500 MeV. Above this energy some very small influence of the $N^*(1440)$ is found in the phase shifts and inelasticities.
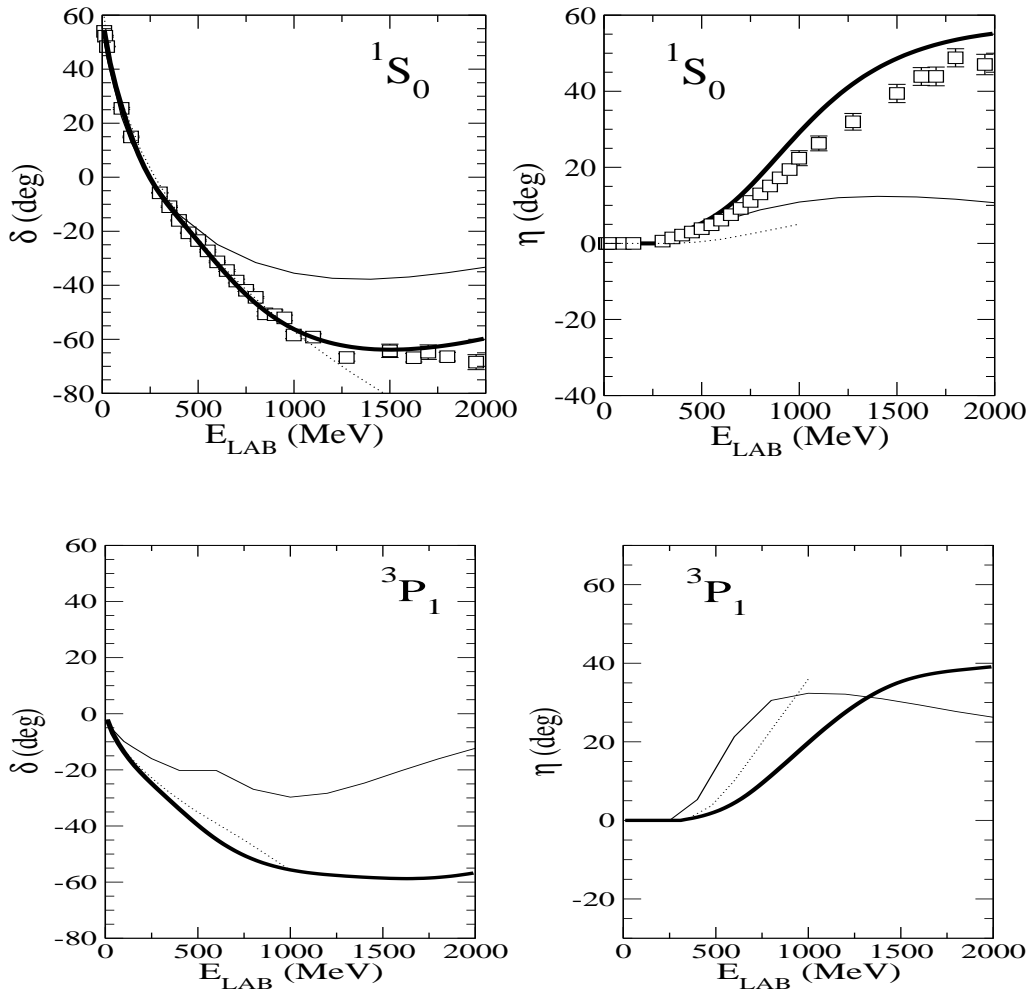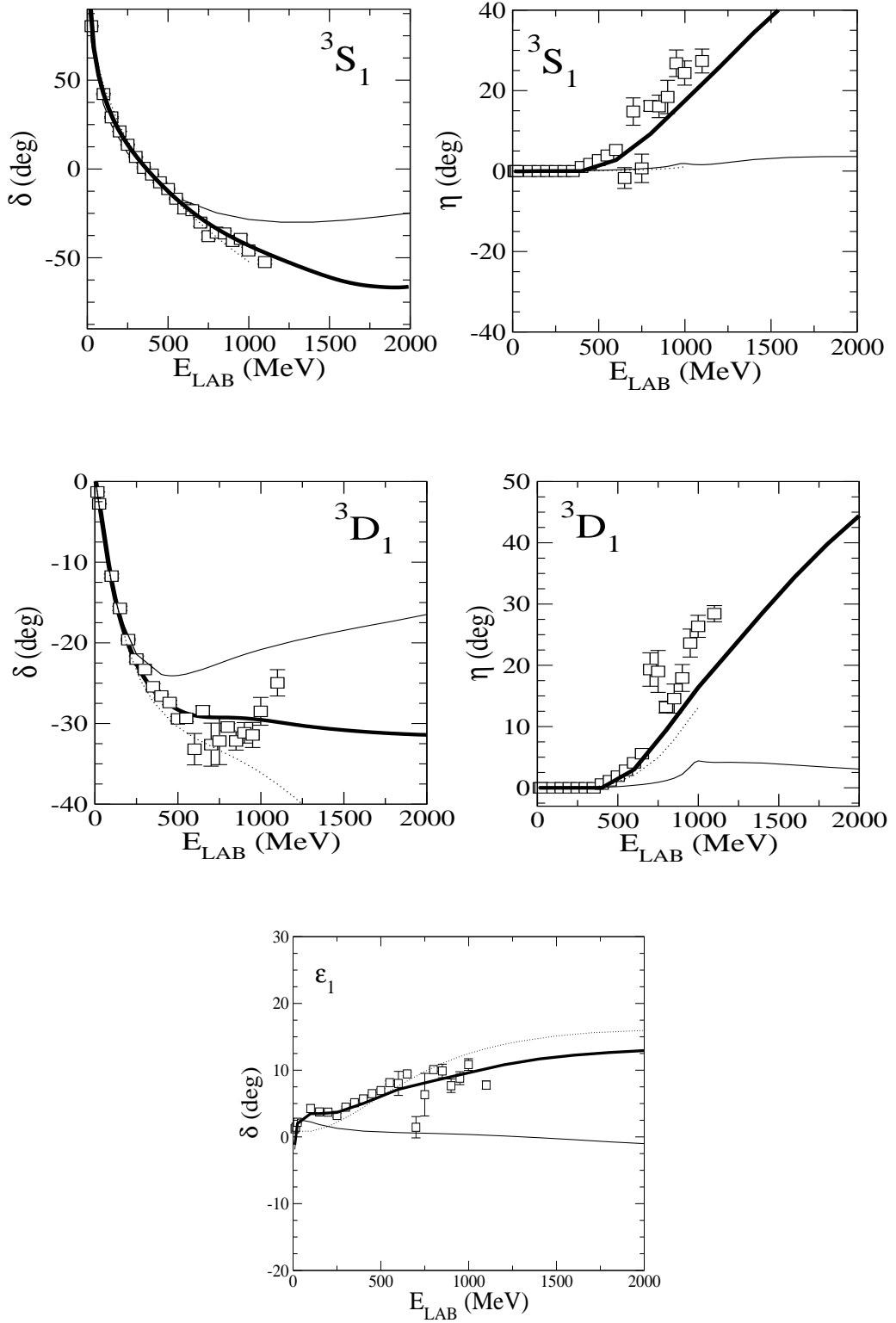

Figure 7.2: Phase shift and inelasticity for the $^1S_0$ and $^3P_1$ partial waves. The thick solid line corresponds to the experimental analysis of Arndt et al. [153]. The solid line is the result using our quark model potentials. The dotted line corresponds to the calculation of Ref. [158] where they give results up to 1000 MeV. No $N^*(1440)$ resonance is included.
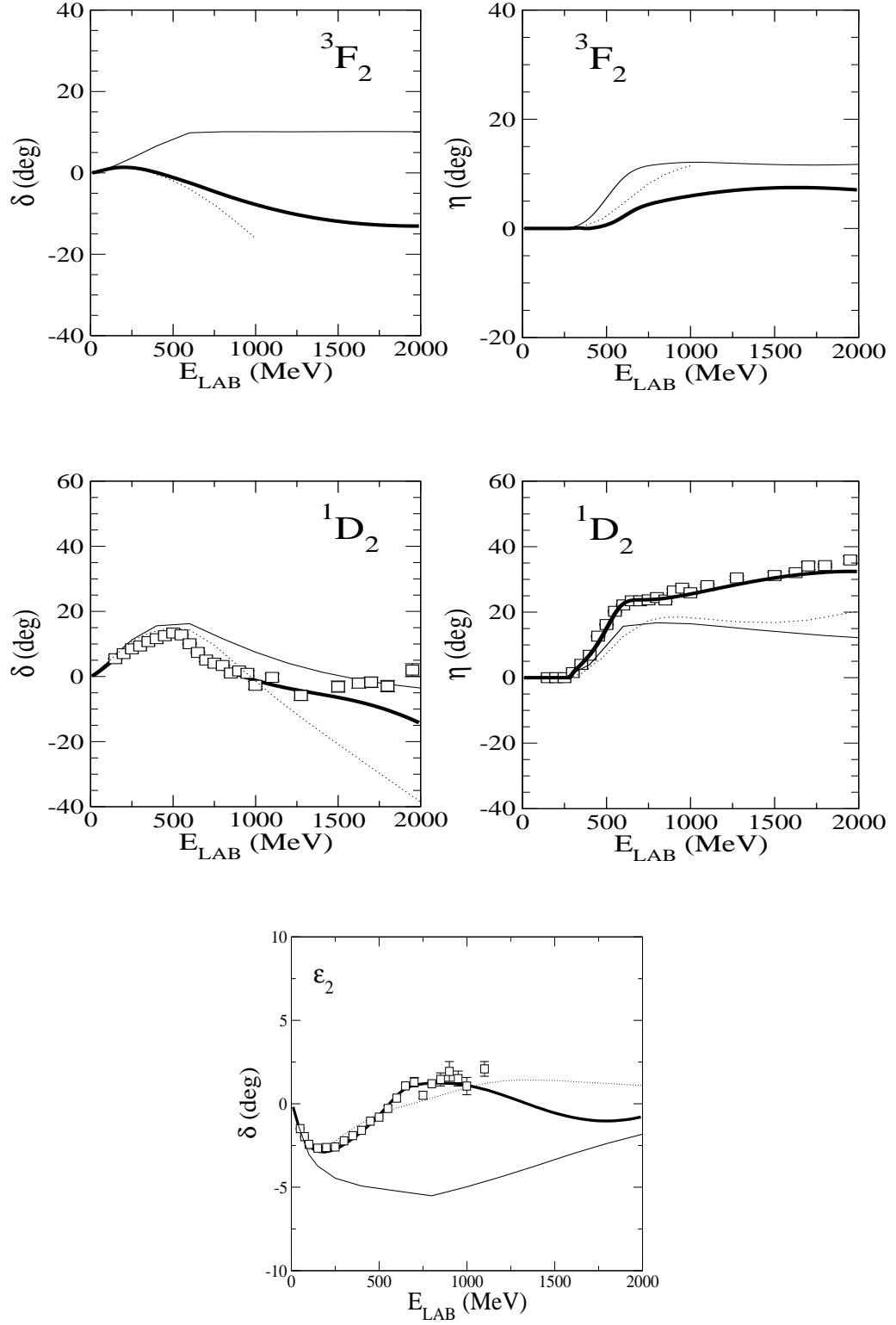
Figure 7.3: Same as Fig. 7.2 but for the $^3F_2$ and $^1D_2$ partial waves and for ε_2.
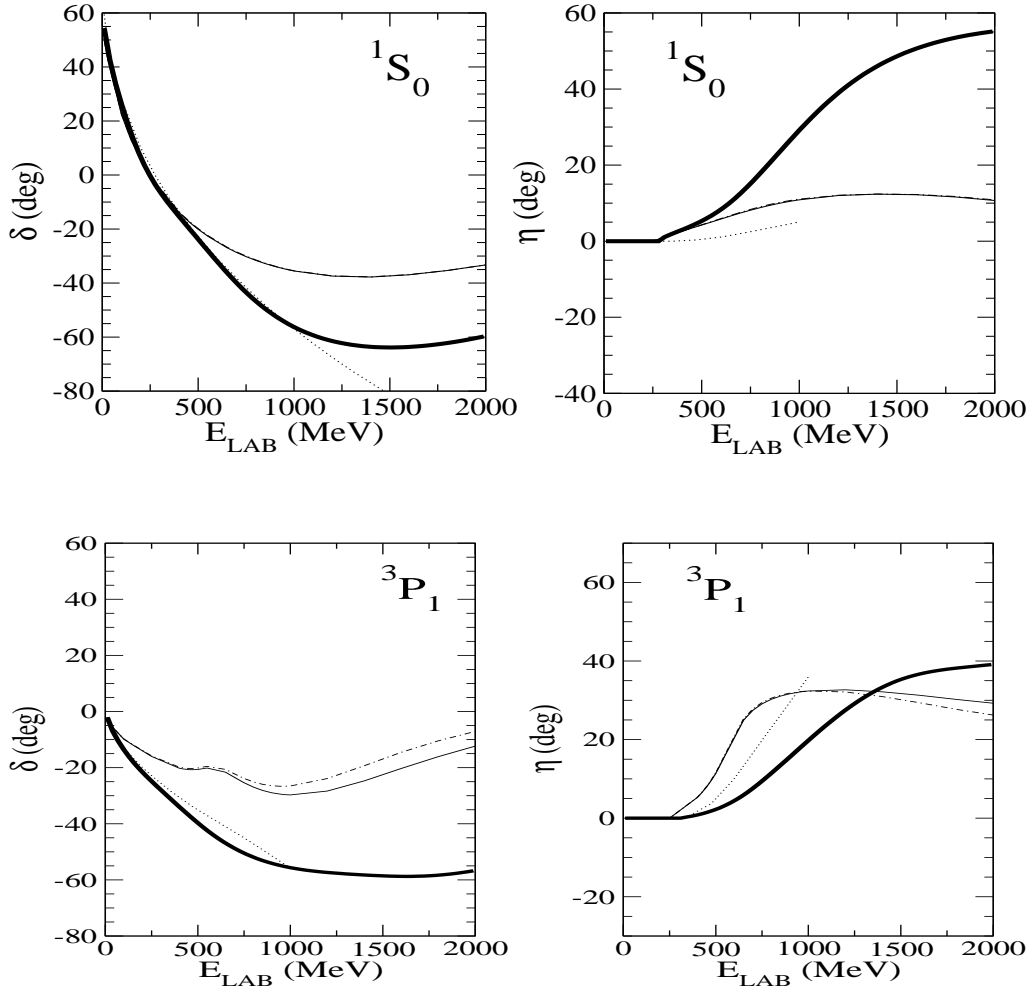
Figure 7.4: Phase shift and inelasticity for the $^1S_0$ and $^3P_1$ partial waves. The thick solid line corresponds to the experimental analysis of Arndt et al. [153]. The solid line is the result not including $N^*(1440)$ resonances. The dot-dashed line is the full calculation. The dotted line corresponds to the calculation of Ref. [158].

7.2.2 Isospin 0 channels

The inclusion of $NN^*(1440)$ channels in the formalism was first considered as a possible way to understand the experimental data in those channels which cannot couple to $N\Delta$. This is the case of Ref. [158] where they incorporate this transition to try to describe the NN data also in $T = 0$ channels. In our study we will not present results for Pauli blocked channels, such as the $^1P_1$ partial wave. The study of Pauli blocked channels would require many technical steps in the RGM [159].

$^3S_1$, $^3D_1$, and ε_1: NN and $NN^*(1440)$

These channels were studied in Chapter 4 when we calculated the triton binding energy. There we showed, see Fig. 4.2, the phase shifts at energies below 300 MeV and clearly saw that the agreement with the experimental data was very good. In Fig. 7.5 we present the phase shift obtained for the $^3S_1$ partial wave. The correct description of the energy dependence of the phase shift at low energies is not altered by the inclusion of the $N^*(1440)$. On the other hand at higher energies, above 500 MeV, we find similar effects as the ones already discussed for the $^1S_0$ partial wave. That is, our theoretical predictions saturate earlier than the experimental data. Similarly, for the $^3D_1$ partial wave our results are more attractive than the experimental data at energies above 400 MeV.

The description of the inelasticity in the $^3S_1$ channel is not too appealing. The coupling to the $NN^*(1440)$ system does not provide the experimental inelasticity in the $^3S_1$ partial wave. Similar to the result obtained in Ref. [158]. However in the $^3D_1$ partial wave the results are in better agreement with the data.

Figure 7.5: Phase shift and inelasticity for the $^3S_1$, $^3D_1$ and ε_1 partial waves. The thick solid line corresponds to the experimental analysis of Arndt et al. [153]. The boxes are single data from [153]. The solid line corresponds to the quark model, the dotted line corresponds to the calculation of Ref. [158].

Model	$V_{NN\to NN}$	$V_{NN\to N\Delta}$	$V_{N\Delta\to N\Delta}$	$V_{NN\to NN^*}$	$V_{NN^*\to NN^*}$	Width
RGM	RGM	RGM	RGM	BO	BO	Quark Model
BO	BO	BO	BO	BO	BO	Lee

Table 7.2: Building blocks of the two approaches described in the text.

7.3   A model for comparison

In the previous section we have presented our quark model results. The agreement with the experimental data is quite satisfactory up to 1000 MeV in some partial waves. In this section we build a model which will permit us to investigate whether our results can be improved by using a different potential or a different parametrization of the width. The calculation will be done using the coupled channel model already explained in Sect. 7.1. The only differences come from the direct and transition potentials employed. In this approach, that we denote as BO, we take the NN, $N\Delta$ and $N^*(1440)$ pieces, $V_{NN\to NN}, V_{NN\to N\Delta}$, $V_{N\Delta\to N\Delta}$, $V_{NN\to NN^*}$ and $V_{NN^*\to NN^*}$, obtained using the BO method as described in Chapter 3. The width of the resonances is taken from the works of Lee [158] [5]. There he calculates the width of the resonance from a phenomenological point of view taking into account one and two-pion contributions to the self-energy of the Δ and $N^*(1440)$ in a meson-baryon formalism. The parameters are fixed to reproduce the πN scattering phase shifts for the P_{11} and P_{33} channels up to 1900 MeV (center of mass energy).

The definition of the width is [158]:

$$\Sigma_\alpha(w) = \Sigma_{\alpha,\pi}(w) + \Sigma_{\alpha,2\pi}(w) \tag{7.9}$$

where α refers to Δ or $N^*(1440)$. They can be calculated with the vertex interactions, $h_{\alpha\beta}$ shown in Fig. 7.6,

$$
\begin{aligned}
\Sigma_{\alpha,\pi}(w) &= \int_0^\infty \frac{|h_{0\alpha}(q')|^2\ q'^2 dq'}{w - E_\pi(q') - E_N(q') + i\epsilon} \\
\Sigma_{\alpha,2\pi}(w) &= \int_0^\infty \frac{|h_{\alpha 3}(q')|^2\ q'^2 dq'}{w - E_\pi(q') - E_\alpha(q') - \Pi_\alpha(w,q')}\ ,
\end{aligned}
\tag{7.10}
$$

with

$$\Pi_{\alpha,q'} = \int_0^\infty \frac{|h_{01}(q'')|^2\ q''^2 dq''}{w - E_\pi(q') - ([E_\pi(q'') + E_N(q'')]^2 + q'^2)^{1/2} + i\epsilon} \tag{7.11}$$

In Table 7.2 we summarize the two approaches that we consider. We denote RGM to the quark model presented in the previous section.

---

[5]We will explore the dependence of our results on the parametrization employed for the width.
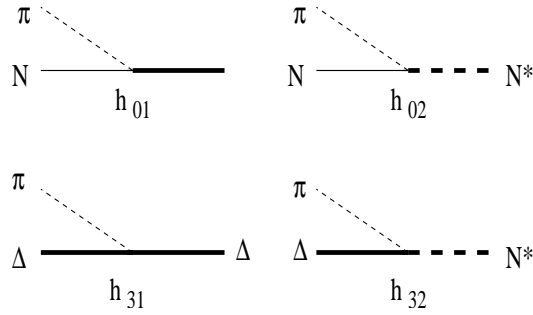
Figure 7.6: Vertex interactions used in [158].

7.3.1 Results

In Fig. 7.7 we show the results obtained using both schemes for the $^1S_0$ partial wave. The good agreement already stated for energies below 300 MeV is again obtained with the BO model. However, we observe that in both cases the energy dependence of the phase shifts at energies above 500 MeV is not well described. In the BO model the saturation of the phase shift occurs earlier than in the RGM one, giving a poorer description at energies above 1000 MeV. Regarding the inelasticity, η, both the RGM and BO provide a similar description.
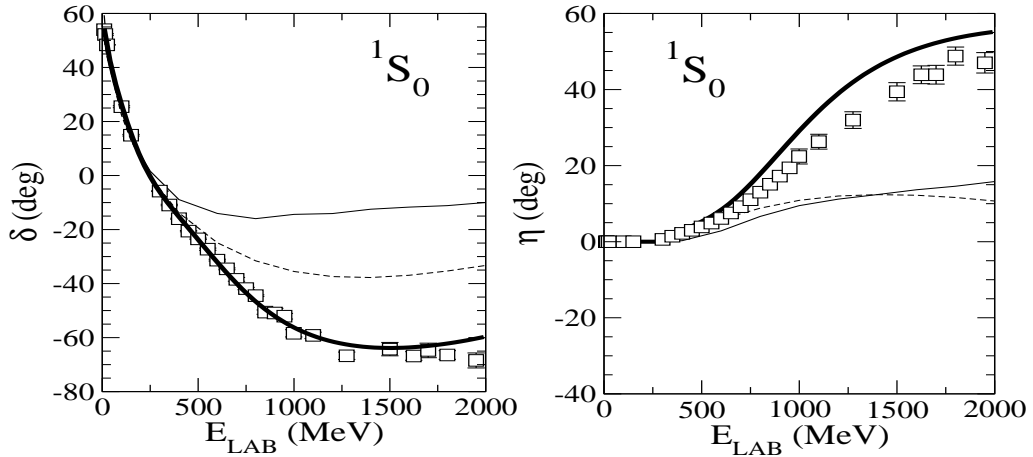
Figure 7.7: Phase shift and inelasticity for the $^1S_0$ partial wave. The thick solid line corresponds to the experimental analysis of Arndt et al. [153]. The solid line is BO result, where all the interactions are obtained using the BO. The dashed line corresponds to the RGM.

In Fig. 7.8 we present the phase shift obtained for the $^3S_1$ partial wave for both the BO and RGM models. The energy dependence of the phase shift at low-energies is again described and is not altered by the inclusion of the $N^*(1440)$. We again find that the BO model does saturate earlier than the RGM one providing a poorer description of the data at energies above 500 MeV. The description of the inelasticity in the $^3S_1$ channel is not too appealing in neither case. The coupling to the $NN^*(1440)$ system does not account for the experimental inelasticity. At energies above 600 MeV the BO gives a better agreement for this channel though it fails to follow the data above 1000 MeV.

The soft energy dependence present in the $^1D_2$ phase shift, Fig. 7.8, is also described by the BO model. However, in this case the BO model contains more attraction in the whole energy domain. The experimental structure seen in the inelasticity is reasonably reproduced in both models. In this case we are again in the same situation as with the RGM model, the phase shift is more atractive but in this case the agreement for the inelasticity is better than in the RGM. This is what usually happens: if one gets the correct inelasticity the phase shift is above the data while if the phase shift is correctly described the inelasticity is below the data [157].

7.3.2   Dependence on the parametrization of the width

We have considered two different parametrizations of the width of the resonances. One is defined in Eqs. (7.7) and (7.8), the second one is defined in Eq. (7.9). The first one was obtained within the quark model, and therefore has no free parameters, while the second one was obtained in a meson-baryon formalism and its free parameters were fitted to reproduce the experimental $\pi\pi$ phase shifts. In order to clarify the importance of the parametrization for the width, we present a calculation of the phase shifts and inelasticities of two partial waves using the BO model as it is in Table 7.2 but making use of the two different parametrizations of the width.

The results for the $^3S_1$ partial wave, see Fig. 7.9, show very minor differences when using the two different expressions for the width. Slightly different is the situation for the $^3D_1$ partial wave. There the use of the quark model width worsens the description of both the phase shift and the inelasticity but does not modify considerably the energy dependence.
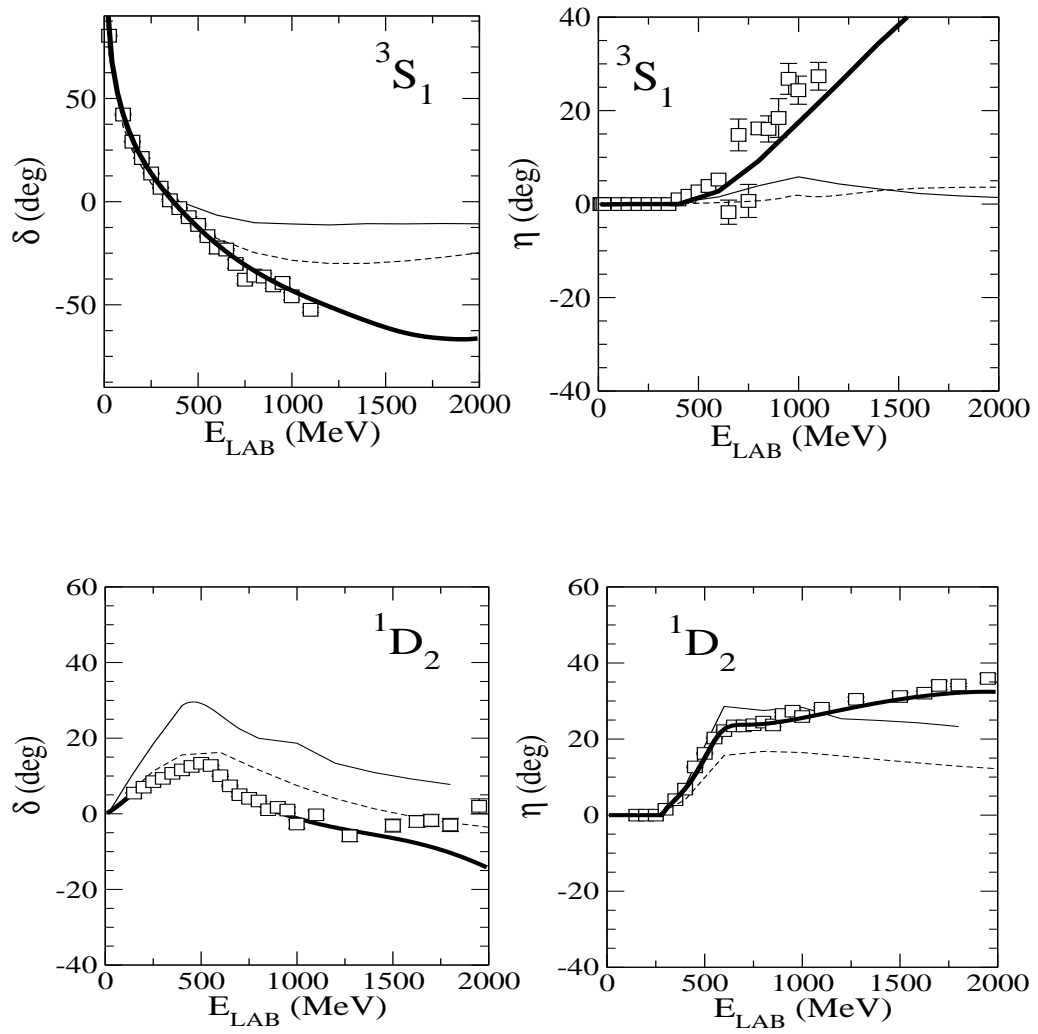
Figure 7.8: Same as Fig. 7.7 but for the $^3S_1$ and $^1D_2$ partial waves.
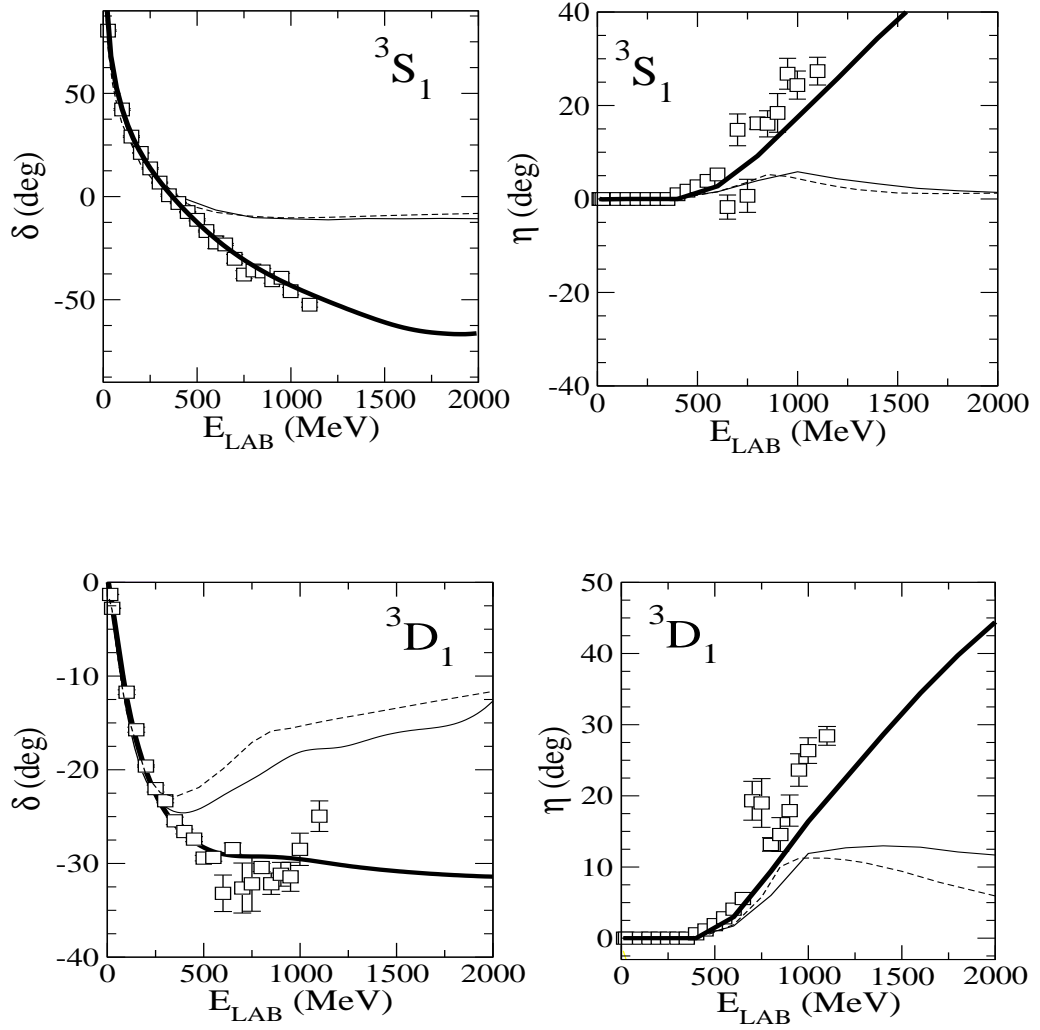
Figure 7.9: Phase shift and inelasticity for the $^3S_1$ and $^3D_1$ partial waves. The thick solid line is the solution of Arndt. The boxes are the experimental data. For our calculation we use only the BO derived potentials. The thin solid line is obtained using the width of the $N^*(1440)$ as written in Eqs. (7.7) and (7.8) while the dashed one is corresponds to the expression of Eq. (7.9).

8 CONCLUSIONS

This thesis represents a first step towards the application of quark-model based baryon-baryon interactions to the study of few-body systems. For this purpose, we have used a chiral constituent quark model that was developed in order to understand the NN system below pion threshold and the low-lying baryon spectrum. Such a model has been extended in two directions: the study of systems with more than two nucleons (triton) and the study of reactions where nucleon resonances other than the Δ could play a role.

We have first of all made a detailed analysis of the simplest few-body system, the triton. We calculate the binding energy by previously deriving EST separable expansions of the low partial waves included in the three-body calculation. The result obtained is in the range of the experimental value and is also close to the results obtained utilizing other baryonic models available in the literature. Those EST expansions could be tested against any other many-nucleon system. Our result is ~ 800 MeV smaller than the experimental data. This underprediction, reported in many other theoretical calculations, has been the object of extensive study during the last years. It has been suggested that the non-local structure of the NN interaction could be responsible for this disagreement. We have estimated the effect of the non-localities inherent to the RGM derivation of the quark-model based potential. Our results predict more binding for the non-local calculation in the order of 200 MeV.

Later on we have presented the way in which any baryon-baryon interaction can be derived from the basic quark-model Hamiltonian. The main advantage of constituent quark models is that they permit to obtain any baryon-baryon interaction in a consistent way. The microscopic model of quarks, gluons and Goldstone modes, defines a framework in which any transition or direct potential between two-baryons can be derived. In particular, the potentials involving N's and $N^*(1440)$'s have been studied in detail. There are several reasons for that. On one hand the elusive structure of the $N^*(1440)$ resonance and on the other hand the increasing number of data from processes involving higher nucleon resonances.

First of all, we studied the direct $NN^*(1440) \rightarrow NN^*(1440)$ potential. This system is composed of non-identical baryons and thus there is no selection rule on its quantum numbers at baryonic level. The detailed analysis of the contribution of each part of the quark Hamiltonian makes it apparent that the short-range part of the potential is dominated by antisymmetry requirements. As a consequence, the Pauli principle at the quark level has important implications for those partial waves that are forbidden for the

NN case: we find strong short-range barriers. Moreover our potential exhibits different behavior when the isospin is changed, e.g. $L = 0$, $S = 0$, $T = 1$ compared to $L = 0$, $S = 0$, $T = 0$. This result should prevent about baryonic potentials obtained from the *NN* potential by naive SU(2) scaling of the boson coupling constants. The transition piece has also been obtained, $NN \rightarrow NN^*(1440)$. The main differences between the direct and transition potentials come from the fact that in the latter, due to the conservation of isospin by the strong force, we do not have partial waves with no counterpart in the *NN* system. Regarding the role played by the different pieces of the quark-quark Hamiltonian, some features can be outlined for both cases: the OPE drives the very-long range part of the interaction between the two baryons, the OSE is mainly responsible for the medium-range part of the interaction while the OGE affects only to the short range behavior.

We have applied the $NN^*(1440)$ interactions to the study of different subjects. First of all, the non-nucleonic structure of the deuteron has been studied in the framework of a non-relativistic coupled channel scheme. The inclusion of other resonance components is free of any additional parameter and therefore our estimates greatly reduce the model dependence. The results show that the $NN^*(1440)$ probability is small, $\leq 0.1\%$. It does agree with other previous estimations of $\leq 1\%$ for resonance admixture to the deuteron wave function which are mainly shared between $NN^*(1440)$ and $\Delta\Delta$ parts. The $NN^*(1440)$ baryon resonance probabilities in the deuteron, being smaller than the $\Delta\Delta$ ones, should be included in any detailed deuteron structure calculation. Our results support recent experimental data where $NN^*(1440)$ components were induced from processes like subthreshold antiproton production on $d - p$ collisions or $pd \rightarrow dp$ reactions.

Secondly, our baryon-baryon potentials allow to determine the coupling constants that in hadronic theories had to be fitted to the experimental data. The effect of antisymmetry vanishes at distances of the order of $1.5-2$ fm. This means that at long-enough distances we are left with the original structures. This permits to extract the baryon-baryon-Goldstone meson coupling constant from the long-range part of the transition potentials. We have obtained scheme-dependent values for $g_{\pi NN^*(1440)}$ and $g_{\sigma NN^*(1440)}$, an almost scheme-independent result for $g_{\pi NN^*(1440)}/g_{\pi NN}$ and $g_{\sigma NN^*(1440)}/g_{\sigma NN}$ and a very definite prediction for the quotient between the latter.

In the third place, we have studied a reaction that is mediated by a Roper excitation in an isosinglet channel. We have analyzed the most prominent model dependencies of the results obtained determining the strong dependence of the results on the form factor chosen and the model-dependent method used to extract the experimental data. This fact was also stressed when the $N^*(1440)$ coupling constants were extracted. An extremely interesting result is that in the quark-model calculation one obtains contributions to the cross-section coming not only from the scalar exchange at quark level but also from the other exchanges present in the quark-model Hamiltonian.

Finally, with respect to the $NN^*(1440)$ direct potential, unfortunately there are no experimental data for the forbidden channels (this is not the case for the $N\Delta$ system,

where indirect data obtained from the πd elastic scattering support the strong repulsive barriers obtained). So our study of the NN system above pion threshold only involves allowed channels. This study has been done by means of the Coupled Channel Method including N's, Δ's and N^*'s. The set of potentials which enters in a Lippmann-Schwinger formulation of the problem has been derived in a consistent way from the same underlying quark Hamiltonian. We extend the study of the NN interaction well above the domain where the Δ is expected to account for most of the inelasticity. Our results show that, corroborating other phenomenological approaches, the coupling to the $N\Delta$ system is essential to reproduce the NN interaction even at low energies, being the dominant resonance configuration when higher energies are also considered. The effect of the $N^*(1440)$ on those channels where the system can also couple to Δ ones is found to be very small. On the other hand, some effects are found in those channels which cannot couple to Δ ones, isospin 0 channels. In the latter, the $N^*(1440)$ gives a small fraction of the experimental inelasticity. However, its contribution is in general very small not being responsible for the disagreement observed with respect to the experimental data.

Therefore, we have demonstrated the capability of quark-model based baryon-baryon potentials to study medium-energy phenomenology: few-body problems such as the triton binding energy and nuclear reactions: $p(d, d')$ and NN scattering. The results obtained for processes where only allowed channels appear are comparable to any other baryon theory but in our case with a restricted number of free parameters. The study of processes where the presence of forbidden channels can occur could put some light on the predictions of quark-model calculations. This kind of calculations should serve either as a first step for more refined calculations or as a possible guide for phenomenological applications.

Appendix A MATHEMATICAL FORMULAE

Yukawa functions

$$Y(x) = \frac{e^{-x}}{x} \tag{A.1}$$

$$H(x) = \left(1 + \frac{3}{x} + \frac{3}{x^2}\right) Y(x) \tag{A.2}$$

Gaussian integrals

$$
\begin{aligned}
\int d\vec{x}\, e^{-a^2\, x^2} &= \frac{\pi^{3/2}}{a^3} \\
\int d\vec{x}\, |\vec{x}|^2\, e^{-a^2\, x^2} &= \frac{3}{2}\frac{\pi^{3/2}}{a^5} \\
\int d\vec{x}\, |\vec{x}|^4 e^{-a^2\, x^2} &= \frac{15}{4}\frac{\pi^{3/2}}{a^7} \\
\int d\vec{x}\, (\vec{a}\cdot\vec{x})\,(\vec{b}\cdot\vec{x})\, e^{-a^2\, x^2} &= (\vec{a}\cdot\vec{b})\,\frac{3}{2}\frac{\pi^{3/2}}{2a^5}
\end{aligned} \tag{A.3}
$$

Useful expansions

- With Legendre Polynomia

$$
\begin{aligned}
\sum_{\ell=0}^{\infty}(2\ell+1)\,P_\ell(\mu)\,\imath_\ell(x)\,\mu &= \sum_{\ell=0}^{\infty}(2\ell+1)\,P_\ell(\mu)\,F_1(\ell,x) \\
\sum_{\ell=0}^{\infty}(2\ell+1)\,P_\ell(\mu)\,\imath_\ell(x)\,\mu^2 &= \sum_{\ell=0}^{\infty}(2\ell+1)\,P_\ell(\mu)\,F_2(\ell,x)
\end{aligned} \tag{A.4}
$$

with

$$F_1(\ell,x) = \frac{\ell}{2\ell+1}\imath_{\ell-1}(x) + \frac{\ell+1}{2\ell+1}\imath_{\ell+1}(x) \tag{A.5}$$

$$
\begin{aligned}
F_2(\ell,x) = {}& \frac{\ell(\ell-1)}{(2\ell+1)(2\ell-1)}\imath_{\ell-2}(x) + \frac{2\ell^2+2\ell-1}{(2\ell+3)(2\ell-1)}\imath_\ell(x) \\
&+ \frac{(\ell+2)(\ell+1)}{(2\ell+3)(2\ell+1)}\imath_{\ell+2}(x)
\end{aligned} \tag{A.6}
$$

where $P_\ell(x)$ are Legendre polynomia which can be obtained using Rodrigues formula,

$$P_\ell(x) = \frac{1}{2^{\ell+1}\ell!}\frac{d^\ell}{dx^\ell}(x^2-1)^\ell \tag{A.7}$$

- Expansions of the exponential

$$e^{\vec{A}\cdot\vec{B}} = 4\pi \sum_{LM} Y_{LM}(\hat{A})\, Y_{LM}^*(\hat{B})\, \imath_L(AB) \tag{A.8}$$

$$e^{i\vec{A}\cdot\vec{B}} = 4\pi \sum_{LM} i^L\, Y_{LM}(\hat{A})\, Y_{LM}^*(\hat{B})\, \jmath_L(AB) \tag{A.9}$$

where $\jmath_L$ are the spherical Bessel functions which can be defined as,

$$\begin{aligned}
\jmath_0(z) &= \frac{\sin(z)}{z} \\
\jmath_1(z) &= \frac{\sin(z)}{z^2} - \frac{\cos(z)}{z} \\
\jmath_{n-1}(z) + \jmath_{n+1}(z) &= (2n+1)\frac{\jmath_n(z)}{z}
\end{aligned} \tag{A.10}$$

and $\imath_L$ are the modified spherical Bessel functions defined as,

$$\begin{aligned}
\imath_0(z) &= \frac{\sinh(z)}{z} \\
\imath_1(z) &= \frac{\sinh(z)}{z^2} + \frac{\cosh(z)}{z} \\
\imath_{n-1}(z) - \imath_{n+1}(z) &= (2n+1)\frac{\imath_n(z)}{z}
\end{aligned} \tag{A.11}$$

Angular Momentum Formulae

- Three spherical harmonics

$$\int Y_{l'm'}^*(\hat{A})\, Y_{LM}(\hat{A})\, Y_{lm}(\hat{A})\, d\hat{A} = (-1)^{m'}\sqrt{\frac{(2l'+1)(2L+1)(2l+1)}{4\pi}} \\
\begin{pmatrix} l' & L & l \\ -m' & M & m \end{pmatrix}\begin{pmatrix} l' & L & l \\ 0 & 0 & 0 \end{pmatrix} \tag{A.12}$$

- Sums over 3-j symbols

$$\sum_{\mu_1\mu_2\mu_3}(-1)^{l_1+l_2+l_3+\mu_1+\mu_2+\mu_3}\begin{pmatrix} j_1 & l_2 & l_3 \\ m_1 & \mu_2 & -\mu_3 \end{pmatrix}\begin{pmatrix} l_1 & j_2 & l_3 \\ -\mu_1 & m_2 & \mu_3 \end{pmatrix} \\
\begin{pmatrix} l_1 & l_2 & j_3 \\ \mu_1 & -\mu_2 & m_3 \end{pmatrix} = \begin{pmatrix} j_1 & j_2 & j_3 \\ m_1 & m_2 & m_3 \end{pmatrix}\begin{Bmatrix} j_1 & j_2 & j_3 \\ l_1 & l_2 & l_3 \end{Bmatrix} \tag{A.13}$$

- Matrix element of irreducible tensors

$$
\begin{aligned}
\langle \alpha \jmath_1 \jmath_2 \jmath m | T^{(k)} \cdot U^{(k)} | \alpha' \jmath_1' \jmath_2' \jmath' m' \rangle \;=\;& (-1)^{\jmath + \jmath_2 + \jmath_1'} \, \delta_{\jmath \jmath'} \, \delta_{mm'} \left\{ \begin{array}{ccc} \jmath_1' & \jmath_2' & \jmath' \\ \jmath_2 & \jmath_1 & k \end{array} \right\} \quad\text{(A.14)} \\
& \sum_{\alpha''} \langle \alpha \jmath_1 || T^{(k)} || \alpha'' \jmath_2 \rangle \langle \alpha'' \jmath_2 || U^{(k)} || \alpha' \jmath_2' \rangle
\end{aligned}
$$

- Four angular momentum recoupling formula

$$
\begin{aligned}
|(\ell_1 \ell_2)\ell_{12}, (\ell_3 \ell_4)\ell_{34}; JM\rangle \;=\;& \sum_{\ell_{13}\ell_{24}} \sqrt{\hat{\ell}_{12}\hat{\ell}_{34}\hat{\ell}_{13}\hat{\ell}_{24}} \left\{ \begin{array}{ccc} \ell_1 & \ell_3 & \ell_{13} \\ \ell_2 & \ell_4 & \ell_{24} \\ \ell_{12} & \ell_{34} & J \end{array} \right\} \\
& |(\ell_1 \ell_3)\ell_{13}, (\ell_2 \ell_4)\ell_{24}; JM\rangle \quad\quad\quad \text{(A.15)}
\end{aligned}
$$

where $\hat{a} = 2a + 1$.

Appendix B EST EXPANSIONS

In Chapter 4 we make use of separable expansions of the two-body baryon-baryon potentials to calculate the triton bound state. Here we explain the construction of an EST expansion of a general two-body potential following Refs. [100, 102, 160].

The method can also be found in the original work of Ernst et al. [160]. In Sect. B.1 we review the concept of separable kernels for integral equations. Then in Sect. B.2 we consider a particular integral equation which is relevant: Lippmann-Schwinger equation. The use of separable kernels is of interest when many body problems are being considered. However, we consider the two-body problem as it illustrates their convenience.

B.1 Mathematical introduction

Let us consider the following general mathematical problem:

$$f = h + K[f]\,, \tag{B.1}$$

where h is a known function, K is called the kernel of the problem and f is the unknown function we want to find.

As an example we can consider the problem in one dimension:

$$f(x) = h(x) + \int dy\, K(x,y)\, f(y)\,. \tag{B.2}$$

One of the easiest cases where this integral equation can be readily solved corresponds to the case when the kernel is *separable*. That corresponds to the case where the kernel accepts the following factorization:

$$K(x,y) = \bar{\varphi}(x)\varphi(y)\,, \tag{B.3}$$

in this case the solution of Eq. (B.2) can be obtained analytically in a few steps:

$$f(x) = h(x) + c\bar{\varphi}(x) \tag{B.4}$$

with

$$
\begin{aligned}
c &= \int dy\, \varphi(y) f(y) = \int dy\, \varphi(y) h(y) + c \int dy\, \varphi(y)\bar{\varphi}(y) \\
&\Rightarrow\ c = \frac{\int dy\, \varphi(y)\, h(y)}{1 - \int dy\varphi(y)\bar{\varphi}(y)}
\end{aligned}
\tag{B.5}
$$

This shows that an, in principle, difficult to treat problem as is Eq. (B.2) turns out to be analytically solvable when the kernel appearing in the integral equation can be written as in a separable form. This suggests a possible way of obtaining approximate solutions to integral equations: finding separable expansions of the kernels so that the equation can be split up in several easily solvable parts.

B.2   Physical example: Two-body scattering

In scattering theory and many body physics we deal with equations similar to Eq. (B.1) as are the Lippmann-Schwinger (LS) (or any integral version of the Schödinger equation) and the Faddeev equations. We concentrate on the first one as it serves to illustrate the method and also because it is used when building separable representations of two-body forces.

The Lippmann-Schwinger equation for the wave function reads

$$\left|\phi^{(+)}(\vec{p})\right\rangle = |\vec{p}\rangle + g_0(e_p + i0)\, v\, \left|\phi^{(+)}(\vec{p})\right\rangle , \qquad (B.6)$$

where

$$
\begin{aligned}
g_0(z) &= \frac{1}{z - h_0}, \\
g(z) &= \frac{1}{z - h}, \\
|\vec{p}\rangle &= i0\, g_0(e_p + i0)\, |\vec{p}\rangle , \\
\left|\phi^{(+)}(\vec{p})\right\rangle &= i0 g(e_p + i0)\, .\, |\vec{p}\rangle
\end{aligned}
\qquad (B.7)
$$

$i0$ stands for $\lim_{\varepsilon \to 0} i\varepsilon$.

In the next section we give the precise definition of the separable potential for a given two-body interaction. We explain in detail the solution of the LS equation. However we should notice that the construction of the separable version needs the numerical solution of the LS equation first so it makes no sense to build a separable version of a given potential to calculate two-body scattering. The interest in building such expansions is clearly seen when many-body problems are considered.

B.3   Definition of the Separable expansion

We define our separable version of the original potential in the following way,

$$\bar{v} = \sum_{\pi J T M_J M_T} \sum_{ij} \left|g^{i\pi JT}; M_J, M_T\right\rangle \lambda^{(i\pi JT)(j\pi JT)} \left\langle g^{j\pi JT}; M_J, M_T\right| . \qquad (B.8)$$

In the case we are considering, baryon-baryon systems, the strong force does not connect states with different J, π or T and thus in the following we can restrict ourselves to certain

J, π, T:

$$\bar{v} = \sum_{ij} \left| g^i \right\rangle \lambda^{ij} \left\langle g^j \right| . \qquad (B.9)$$

The EST method wants the original potential, v, and its separable version, $\bar{v}$, to produce the same on and half-off-shell t matrix for a certain set of energies, E_i, with corresponding momenta, p_i, and orbital angular momentum, L_i.

To define the objects appearing in Eq. (B.8) we first introduce the following set of states,

$$\left| \psi^i \right\rangle \equiv \begin{cases} |\text{deuteron wave}\rangle & \text{if in } {}^3S_1 - {}^3D_1 \\ |\phi(z_i, p_i)(L_i, S_i)T\rangle \equiv |\psi_{\alpha_i}\rangle \end{cases} \qquad (B.10)$$

satisfying equation,

$$|\psi_{\alpha_i}\rangle = |\phi_i\rangle + \mathcal{P} \; g_0(z_i) v \, |\psi_{\alpha_i}\rangle \; , \qquad (B.11)$$

with $\mathcal{P}$ being a principal value integration. This definition includes two different kind of states $|\psi_{\alpha_i}\rangle$:

- if $z_i = \frac{p_i^2}{2\mu}$ then $|\psi_{\alpha_i}\rangle$ is a scattering state

- if $z_i < 0$ then $|\psi_{\alpha_i}\rangle$ has no physical meaning

The form factors $\left| g^i \right\rangle$ and the matrix λ^{ij} are defined in the following way,

$$\begin{aligned} \left| g^i \right\rangle &\equiv v \left| \psi^i \right\rangle \\ \sum_j \lambda^{ij} \langle \psi^j | v | \psi^k \rangle &\equiv \delta_{ik} . \end{aligned} \qquad (B.12)$$

It is easy to proof that the second definition in Eq. (B.12) ensures that,

$$v \left| \psi^i \right\rangle = \bar{v} \left| \psi^i \right\rangle \; , \qquad (B.13)$$

lets see,

$$\begin{aligned} v \left| \psi^i \right\rangle &= \sum_j \left[\sum_k \lambda^{jk} \langle \psi^k | v | \psi^i \rangle \right] v \left| \psi^j \right\rangle \\ &= \bar{v} \left| \psi^i \right\rangle . \end{aligned} \qquad (B.14)$$

R matrix

Now we can obtain an analytic expression for the R matrix corresponding to the separable potential:

$$\begin{aligned} \bar{R}(z) &= \bar{v} + \bar{v} \, \mathcal{P} g_0(z) \, \bar{R}(z) \\ &= \sum_{ij} \left| g^i \right\rangle D_{ij}(z) \left\langle g^j \right| , \end{aligned} \qquad (B.15)$$

with

$$D_{ij} = \left[\Lambda^{-1} - G(E) \right]_{ij}^{-1} \tag{B.16}$$

and

$$\begin{aligned}
(\Lambda)_{ij} &= \lambda_{ij} \\
(G(E))_{ij} &= \langle g^i | \mathcal{P} g_0(E) | g^j \rangle \,.
\end{aligned} \tag{B.17}$$

It is important to note that the separable expansion itself does not contain any energy dependence, all the energy dependence comes from the resolvent.

We need to prove that both the original R matrix and the separable one $\bar{R}$ have the same half-off shell values for the set of energies E_i. Consider,

$$\begin{aligned}
\bar{R}(E) &= \sum_{ij} \left| g^i \right\rangle D_{ij}(E) \left\langle g^j \right| \\
\text{with} \qquad D_{ij}^{-1}(E) &= (\Lambda^{-1})_{ij} - G_{ij}(E) \\
(\Lambda^{-1})_{ij} &= \langle \psi^i | v | \psi^j \rangle \\
G_{ij}(E) &= \langle \psi^i | v \, \mathcal{P} g_0(E) \, v | \psi^j \rangle \\
\Rightarrow \qquad D_{ij}^{-1}(E) &= \langle \psi^i | v - v \mathcal{P} g_0(E) \, v | \psi^j \rangle \\
\Rightarrow \qquad \sum_j D_{ij}(E) \langle \psi^j | v - v \mathcal{P} g_0(E) \, v | \psi^k \rangle &= \delta_{ik} \,.
\end{aligned} \tag{B.18}$$

If $\left| \psi^j \right\rangle$ is a scattering state we have,

$$[v - v \, \mathcal{P} g_0(E_j) \, v] \left| \psi^j \right\rangle = v \left| \phi^j \right\rangle \tag{B.19}$$

The half off-shell is,

$$\begin{aligned}
\bar{R}(E_K) \left| \phi^k \right\rangle &= \sum_{ij} \left| g^i \right\rangle D^{ij}(E_k) \langle g^i | \phi_k \rangle \\
&= \sum_{ij} \left| g^i \right\rangle D^{ij}(E_k) \langle \psi^j | v - v \mathcal{P} g_0(E_k) \, v | \psi^k \rangle \\
&= \left| g^k \right\rangle = v \left| \psi^k \right\rangle = R(E_k) \left| \phi^k \right\rangle \,.
\end{aligned} \tag{B.20}$$

B.4 Numerical implementation

For the method to be operational one needs to cast the form factors $\langle pLS | g^i \rangle$ into analytic functions. The way to achieve that is to first calculate them on a mesh of gauss-legendre points solving the following equations.

- if $\left| \psi^i \right\rangle$ is a scattering state

$$\begin{aligned}
\langle pLS | v | \psi_{\alpha_i} \rangle &= \langle pLS | R(E_i) | \phi_{\alpha_i} \rangle \\
&= R_{L\ell_i S s_i}^T(p, p_i)
\end{aligned} \tag{B.21}$$

and these quantities satisfy,

$$
\begin{aligned}
R^T_{L'S'LS}(q',q) &= V^T_{L'S'LS}(q',q) \\
&+ \frac{2}{\pi} \sum_{L''S''} \int_0^\infty dk \; k^2 \; V^T_{L''S''LS}(q',k) \mathcal{P} \frac{1}{E_q - E_k} R^T_{L'S'LS}(k,q) \,.
\end{aligned}
\tag{B.22}
$$

- If $|\psi^i\rangle$ is a bound state We have a similar equation, without poles in this case, for the state,

$$
|\psi_d\rangle = g_0(e_d) \; v \; |\psi_d\rangle \,.
\tag{B.23}
$$

The Hanover-Jülich group [102] casts the form factors into analytic functions which are essentially Gegenbauer polynomials,

$$
\langle pLS|g^i\rangle = \frac{p^L}{(p^2 + \beta_{2i}^2)^m} \left\{ \beta_{1i} + p^2 \left[C_{1i} + (C_{2i}x - C_{3i}) \sum_n a_n G_n^{5/2}(x) \right] \right\} ,
\tag{B.24}
$$

with

$$
x = \frac{p^2/\beta_{3i}^2 - 1}{p^2/\beta_{3i}^2 + 1} \,.
\tag{B.25}
$$

Appendix C NN^* NORM

We give the explicit expression for the overlapping of the $NN^*(1440)$ wave function appeared in Eq. (5.1) of Chapter 5

$$
\begin{aligned}
\mathcal{N}_L^{\mathrm{di}}(R) &= \left[\frac{2}{3}T_1 + \frac{1}{3}T_7 + (-)^f\frac{2}{3}T_2\right] \\
\mathcal{N}_L^{\mathrm{ex}}(R) &= \left[\frac{2}{3}T_3 + \frac{1}{3}T_8 + (-)^f\frac{2}{3}T_4\right] + 2\left[\frac{2}{3}T_5 + (-)^f\frac{2}{3}T_6\right]
\end{aligned}
\tag{C.1}
$$

with

$$
\begin{aligned}
T_1 &= 8\pi e^{-\alpha}\left\{\imath_L(\alpha) - \frac{R^2}{6b^2}\imath_L(\alpha) + \frac{R^2}{6b^2}F_1(L,\alpha)\right. \\
&\qquad\left. + \frac{R^4}{96b^4}\imath_L(\alpha) - \frac{R^4}{48b^4}F_1(L,\alpha) + \frac{R^4}{96b^4}F_2(L,\alpha)\right\} \\
T_2 &= 8\pi e^{-\alpha}\left\{\frac{R^4}{96b^4}\imath_L(\alpha) - \frac{R^4}{48b^4}F_1(L,\alpha) + \frac{R^4}{96b^4}F_2(L,\alpha)\right\} \\
T_3 &= 8\pi e^{-\alpha}\left\{\frac{R^4}{96b^4}\imath_L(\beta) + \frac{R^4}{48b^4}F_1(L,\beta) + \frac{R^4}{96b^4}F_2(L,\beta)\right\} \\
T_4 &= 8\pi e^{-\alpha}\left\{\imath_L(\beta) - \frac{R^2}{6b^2}\imath_L(\beta) - \frac{R^2}{6b^2}F_1(L,\beta)\right. \\
&\qquad\left. + \frac{R^4}{96b^4}\imath_L(\beta) + \frac{R^4}{48b^4}F_1(L,\beta) + \frac{R^4}{96b^4}F_2(L,\beta)\right\} \\
T_5 &= 8\pi e^{-\alpha}\left\{\imath_L(\beta) - \frac{R^2}{6b^2}\imath_L(\beta) + \frac{R^2}{6b^2}F_1(L,\beta)\right. \\
&\qquad\left. + \frac{R^4}{96b^4}\imath_L(\beta) - \frac{R^4}{48b^4}F_1(L,\beta) + \frac{R^4}{96b^4}F_2(L,\beta)\right\} \\
T_6 &= 8\pi e^{-\alpha}\left\{\frac{R^4}{96b^4}\imath_L(\beta) - \frac{R^4}{48b^4}F_1(L,\beta) + \frac{R^4}{96b^4}F_2(L,\beta)\right\} \\
T_7 &= 8\pi e^{-\alpha}\left\{\imath_L(\alpha) - \frac{R^2}{6b^2}\imath_L(\alpha) + \frac{R^2}{6b^2}F_1(L,\alpha)\right.
\end{aligned}
\tag{C.2}
$$

$$+ \frac{R^4}{48b^4} \imath_L(\alpha) - \frac{R^4}{24b^4} F_1(L, \alpha) + \frac{R^4}{48b^4} F_2(L, \alpha) \Big\}$$

$$T_8 = 8\pi e^{-\alpha} \left\{ \imath_L(\beta) - \frac{R^2}{6b^2} \imath_L(\beta) + \frac{R^2}{6b^2} F_1(L, \beta) \right.$$

$$\left. + \frac{R^4}{48b^4} \imath_L(\beta) - \frac{R^4}{24b^4} F_1(L, \beta) + \frac{R^4}{48b^4} F_2(L, \beta) \right\} , \qquad \text{(C.3)}$$

where α and β are defined by:

$$\alpha = \frac{3R^2}{4b^2}$$

$$\beta = \frac{R^2}{4b^2} , \qquad \text{(C.4)}$$

and the functions F_1 and F_2 are given in Eq. (A.6) where $\imath_L(x)$ is the modified spherical Bessel function of the first kind.

Appendix D $NN^* \rightarrow NN^*$ POTENTIALS

We describe in detail the technical steps to calculate the direct NN^* potential [1].

The local potential is defined in Chapter 3, Eq. (3.28).

We explain the procedure to calculate the interaction potential for those diagrams containing a quark in an orbital state ϕ_{1s} in both the initial and final states. The remaining terms can be obtained using analogous procedures.

Let us suppose for the sake of generality that we are calculating a tensor term, the particular case of central potentials will be easily reduced from this one.

D.0.1 Wave functions, normalizations and overlappings

Let us denote Ψ_{6q} the 6 quark wave function. As explained in Chapter 3, three of the quarks are building one baryon and the other three are making the other baryon.

$$\int \Psi_{6q}(\mathbf{r_1}, \mathbf{r_2}, \mathbf{r_3}, \mathbf{r_4}, \mathbf{r_5}, \mathbf{r_6}, \mathbf{R}). \tag{D.1}$$

This wave function has a well defined spin-isospin and color parts. We can construct the angular momentum projection and consider the states:

$$[\Psi_{6q}^{LS}]^J = [\Psi_{6q}^L \otimes \chi_{ST}]^J \xi_c. \tag{D.2}$$

The tensor interactions we consider, scalar interactions can be readily obtained from these ones, are of the general form,

$$V(\mathbf{r}_{ij}) = V(r_{ij}) S_{ij} \tau_i \cdot \tau_j \tag{D.3}$$

where $\mathbf{r}_{ij} = |\mathbf{r_i} - \mathbf{r_j}|$, S_{ij} is the quark tensor operator and τ_i are the Pauli matrices.

The single quark wave functions are taken as harmonic oscillator states. We are going to consider the components which only include quarks in 0s and 1s harmonic oscillator wave functions:

$$
\begin{aligned}
\phi_{0S} &= \left(\frac{1}{\pi b^2}\right)^{3/4} e^{-\frac{r^2}{2b^2}} \\
\phi_{1S} &= \sqrt{\frac{2}{3}} \left(\frac{1}{\pi b^2}\right)^{3/4} e^{-\frac{r^2}{2b^2}} \left[\frac{3}{2} - \frac{r^2}{b^2}\right].
\end{aligned} \tag{D.4}
$$

_____

[1] We denote the three vectors as $\mathbf{r}$ instead of $\vec{r}$ to make the expressions clearer.

They are orthonormalized in the following way,

$$
\begin{aligned}
\int d\mathbf{r}\, \phi_{0S}(\mathbf{r})\, \phi_{0S}(\mathbf{r}) &= 1 \\
\int d\mathbf{r}\, \phi_{1S}(\mathbf{r})\, \phi_{1S}(\mathbf{r}) &= 1 \\
\int d\mathbf{r}\, \phi_{1S}(\mathbf{r})\, \phi_{0S}(\mathbf{r}) &= 0\,.
\end{aligned}
\tag{D.5}
$$

In the calculation we are performing one often has overlappings between the non-interacting quarks that can be obtained analytically. Here we write the ones we use,

$$
\begin{aligned}
\Delta(\mathbf{A},\mathbf{B}) = \int d\mathbf{r}\, \phi_{0S}(\mathbf{r}-\mathbf{A})\, \phi_{0S}(\mathbf{r}-\mathbf{B}) &= e^{\frac{-1}{4b^2}(\mathbf{A}-\mathbf{B})^2} \\
\Sigma(\mathbf{A},\mathbf{B}) = \int d\mathbf{r}\, \phi_{0S}(\mathbf{r}-\mathbf{A})\, \phi_{1S}(\mathbf{r}-\mathbf{B}) &= -\sqrt{\frac{2}{3}}\frac{(\mathbf{A}-\mathbf{B})^2}{4b^2}e^{\frac{-1}{4b^2}(\mathbf{A}-\mathbf{B})^2} \\
\Lambda(\mathbf{A},\mathbf{B}) = \int d\mathbf{r}\, \phi_{1S}(\mathbf{r}-\mathbf{A})\, \phi_{1S}(\mathbf{r}-\mathbf{B}) &= e^{\frac{-1}{4b^2}(\mathbf{A}-\mathbf{B})^2}\left\{1 - \frac{(\mathbf{A}-\mathbf{B})^2}{3b^2} + \frac{(\mathbf{A}-\mathbf{B})^4}{24b^4}\right\}.
\end{aligned}
\tag{D.6}
$$

D.0.2 The interaction kernel

The interaction potential is defined as (without the norm),

$$
V^{LL'SS'}(R) = \langle [\Psi_{6q}^{L'S'}]^J | V(\mathbf{r}_{ij}) | [\Psi_{6q}^{LS}]^J \rangle\,.
\tag{D.7}
$$

That using the relation given in Eq. (A.15) can be written as,

$$
\begin{aligned}
V^{LL'SS'}(R) &= \sqrt{6}(-)^{L+S'+J}\left\{\begin{array}{ccc} L & S & J \\ S' & L' & 2 \end{array}\right\} \langle \chi_{S'T} || V^{S\rightarrow S'TC} || \chi_{ST}\rangle \\
&\times\; \langle \Psi_{6q}^{L'}(\mathbf{r_1},...,\mathbf{r_6},R) || V^{L\rightarrow L'}(\mathbf{r}_{ij}) || \Psi_{6q}^{L}(\mathbf{r_1},...,\mathbf{r_6},R)\delta(R-R')\,.
\end{aligned}
\tag{D.8}
$$

The spin-isospin-color part can be obtained independently,

$$
C^{SS'TC} = \langle \xi_c \chi_{S'T} || V^{S\rightarrow S'TC} || \xi_c \chi_{ST}\rangle\,.
\tag{D.9}
$$

The presence of the quark antisymmetry operator together with the sum over the various quark pairs implicit in Eq. (D.7) gives rise to many terms depending on which quarks are interacting. We consider only one of them, the one which corresponds to interaction between quarks 2 and 5, V_{25}. Therefore, the remaining radial integral we need to calculate is the following,

$$
\begin{aligned}
H = \;&\int d\hat{R}\int d\hat{R}'\, Y_{L'0}(\hat{R}')Y_{L0}(\hat{R})\int d\mathbf{r_1}..d\mathbf{r_6} \\
&\phi_{0S}(\mathbf{r_1}-\mathbf{A_1})\,\phi_{1S}(\mathbf{r_2}-\mathbf{B_1})\,\phi_{0S}(\mathbf{r_3}-\mathbf{C_1}) \\
&\phi_{0S}(\mathbf{r_4}-\mathbf{D_1})\,\phi_{0S}(\mathbf{r_5}-\mathbf{E_1})\,\phi_{0S}(\mathbf{r_6}-\mathbf{F_1}) \\
&V(r_{25}) \\
&\phi_{0S}(\mathbf{r_1}-\mathbf{A_2})\,\phi_{1S}(\mathbf{r_2}-\mathbf{B_2})\,\phi_{0S}(\mathbf{r_3}-\mathbf{C_2}) \\
&\phi_{0S}(\mathbf{r_4}-\mathbf{D_2})\,\phi_{0S}(\mathbf{r_5}-\mathbf{E_2})\,\phi_{0S}(\mathbf{r_6}-\mathbf{F_2})\,.
\end{aligned}
\tag{D.10}
$$

$$H = \frac{2}{3}\left(\frac{1}{\pi b^2}\right)^3 \Delta(\mathbf{A_1}, \mathbf{A_2})\,\Delta(\mathbf{C_1}, \mathbf{C_2})\,\Delta(\mathbf{D_1}, \mathbf{D_2})\,\Delta(\mathbf{F_1}, \mathbf{F_2})$$

$$\int d\hat{R} \int d\hat{R}'\, Y_{L'0}(\hat{R}')\, Y_{L0}(\hat{R}) \int d\mathbf{r_2}\, d\mathbf{r_5} \tag{D.11}$$

$$\exp\left\{\frac{-1}{2b^2}\left[(\mathbf{r_2} - \mathbf{B_1})^2 + (\mathbf{r_5} - \mathbf{E_1})^2\right]\right\}$$

$$\exp\left\{\frac{-1}{2b^2}\left[(\mathbf{r_2} - \mathbf{B_2})^2 + (\mathbf{r_5} - \mathbf{E_2})^2\right]\right\}$$

$$V(r_{25})\left[\frac{3}{2} - \frac{(\mathbf{r_2} - \mathbf{B_1})^2}{b^2}\right]\left[\frac{3}{2} - \frac{(\mathbf{r_2} - \mathbf{B_2})^2}{b^2}\right].$$

$\mathbf{A_1}$, $\mathbf{B_1}$, $\mathbf{C_1}$, $\mathbf{D_1}$, $\mathbf{E_1}$ and $\mathbf{F_1}$ are the positions of the six quarks in the initial configuration that can be either, $\mathbf{R}/2$ or $-\mathbf{R}/2$ while $\mathbf{A_2}$, $\mathbf{B_2}$, $\mathbf{C_2}$, $\mathbf{D_2}$, $\mathbf{E_2}$ and $\mathbf{F_2}$ are the positions of the quarks in the final configuration that can be, $\mathbf{R}'/2$ or $-\mathbf{R}'/2$. The following change of variables leaves the expression in a much simpler form,

$$\mathbf{R_{25}} = \frac{\mathbf{r_2} + \mathbf{r_5}}{2} \tag{D.12}$$
$$\mathbf{r_{25}} = \mathbf{r_2} - \mathbf{r_5},$$

Then we can consider the integral part, I, defined as:

$$I = \exp\left\{\frac{-1}{2b^2}\left[\frac{-(\mathbf{B_1} + \mathbf{E_1} + \mathbf{B_2} + \mathbf{E_2})^2}{4} + B_1^2 + B_2^2 + E_1^2 + E_2^2\right]\right\}$$

$$\int d\mathbf{r_2}\, d\mathbf{r_5}\, V(r_{25}) \exp\left\{\frac{-1}{2b^2}\left[r_{25}^2 - \mathbf{r_{25}} \cdot (\mathbf{B_1} - \mathbf{E_1} + \mathbf{B_2} - \mathbf{E_2})\right]\right\}$$

$$\int d\mathbf{r_{25}} \exp\left\{\frac{-2}{b^2}\left[\mathbf{r_{25}} - \frac{(\mathbf{B_1} + \mathbf{E_1} + \mathbf{B_2} + \mathbf{E_2})}{4}\right]^2\right\} \tag{D.13}$$

$$\left[\frac{3}{2} - \frac{(\mathbf{r_{25}} - \frac{\mathbf{r_{25}}}{2} - \mathbf{E_1})^2}{b^2}\right]\left[\frac{3}{2} - \frac{(\mathbf{r_{25}} - \frac{\mathbf{r_{25}}}{2} - \mathbf{E_2})^2}{b^2}\right],$$

and rearrange the terms in the following way,

$$\begin{array}{lll}
\mathbf{P} &=& \frac{1}{4}(\mathbf{B_1} + \mathbf{E_1} + \mathbf{B_2} + \mathbf{E_2}) \qquad \mathbf{X} &=& \mathbf{r_{25}} - \mathbf{P} \\
\mathbf{S} &=& -\frac{\mathbf{r_{25}}}{2} - \mathbf{E_2} \qquad\qquad\qquad\quad \mathbf{Q} &=& -\frac{\mathbf{r_{25}}}{2} - \mathbf{E_1} \\
\mathbf{PQ} &=& \mathbf{P} - \mathbf{Q} \qquad\qquad\qquad\qquad\quad \mathbf{PS} &=& \mathbf{P} - \mathbf{S}.
\end{array} \tag{D.14}$$

The jacobian of the coordinate transformation (involved in the integral) is one and therefore we get,

$$I = \exp\left\{\frac{-1}{2b^2}\left[\frac{-(\mathbf{B_1} + \mathbf{E_1} + \mathbf{B_2} + \mathbf{E_2})^2}{4} + B_1^2 + B_2^2 + E_1^2 + E_2^2\right]\right\}$$

$$\int d\mathbf{r_{25}}\, V(r_{25}) \exp\left\{\frac{-1}{2b^2}\left[r_{25}^2 - \mathbf{r_{25}} \cdot (\mathbf{B_1} - \mathbf{E_1} + \mathbf{B_2} - \mathbf{E_2})\right]\right\}$$

$$\int d\mathbf{X} \exp\left\{\frac{-2X^2}{b^2}\right\}\left[\frac{3}{2} - \frac{(\mathbf{X} + \mathbf{PQ})^2}{b^2}\right]\left[\frac{3}{2} - \frac{(\mathbf{X} + \mathbf{PS})^2}{b^2}\right], \tag{D.15}$$

it is convenient to remember at this point that $\mathbf{PQ}$ and $\mathbf{PS}$ depend on $\mathbf{X}$ that means $\int d\mathbf{X}$ can be obtained analytically.

$$
\begin{aligned}
I \;=\; & \exp\left\{\frac{-1}{2b^2}\left[\frac{-(\mathbf{B_1}+\mathbf{E_1}+\mathbf{B_2}+\mathbf{E_2})^2}{4}+B_1^2+B_2^2+E_1^2+E_2^2\right]\right\} \\
& \int d\mathbf{r_{25}}V(r_{25})\exp\left\{\frac{-1}{2b^2}\left[r_{25}^2-\mathbf{r_{25}}\cdot(\mathbf{B_1}-\mathbf{E_1}+\mathbf{B_2}-\mathbf{E_2})\right]\right\} \qquad \text{(D.16)} \\
& \frac{\pi^{\frac{3}{2}}b^3}{2^{\frac{3}{2}}}\left[\frac{15}{16}+\frac{\mathbf{PQ}^2+\mathbf{PS}^2}{b^2}\frac{-3}{4}+\frac{\mathbf{PQ}\cdot\mathbf{PS}}{b^2}+\frac{\mathbf{PS}^2\mathbf{PQ}^2}{b^4}\right].
\end{aligned}
$$

We can now return to our full expression,

$$
\begin{aligned}
H \;=\; & \frac{2}{3}\frac{1}{2^{\frac{3}{2}}\pi^{\frac{3}{2}}b^3}\int d\hat{R}\int d\hat{R}'\,Y_{L'0}(\hat{R}')Y_{L0}(\hat{R}) \\
& \exp\left\{\frac{-1}{2b^2}\left[\frac{-(\mathbf{B_1}+\mathbf{E_1}+\mathbf{B_2}+\mathbf{E_2})^2}{4}+B_1^2+B_2^2+E_1^2+E_2^2\right]\right\} \\
& \Delta(\mathbf{A_1},\mathbf{A_2})\Delta(\mathbf{C_1},\mathbf{C_2})\Delta(\mathbf{D_1},\mathbf{D_2})\Delta(\mathbf{F_1},\mathbf{F_2}) \\
& \int d\mathbf{r_{25}}V(r_{25})\exp\left\{\frac{-1}{2b^2}\left[r_{25}^2-\mathbf{r_{25}}\cdot(\mathbf{B_1}-\mathbf{E_1}+\mathbf{B_2}-\mathbf{E_2})\right]\right\} \\
& \left[\frac{15}{16}+\frac{\mathbf{PQ}^2+\mathbf{PS}^2}{b^2}\frac{-3}{4}+\frac{\mathbf{PQ}\cdot\mathbf{PS}}{b^2}+\frac{\mathbf{PS}^2\mathbf{PQ}^2}{b^4}\right].
\end{aligned}
$$

Regrouping the exponential terms in the following way,

$$
\begin{aligned}
\exp\frac{-1}{2b^2}&\left\{r_{25}^2-B\mathbf{S}\cdot\mathbf{r_{25}}-E\mathbf{S}'\cdot\mathbf{r_{25}}-C\mathbf{S}\cdot\mathbf{S}'+ES^2+DS^2\right\} \;=\; \qquad \text{(D.17)} \\
& \Delta(\mathbf{A_1},\mathbf{A_2})\Delta(\mathbf{C_1},\mathbf{C_2})\Delta(\mathbf{D_1},\mathbf{D_2})\Delta(\mathbf{F_1},\mathbf{F_2}) \quad\times \\
\exp\frac{-1}{2b^2}&\left\{\frac{-(\mathbf{B_1}+\mathbf{E_1}+\mathbf{B_2}+\mathbf{E_2})^2}{4}+B_1^2+B_2^2+E_1^2+E_2^2\right\} \quad\times \\
& \exp\frac{-1}{2b^2}\left\{r_{25}^2-\mathbf{r_{25}}\cdot(\mathbf{B_1}-\mathbf{E_1}+\mathbf{B_2}-\mathbf{E_2})\right\} \qquad\qquad ,
\end{aligned}
$$

we have,

$$
\begin{aligned}
H \;=\; & \frac{2}{3}\frac{1}{2^{\frac{3}{2}}\pi^{\frac{3}{2}}b^3}\int d\hat{R}\int d\hat{R}'\,Y_{L'0}(\hat{R}')Y_{L0}(\hat{R})\int d\mathbf{r_{25}}V(r_{25}) \\
& \exp\left\{\frac{-1}{2b^2}\left[r_{25}^2-B\mathbf{S}\cdot\mathbf{r_{25}}-E\mathbf{S}'\cdot\mathbf{r_{25}}-C\mathbf{S}\cdot\mathbf{S}'+ES^2+DS^2\right]\right\} \\
& \left[\frac{15}{16}+\frac{\mathbf{PQ}^2+\mathbf{PS}^2}{b^2}\frac{-3}{4}+\frac{\mathbf{PQ}\cdot\mathbf{PS}}{b^2}+\frac{\mathbf{PS}^2\mathbf{PQ}^2}{b^4}\right]. \qquad \text{(D.18)}
\end{aligned}
$$

This expression is analogous to the one obtained in Ref. [15] for the case of the $NN \rightarrow N\Delta$ transition potential. In our case we have that the integral contains terms, in brackets, with

angular dependence that we need to simplify in a different way.

$$\mathbf{PQ} = \frac{1}{4}(\mathbf{B_1} + \mathbf{E_1} + \mathbf{B_2} + \mathbf{E_2}) - \frac{\mathbf{r_{25}}}{2} - \mathbf{E_1}$$
$$\mathbf{PS} = \frac{1}{4}(\mathbf{B_1} + \mathbf{E_1} + \mathbf{B_2} + \mathbf{E_2}) - \frac{\mathbf{r_{25}}}{2} - \mathbf{E_2} \tag{D.19}$$

Taking into account that $\mathbf{B_1}, \mathbf{E_1}, \mathbf{B_2}, \mathbf{E_2}$ are the initial and final positions of the quarks that interact we can write, PQ and PS in the following way,

$$\mathbf{PQ} = c_1\mathbf{S} + c_2\mathbf{S}' + c_3\mathbf{r_{25}}$$
$$\mathbf{PS} = d_1\mathbf{S} + d_2\mathbf{S}' + d_3\mathbf{r_{25}} \tag{D.20}$$

where c_i and d_j are numbers that depend on the diagram that we are considering.

$$\mathbf{PQ}^2 = b_0 + b_1\mu_1 + b_2\mu_2 + b_3\mu_3$$
$$\mathbf{PS}^2 = e_0 + e_1\mu_1 + e_2\mu_2 + e_3\mu_3 \tag{D.21}$$
$$\mathbf{PS} \cdot \mathbf{PS} = a_0 + a_1\mu_1 + a_2\mu_2 + a_3\mu_3 \,.$$

Where now a_i, b_i and e_i are functions that depend only on the moduli $|\mathbf{S}|$, $|\mathbf{S}'|$ and $|\mathbf{r_{25}}|$ but never on the angles between them.

$$\mu_1 = \cos(\widehat{\mathbf{r_{25}}, \mathbf{R}})$$
$$\mu_2 = \cos(\widehat{\mathbf{r_{25}}, \mathbf{R}'})$$
$$\mu_3 = \cos(\widehat{\mathbf{R}, \mathbf{R}'}) \,. \tag{D.22}$$

So, the integral H in the most general case has the form,

$$H = \frac{2}{3}\frac{1}{2^{\frac{3}{2}}\pi^{\frac{3}{2}}b^3}\int d\hat{R}\int d\hat{R}' Y_{L'0}(\hat{R}')Y_{L0}(\hat{R}) \tag{D.23}$$

$$\int d\mathbf{r_{25}}V(r_{25})\exp\left\{\frac{-1}{2b^2}\left[r_{25}^2 - A\mathbf{S}\cdot\mathbf{r_{25}} - B\mathbf{S}'\cdot\mathbf{r_{25}} - C\mathbf{S}\cdot\mathbf{S}' + ES^2 + DS^2\right]\right\}$$

$$\left[\alpha_{00} + \alpha_{01}\,\mu_1 + \alpha_{02}\,\mu_2 + \alpha_{03}\,\mu_3 + \alpha_{11}\,\mu_1^2 + \alpha_{22}\,\mu_2^2 + \alpha_{33}\,\mu_3^2 + \alpha_{12}\,\mu_1\,\mu_2\right.$$
$$\left. + \alpha_{13}\,\mu_1\,\mu_3 + \alpha_{23}\,\mu_2\,\mu_3\right] \,,$$

being α_{ij} functions again only of the moduli.

$$H = \frac{2}{3}\frac{1}{2^{\frac{3}{2}}\pi^{\frac{3}{2}}b^3}\int d\hat{R}\int d\hat{R}' Y_{L'0}(\hat{R}')\,Y_{L0}(\hat{R})\int d\mathbf{r_{25}}\,V(r_{25})\exp\left\{\frac{-1}{2b^2}\left[r_{25}^2 + ES^2 + DS^2\right]\right\}$$

$$\sum_{l=0}^{\infty}\sum_{l'=0}^{\infty}\sum_{k=0}^{\infty}(2l + 1e)(2l' + 1)(2k + 1)P_l(\mu_1)P_{l'}(\mu_2)P_k(\mu_3)\imath_l(x_1)\imath_{l'}(x_2)\imath_k(x_3)$$

$$\left[\alpha_{00} + \alpha_{01}\,\mu_1 + \alpha_{02}\,\mu_2 + \alpha_{03}\,\mu_3 + \alpha_{11}\,\mu_1^2 + \alpha_{22}\,\mu_2^2 + \alpha_{33}\,\mu_3^2 + \alpha_{12}\,\mu_1\,\mu_2\right. \tag{D.24}$$
$$\left. + \alpha_{13}\,\mu_1\,\mu_3 + \alpha_{23}\,\mu_2\,\mu_3\right] \,,$$

with $x_1 = \frac{ASr_{25}}{2b^2}$, $x_2 = \frac{BS'r_{25}}{2b^2}$ and $x_3 = \frac{CSS'}{2b^2}$. Now we make use of Eq. (A.4) obtaining,

$$
\begin{aligned}
H \;=\; & \frac{2}{3}\frac{1}{2^{\frac{3}{2}}\pi^{\frac{3}{2}}b^3}\int d\hat{R}\int d\hat{R}'\,Y_{L'0}(\hat{R}')Y_{L0}(\hat{R})\int d\mathbf{r_{25}}V(r_{25})\exp\left\{\frac{-1}{2b^2}\left[r_{25}^2+ES^2+DS^2\right]\right\} \\
& \sum_{l=0}^{\infty}\sum_{l'=0}^{\infty}\sum_{k=0}^{\infty}(2l+1)(2l'+1)(2k+1)P_l(\mu_1)P_{l'}(\mu_2)P_k(\mu_3) \\
& \begin{aligned}[t]
[\,&\alpha_{00}\,\imath_l(x_1)\,\imath_{l'}(x_2)\,\imath_k(x_3)+ && \alpha_{01}\,F_1(l,x_1)\,\imath_{l'}(x_2)\,\imath_k(x_3)+ \\
&\alpha_{02}\,\imath_l(x_1)\,F_1(l',x_2)\,\imath_k(x_3)+ && \alpha_{03}\,\imath_l(x_1)\,\imath_{l'}(x_2)\,F_1(k,x_3)+ \\
&\alpha_{11}\,F_2(l,x_1)\,\imath_{l'}(x_2)\,\imath_k(x_3)+ && \alpha_{22}\,\imath_l(x_1)\,F_2(l',x_2)\,\imath_k(x_3)+ \\
&\alpha_{33}\,\imath_l(x_1)\,\imath_{l'}(x_2)\,F_2(k,x_3)+ && \alpha_{12}\,F_1(l,x_1)\,F_1(l',x_2)\,\imath_k(x_3)+ \\
&\alpha_{13}\,F_1(l,x_1)\,\imath_{l'}(x_2)\,F_1(k,x_3)+ && \alpha_{23}\,\imath_l(x_1)\,F_1(l',x_2)\,F_1(k,x_3)\,].
\end{aligned}
\end{aligned}
\tag{D.25}
$$

The term in brackets will be shortened as $\{...\}$

$$
\begin{aligned}
H \;=\; & \frac{2}{3}\frac{1}{2^{\frac{3}{2}}\pi^{\frac{3}{2}}b^3}\int d\hat{R}\int d\hat{R}'\,Y_{L'0}(\hat{R}')\,Y_{L0}(\hat{R})\int d\mathbf{r_{25}}V(r_{25})\exp\left\{\frac{-1}{2b^2}\left[r_{25}^2+ES^2+DS^2\right]\right\} \\
& \sum_{l=0}^{\infty}\sum_{l'=0}^{\infty}\sum_{k=0}^{\infty}(2l+1)(2l'+1)(2k+1)P_l(\mu_1)P_{l'}(\mu_2)P_k(\mu_3)\{...\},
\end{aligned}
\tag{D.26}
$$

$$
\begin{aligned}
H \;=\; & \frac{2}{3}\frac{(4\pi)^3}{2^{\frac{3}{2}}\pi^{\frac{3}{2}}b^3}\int d\hat{R}\int d\hat{R}'\,Y_{L'0}(\hat{R}')\,Y_{L0}(\hat{R})\int d\mathbf{r_{25}}V(r_{25})\exp\left\{\frac{-1}{2b^2}\left[r_{25}^2+ES^2+DS^2\right]\right\} \\
& \sum_{l,l',k=0}^{\infty}\sum_{m,m',p}\{...\}Y_{lm}(\hat{R})\,Y_{lm}^*(\hat{r_{25}})\,Y_{l'm'}(\hat{R}')\,Y_{l'm'}^*(\hat{r_{25}})\,Y_{kp}(\hat{R})\,Y_{kp}^*(\hat{R}')
\end{aligned}
\tag{D.27}
$$

where we have used,

$$
P_l(\hat{A}\hat{B}) = \frac{4\pi}{2l+1}\sum_{m=-l}^{l}Y_{lm}(\hat{A})\,Y_{lm}^*(\hat{B})\,.
\tag{D.28}
$$

Reordering the integrations and writing the tensor dependence of the interaction in an explicit form, $(Y_{20}(\hat{r_{25}}))$:

$$
\begin{aligned}
H \;=\; & \frac{2}{3}\frac{(4\pi)^3}{2^{\frac{3}{2}}\pi^{\frac{3}{2}}b^3}\sqrt{\frac{4\pi}{5}}\sum_{l,l',k=0}^{\infty}\int dr_{25}\,r_{25}^2 V(r_{25})\exp\left\{\frac{-1}{2b^2}\left[r_{25}^2+ES^2+DS^2\right]\right\}\{...\} \\
& \sum_{m,m',p}\int d\hat{R}\,Y_{L0}(\hat{R})\,Y_{lm}(\hat{R})\,Y_{kp}(\hat{R}) \\
& \int d\hat{R}'\,Y_{L'0}(\hat{R}')\,Y_{l'm'}(\hat{R}')\,Y_{kp}^*(\hat{R}') \\
& \int d\Omega_{25}\,Y_{lm}^*(\hat{r_{25}})\,Y_{l'm'}^*(\hat{r_{25}})\,Y_{20}(\hat{r_{25}})\,.
\end{aligned}
\tag{D.29}
$$

We can integrate the spherical harmonics using Eq. (A.12),

$$
\begin{aligned}
H \;=\; & \frac{2}{3}\frac{(4\pi)^3}{2^{\frac{3}{2}}\pi^{\frac{3}{2}}b^3}\sum_{l,l',k=0}^{\infty}\sqrt{\frac{(2l+1)(2L+1)(2k+1)}{4\pi}}\begin{pmatrix} l & L & k \\ 0 & 0 & 0 \end{pmatrix} \\
& \sqrt{\frac{(2l'+1)(2L'+1)(2k+1)}{4\pi}}\begin{pmatrix} l' & L' & k \\ 0 & 0 & 0 \end{pmatrix}\sqrt{(2l+1)(2l'+1)} \\
& \sum_{m}(-1)^m\begin{pmatrix} l' & 2 & l \\ -m & 0 & m \end{pmatrix}\begin{pmatrix} l & L & k \\ -m & 0 & m \end{pmatrix}\begin{pmatrix} l' & L' & k \\ -m & 0 & m \end{pmatrix} \\
& \int dr_{25}\, r_{25}^2\, V(r_{25})\exp\left\{\frac{-1}{2b^2}\left[r_{25}^2+ES^2+DS^2\right]\right\}\{...\}\begin{pmatrix} l' & 2 & l \\ 0 & 0 & 0 \end{pmatrix}. \quad \text{(D.30)}
\end{aligned}
$$

Using now Eq. (A.13) we get:

$$
\begin{aligned}
H \;=\; & \frac{2}{3}\frac{(4\pi)^3}{2^{\frac{3}{2}}\pi^{\frac{3}{2}}b^3}\sum_{l,l',k=0}^{\infty}(-1)^k\sqrt{\frac{(2l+1)(2L+1)(2k+1)}{4\pi}}\begin{pmatrix} l & L & k \\ 0 & 0 & 0 \end{pmatrix} \\
& \sqrt{\frac{(2l'+1)(2L'+1)(2k+1)}{4\pi}}\begin{pmatrix} l' & L' & k \\ 0 & 0 & 0 \end{pmatrix}\sqrt{(2l+1)(2l'+1)} \\
& \begin{pmatrix} 2 & L' & L \\ 0 & 0 & 0 \end{pmatrix}\begin{Bmatrix} 2 & L' & L \\ k & l & l' \end{Bmatrix}\begin{pmatrix} l' & 2 & l \\ 0 & 0 & 0 \end{pmatrix} \\
& \int dr_{25}\, r_{25}^2\, V(r_{25})\exp\left\{\frac{-1}{2b^2}\left[r_{25}^2+ES^2+DS^2\right]\right\}\{...\}. \qquad \text{(D.31)}
\end{aligned}
$$

This last expression can already be efficiently implemented in a computer in a reasonable time.

Appendix E SPIN-ISOSPIN-COLOR COEFFICIENTS

The techniques for the calculation of these matrix elements has been already given in several works, e.g. [15, 40]. In this section we only want to introduce the techniques.

The spin-isospin-color matrix element can be split into a color and a spin-isospin parts.

$$C^{SS'Tc} = \langle \xi_c || V^c || \xi_c \rangle \langle \chi_{S'T} || V^{S \to S'T} || \chi_{ST} \rangle, \tag{E.1}$$

$S(S')$ and T stand for the initial(final) spin and the isospin of the two-baryon system. c stands for color.

E.0.3   Color part

The six-quark color singlet state is constructed in the following way,

$$\xi_s^{6q} = \xi_s(123)\, \xi_s(456) \tag{E.2}$$

where $\xi_s(123)$ is the three-quark color singlet.

The matrix elements we are interested in are of the form,

$$\langle \xi_s^{6q} | \vec{\lambda}_i \cdot \vec{\lambda}_j \; P_{36}^c | \xi_s^{6q} \rangle \tag{E.3}$$

The permutator operator of the $SU(3)_c$ group can be written in the following way,

$$P_{ij}^c = \frac{1}{3} + \frac{\vec{\lambda}_i \cdot \vec{\lambda}_j}{2} \tag{E.4}$$

The direct terms (not involving the exchange operator) can be calculated readily,

$$\langle \xi_c^{6q} | \vec{\lambda}_i \cdot \vec{\lambda}_j | \xi_c^{6q} \rangle = \begin{cases} -\frac{8}{3} & \text{Quarks in the same cluster} \\ 0 & \text{Quarks in a different cluster} \end{cases} \tag{E.5}$$

The exchange terms can be obtained using similar arguments.

E.0.4   Spin-isospin part

We give the simplest case, which is at the same time very illustrative, of the techniques used to calculate the spin-isospin matrix elements. Let us consider the following matrix element,

$$M(S,T) = \langle B_1 B_2 | P_{36}^{ST} | B_1 B_2 \rangle, \tag{E.6}$$

where $|B_1 B_2\rangle$ is a state of six quarks with total spin S and isospin T. All the other spin-isospin-color matrix elements which appear in the derivation can be obtained using similar tools. In our derivation we will consider only the two-nucleon system, which is exactly the same as considering the $NN^*(1440)$ system in spin-isospin space.

For the case under consideration, which is, N and $N^*(1440)$ resonance we have that the two baryon wave function in spin and isospin can be written as,

$$|NN\rangle_{ST} = \frac{1}{2} \sum_{ll'=0}^{1} |(l,\frac{1}{2}),\frac{1}{2};(l',\frac{1}{2}),\frac{1}{2};S,M_S\rangle \otimes \frac{1}{2}|(l,\frac{1}{2}),\frac{1}{2};(l',\frac{1}{2}),\frac{1}{2};T,M_T\rangle \qquad (\text{E.7})$$

$$|NN^*\rangle_{ST} = \frac{1}{2} \sum_{ll'=0}^{1} |(l,\frac{1}{2}),\frac{1}{2};(l',\frac{1}{2}),\frac{1}{2};S,M_S\rangle \otimes \frac{1}{2}|(l,\frac{1}{2}),\frac{1}{2};(l',\frac{1}{2}),\frac{1}{2};T,M_T\rangle \qquad (\text{E.8})$$

to get these two-baryon wave functions one needs to take into account the fact that the nucleon and the roper are spin and isospin 1/2 particles themselves. The matrix element we are interested in evaluating is thus,

$$\begin{aligned} M(S,T) &= \frac{1}{4} \sum_{ll'l_1 l_1'} \langle (l_1,\frac{1}{2}),\frac{1}{2};(l_1',\frac{1}{2}),\frac{1}{2};T,M_T|P_{36}^T|(l,\frac{1}{2}),\frac{1}{2};(l',\frac{1}{2}),\frac{1}{2};T',M_T'\rangle \\ &\times \langle (l_1,\frac{1}{2}),\frac{1}{2};(l_1',\frac{1}{2}),\frac{1}{2};S,M_S|P_{36}^S|(l,\frac{1}{2}),\frac{1}{2};(l',\frac{1}{2}),\frac{1}{2};S',M_S'\rangle\,. \end{aligned} \qquad (\text{E.9})$$

This case we are considering appears when evaluating the exchange kernels of the OSE. We can define the following function,

$$\eta_T^{NN}(l,l') = \langle l,l';T,M_T|P_{36}^T|l,l';T,M_T\rangle \qquad (\text{E.10})$$

which simplify the matrix element giving,

$$M(S,T) = \frac{1}{4}\sum_{l,l'}\eta_T^{NN}(l,l')\eta_S^{NN}(l,l')\,. \qquad (\text{E.11})$$

The idea is to recouple the angular momenta involved in the problem till the matrix element of the two-body operator is acting on one of its eigenfunctions and then recouple back again. To do so it is very useful to consider the angular momentum recoupling formula Eq. (A.15). So we get for the η_T function:

$$\begin{aligned} \eta_T^{NN}(l,l') &= \sum_{t_{1245},t'_{1245},t_{36},t'_{36}} 4\sqrt{\hat{t}_{1245}\hat{t}'_{1245}\hat{t}_{36}\hat{t}'_{36}} \begin{Bmatrix} l & l' & t_{1245} \\ \frac{1}{2} & \frac{1}{2} & t_{36} \\ \frac{1}{2} & \frac{1}{2} & T \end{Bmatrix} \begin{Bmatrix} l & l' & t'_{1245} \\ \frac{1}{2} & \frac{1}{2} & t'_{36} \\ \frac{1}{2} & \frac{1}{2} & T \end{Bmatrix} \\ &\quad \langle (l,l')t_{1245};(\frac{1}{2},\frac{1}{2})t_{36}|P_{36}^T|(l,l')t'_{1245};(\frac{1}{2},\frac{1}{2})t'_{36}\rangle\,, \end{aligned} \qquad (\text{E.12})$$

with $\hat{a} = 2a+1$. At this point we can calculate the action of P_{36}^T explicitly,

$$\langle (l,l')t_{1245};(\frac{1}{2},\frac{1}{2})t_{36}|P_{36}^T|(l,l')t'_{1245};(\frac{1}{2},\frac{1}{2})t'_{36}\rangle = \delta_{t_{1245},t'_{1245}}\delta_{t_{36},t'_{36}}(-1)^{1+t_{36}} \qquad (\text{E.13})$$

and we finally get,

$$M(S,T) = 4 \sum_{ll'} \left\{ \begin{matrix} l & \frac{1}{2} & \frac{1}{2} \\ \frac{1}{2} & l' & \frac{1}{2} \\ \frac{1}{2} & \frac{1}{2} & S \end{matrix} \right\} \left\{ \begin{matrix} l & \frac{1}{2} & \frac{1}{2} \\ \frac{1}{2} & l' & \frac{1}{2} \\ \frac{1}{2} & \frac{1}{2} & T \end{matrix} \right\} . \tag{E.14}$$

Index

References:

[1] E. Rutherford, Phil. Mag. **21**, 669 (1911).

[2] J. Chadwick, Nature **129**, 312 (1932).

[3] J. Chadwick, Proc. Roy. Soc **136**, 692 (1932).

[4] H. Yukawa, Proc. Phys. Math. Soc. Jap. **17**, 48 (1935).

[5] C. M. G. Lattes, G. P. S. Occhialini, and C. F. Powell, Nature **160**, 453 (1947).

[6] S. H. Neddermeyer and C. D. Anderson, Phys. Rev. **51**, 884 (1937).

[7] J. C. Street and E. C. Stevenson, Phys. Rev. **52**, 1003 (1937).

[8] E. Segre, *From X-rays to Quarks. Modern Physicists and their Discoveries* (San Francisco, USA: Freeman, 1980).

[9] G. Kallen, *Elementary Particle Physics* (Addison-Wesley, 1964).

[10] M. Gell-Mann, Phys. Lett. **8**, 214 (1964).

[11] G. Zweig, CERN-TH-412 (1964).

[12] V. E. Barnes et al., Phys. Rev. Lett. **12**, 204 (1964).

[13] N. Isgur and G. Karl, Phys. Today **36**, 36 (1983).

[14] F. Fernández, A. Valcarce, U. Straub, and A. Faessler, J. Phys. **G19**, 2013 (1993).

[15] A. Valcarce, Ph.D. thesis, Universidad de Salamanca (1993).

[16] R. Machleidt, K. Holinde, and C. Elster, Phys. Rep. **149**, 1 (1987).

[17] V. G. J. Stoks, R. A. M. Klomp, C. P. F. Terheggen, and J. J. de Swart, Phys. Rev. **C49**, 2950 (1994), `nucl-th/9406039`.

[18] M. Lacombe et al., Phys. Rev. **C21**, 861 (1980).

[19] V. G. Neudachin, Y. F. Smirnov, and R. Tamagaki, Prog. Theor. Phys. **58**, 1072 (1977).

[20] J. E. T. Ribeiro, Z. Phys. **C5**, 27 (1980).

[21] H. Toki, Z. Phys. **A294**, 173 (1980).

[22] M. Oka and K. Yazaki, Phys. Lett. **B90**, 41 (1980).

[23] Y. Fujiwara and K. T. Hecht, Phys. Lett. **B171**, 17 (1986).

[24] M. Wakamatsu, R. Yamamoto, and Y. Yamauchi, Phys. Lett. **B146**, 148 (1984).

[25] S. Takeuchi, K. Shimizu, and K. Yazaki, Nucl. Phys. **A504**, 777 (1989).

[26] A. Valcarce, F. Fernández, A. Buchmann, and A. Faessler, Phys. Rev. **C50**, 2246 (1994).

[27] A. Valcarce, F. Fernández, P. González, and V. Vento, Phys. Lett. **B367**, 35 (1996), `nucl-th/9509009`.

[28] V. G. J. Stoks, R. A. M. Klomp, M. C. M. Rentmeester, and J. J. de Swart, Phys. Rev. **C48**, 792 (1993).

[29] S. Takeuchi, T. Cheon, and E. F. Redish, Phys. Lett. **B280**, 175 (1992).

[30] R. L. Kelly and R. E. Cutkosky, Phys. Rev. **D20**, 2782 (1979).

[31] R. Koch and E. Pietarinen, Nucl. Phys. **A336**, 331 (1980).

[32] D. M. Manley and E. M. Saleski, Phys. Rev. **D45**, 4002 (1992).

[33] V. D. Burkert (2002), `hep-ph/0210321`.

[34] F. X. Lee et al. (2002), `hep-lat/0208070`.

[35] O. Krehl, C. Hanhart, S. Krewald, and J. Speth, Phys. Rev. **C62**, 025207 (2000), `nucl-th/`

9911080.

[36] S. Hirenzaki, P. Fernández de Cordoba, and E. Oset, Phys. Rev. **C53**, 277 (1996), `nucl-th/9511036`.

[37] S. Hirenzaki, E. Oset, C. Djalali, and M. Morlet, Phys. Rev. **C61**, 044605 (2000), `nucl-th/0001004`.

[38] S. Huber and J. Aichelin, Nucl. Phys. **A573**, 587 (1994).

[39] A. Valcarce, F. Fernández, P. González, and V. Vento, Phys. Rev. **C52**, 38 (1995).

[40] D. R. Entem, Ph.D. thesis, Universidad de Salamanca (2000).

[41] P. Pascual and R. Tarrach, Lect. Notes Phys. **194**, 1 (1984).

[42] F. J. Yndurain, *The Theory of Quark and Gluon Interactions* (Springer: Berlin, Germany, 1999).

[43] K. Hagiwara et al. (Particle Data Group), Phys. Rev. **D66**, 010001 (2002).

[44] S. R. Coleman, J. Math. Phys. **7**, 787 (1966).

[45] A. Pich (1995), `hep-ph/9505231`.

[46] J. Goldstone, Nuovo Cim. **19**, 154 (1961).

[47] A. Manohar and H. Georgi, Nucl. Phys. **B234**, 189 (1984).

[48] M. B. Hecht, C. D. Roberts, and S. M. Schmidt (2001), `nucl-th/0106011`.

[49] Y. Fujiwara, M. Kohno, C. Nakamoto, and Y. Suzuki, Phys. Rev. **C64**, 054001 (2001), `nucl-th/0106052`.

[50] L. A. Blanco, Ph.D. thesis, Universidad de Salamanca (2001).

[51] L. Y. Glozman and D. O. Riska, Phys. Rep. **268**, 263 (1996), `hep-ph/9505422`.

[52] D. Bartz, Ph.D. thesis, Université de Liegé (2002), `hep-ph/0205138`.

[53] N. Isgur, Phys. Rev. **D62**, 054026 (2000), `nucl-th/9908028`.

[54] C. Nakamoto and H. Toki, Prog. Theor. Phys. **99**, 1001 (1998).

[55] M. Furuichi and K. Shimizu, Phys. Rev. **C65**, 025201 (2002).

[56] L. Y. Glozman, W. Plessas, K. Varga, and R. F. Wagenbrunn, Phys. Rev. **D58**, 094030 (1998), `hep-ph/9706507`.

[57] K. G. Wilson, Phys. Rev. **D10**, 2445 (1974).

[58] G. S. Bali, Phys. Rep. **343**, 1 (2001), `hep-ph/0001312`.

[59] K. Shimizu, Rep. Prog. Phys. **52**, 1 (1989).

[60] A. de Rujula, H. Georgi, and S. L. Glashow, Phys. Rev. **D12**, 147 (1975).

[61] M. D. Scadron, Phys. Rev. **D26**, 239 (1982).

[62] F. Fernández, A. Valcarce, P. González, and V. Vento, Phys. Lett. **B287**, 35 (1992).

[63] A. Buchmann, E. Hernández, and K. Yazaki, Phys. Lett. **B269**, 35 (1991).

[64] L. A. Blanco, F. Fernández, and A. Valcarce, Phys. Rev. **C59**, 428 (1999).

[65] R. Bonnaz, L. A. Blanco, B. Silvestre-Brac, F. Fernández, and A. Valcarce, Nucl. Phys. **A683**, 425 (2001).

[66] W. Gloeckle, *The Quantum Mechanical Few-Body Problem* (Springer Verlag, 1983).

[67] Y. Suzuki and K. Varga, Lect. Notes Phys. **M54**, 1 (1998).

[68] H. Garcilazo, A. Valcarce, and F. Fernández, Phys. Rev. **C64**, 058201 (2001), `nucl-th/`

0109004.

[69] A. Faessler, F. Fernández, G. Lübeck, and K. Shimizu, Phys. Lett. **B112**, 201 (1982).

[70] A. Faessler, F. Fernández, G. Lübeck, and K. Shimizu, Nucl. Phys. **A402**, 555 (1983).

[71] H. Garcilazo, F. Fernández, A. Valcarce, and R. D. Mota, Phys. Rev. **C56**, 84 (1997).

[72] H. Garcilazo, A. Valcarce, and F. Fernández, Phys. Rev. **C60**, 044002 (1999).

[73] A. Valcarce, H. Garcilazo, R. D. Mota, and F. Fernández, J. Phys. **G27**, L1 (2001).

[74] Y. C. Tang, M. LeMere, and D. R. Thompson, Phys. Rep. **47**, 167 (1978).

[75] D. A. Liberman, Phys. Rev. **D16**, 1542 (1977).

[76] K. Holinde, Nucl. Phys. **A415**, 477 (1984).

[77] F. E. Close, *An Introduction to Quarks and Partons* (Academic Press/London, 1979).

[78] F. Stancu, *Group Theory in Subnuclear Physics* (Oxford Stud. Nucl. Phys., 1996).

[79] Y. Suzuki and K. T. Hecht, Phys. Rev. **C29**, 1586 (1984).

[80] A. Valcarce, F. Fernández, and P. González, Phys. Rev. **C56**, 3026 (1997).

[81] F. Fernández, A. Valcarce, P. González, and V. Vento, Phys. Rev. **C47**, 1807 (1993).

[82] E. Ferreira and H. G. Dosch, Phys. Rev. **C40**, 1750 (1989).

[83] J. A. Wheeler, Phys. Rev. **52**, 1083 (1937).

[84] K. Shimizu, S. Takeuchi, and A. J. Buchmann, Prog. Theor. Phys. Suppl. **137**, 43 (2000).

[85] D. R. Entem, F. Fernández, and A. Valcarce, Phys. Rev. **C62**, 034002 (2000).

[86] M. Cvetic, B. Golli, N. Mankoc-Borstnik, and M. Rosina, Nucl. Phys. **A395**, 349 (1983).

[87] Y. Suzuki, Nucl. Phys. **A430**, 539 (1984).

[88] N. Isgur and G. Karl, Phys. Rev. **D18**, 4187 (1978).

[89] M. Oka, K. Shimizu, and K. Yazaki, Nucl. Phys. **A464**, 700 (1987).

[90] Z.-Y. Zhang, K. Brauer, A. Faessler, and K. Shimizu, Nucl. Phys. **A443**, 557 (1985).

[91] R. D. Mota, A. Valcarce, F. Fernández, and H. Garcilazo, Phys. Rev. **C59**, 46 (1999).

[92] B. F. Gibson, H. Kohlhoff, H. V. von Geramb, and G. L. Payne, Phys. Rev. **C51**, 465 (1995), nucl-th/9407030.

[93] J. Haidenbauer and K. Holinde, Phys. Rev. **C53**, R25 (1996).

[94] R. Machleidt, F. Sammarruca, and Y. Song, Phys. Rev. **C53**, 1483 (1996), nucl-th/9510023.

[95] C. Elster, E. E. Evans, H. Kamada, and W. Glöckle, Few-Body Syst. **21**, 25 (1996).

[96] P. Doleschall and I. Borbely, Phys. Rev. **C62**, 054004 (2000).

[97] E. F. Redish and K. Stricker-Bauer, Phys. Lett. **B133**, 1 (1983).

[98] C. Hajduk and P. U. Sauer, Nucl. Phys. **A322**, 329 (1979).

[99] D. J. Ernst, C. M. Shakin, and R. M. Thaler, Phys. Rev. **C8**, 46 (1973).

[100] J. Haidenbauer and W. Plessas, Phys. Rev. **C30**, 1822 (1984).

[101] W. Schadow, W. Sandhas, J. Haidenbauer, and A. Nogga, Few-Body Syst. **28**, 241 (2000), nucl-th/9810073.

[102] S. Nemoto et al., Few-Body Syst. **24**, 213 (1998).

[103] D. V. Bugg and R. A. Bryan, Nucl. Phys. **A540**, 449 (1992).

[104] A. Arndt, J. S. Hyslop, and L. D. Roper, Phys. Rev. **D35**, 128 (1987).

[105] Y. Fujiwara, K. Miyagawa, M. Kohno, Y. Suzuki, and H. Nemura, Phys. Rev. **C66**, 021001 (2002), `nucl-th/0205062`.

[106] B. F. Gibson and G. J. Stephenson, Phys. Rev. **C8**, 1222 (1973).

[107] H. P. Morsch and P. Zupranski, Phys. Rev. **C61**, 024002 (2000).

[108] G. E. Brown, J. W. Durso, and M. B. Johnson, Nucl. Phys. **A397**, 447 (1983).

[109] T. Barnes and F. E. Close, Phys. Lett. **B128**, 277 (1983).

[110] C. Schutz, J. Haidenbauer, J. Speth, and J. W. Durso, Phys. Rev. **C57**, 1464 (1998).

[111] E. Oset, H. Toki, and W. Weise, Phys. Rep. **83**, 281 (1982).

[112] P. González and E. L. Lomon, Phys. Rev. **D34**, 1351 (1986).

[113] A. M. Green, Rep. Prog. Phys. **39**, 1109 (1976).

[114] S. A. Coon, M. T. Peña, and D. O. Riska, Phys. Rev. **C52**, 2925 (1995), `nucl-th/9503013`.

[115] L. Alvarez-Ruso, Phys. Lett. **B452**, 207 (1999), `nucl-th/9811058`.

[116] E. L. Lomon, Phys. Rev. **D26**, 576 (1982).

[117] M. T. Peña, D. O. Riska, and A. Stadler, Phys. Rev. **C60**, 045201 (1999), `nucl-th/9902066`.

[118] B. A. Li, C. M. Ko, and G.-Q. Li, Phys. Rev. **C50**, 2675 (1994).

[119] M. T. Peña, H. Henning, and P. U. Sauer, Phys. Rev. **C42**, 855 (1990).

[120] T.-S. H. Lee, Phys. Rev. Lett. **50**, 1571 (1983).

[121] A. Valcarce, A. Faessler, and F. Fernández, Phys. Lett. **B345**, 367 (1995).

[122] A. Valcarce, F. Fernández, H. Garcilazo, M. T. Peña, and P. U. Sauer, Phys. Rev. **C49**, 1799 (1994).

[123] H. J. Weber and H. Arenhovel, Phys. Rep. **36**, 277 (1978).

[124] A. K. Kerman and L. S. Kisslinger, Phys. Rev. **180**, 1483 (1969).

[125] E. Hadjimichael, Phys. Lett. **B46**, 147 (1973).

[126] O. Y. Denisov, S. D. Kuksa, and G. I. Lykasov, Phys. Lett. **B458**, 415 (1999), `nucl-th/9811069`.

[127] Y. L. Dorodnykh, G. I. Lykasov, M. V. Rzyanin, and W. Cassing, Phys. Lett. **B346**, 227 (1995).

[128] Y. N. Uzikov, Phys. Atom. Nucl. **60**, 1616 (1997).

[129] Y. N. Uzikov, Phys. Atom. Nucl. **60**, 1458 (1997).

[130] P. Haapakoski and M. Saarela, Phys. Lett. **B53**, 333 (1974).

[131] H. Arenhovel, M. Danos, and H. T. Williams, Nucl. Phys. **A162**, 12 (1971).

[132] H. J. Weber, Phys. Rev. **C9**, 1771 (1974).

[133] N. R. Nath and H. J. Weber, Phys. Rev. **D6**, 1975 (1972).

[134] E. Rost, Nucl. Phys. **A249**, 510 (1975).

[135] A. M. Kusainov, V. G. Neudatchin, and I. T. Obukhovsky, Phys. Rev. **C44**, 2343 (1991).

[136] L. Y. Glozman and E. I. Kuchina, Phys. Rev. **C49**, 1149 (1994).

[137] I. Maeda, M. Arima, and K. Masutani, Phys. Lett. **B474**, 255 (2000).

[138] K. A. Herbst and F. Gross (1997), `nucl-th/9710020`.

[139] A. M. Green and P. Haapakoski, Nucl. Phys. **A221**, 429 (1974).

[140] D. O. Riska and G. E. Brown, Nucl. Phys. **A679**, 577 (2001), `nucl-th/0005049`.

[141] H. Garcilazo and E. Moya de Guerra, Nucl. Phys. **A562**, 521 (1993).

[142] M. Soyeur, Nucl. Phys. **A671**, 532 (2000), `nucl-th/0003047`.

[143] H. P. Morsch et al., Phys. Rev. Lett. **69**, 1336 (1992).

[144] P. Fernández de Cordoba et al., Nucl. Phys. **A586**, 586 (1995).

[145] R. Machleidt, Adv. Nucl. Phys. **19**, 189 (1989).

[146] T. E. O. Ericson and W. Weise, *Pions and Nuclei* (Oxford, Clarendon, 1988).

[147] E. Epelbaum, W. Glöckle, and U. G. Meißner, Nucl. Phys. **A671**, 295 (2000), `nucl-th/9910064`.

[148] E. L. Lomon and H. Feshbach, Ann. Phys. (N.Y.) **48**, 94 (1968).

[149] H. Pöpping, P. U. Sauer, and X. Zhang, Nucl. Phys. **A474**, 557 (1987).

[150] D. R. Entem, F. Fernández, and A. Valcarce, Phys. Rev. **C67**, 014001 (2003).

[151] H. Garcilazo and T. Mizutani, πNN *systems* (World Scientific, 1990).

[152] M. I. Haftel and F. Tabakin, Nucl. Phys. **A158**, 1 (1970).

[153] R. A. Arndt, I. I. Strakovsky, and R. L. Workman, Phys. Rev. **C62**, 034005 (2000), `nucl-th/0004039`.

[154] A. Valcarce, A. Buchmann, F. Fernández, and A. Faessler, Phys. Rev. **C51**, 1480 (1995).

[155] O. Morimatsu, K. Yazaki, and M. Oka, Nucl. Phys. **A424**, 412 (1984).

[156] Y. Suzuki and K. T. Hecht, Nucl. Phys. **A420**, 525 (1984).

[157] T.-S. H. Lee (2003), private communication.

[158] T.-S. H. Lee, Phys. Rev. **C29**, 195 (1984).

[159] Y. Fujiwara, Y. Suzuki, K. Miyagawa, M. Kohno, and H. Nemura, Prog. Theor. Phys. **107**, 993 (2002), `nucl-th/0201052`.

[160] D. J. Ernst, C. M. Shakin, R. M. Thaler, and D. L. Weiss, Phys. Rev. **C8**, 2056 (1973).

Publications and Contributions

- *Deuteron $NN^*(1440)$ components from a chiral quark model*
  B. Juliá-Díaz, D.R. Entem, A. Valcarce, F. Fernández.
  Phys. Rev. C 66, 047002 (2002).

- *Microscopic $NN \rightarrow NN^*(1440)$ transition potential: Determination of $\pi NN^*(1440)$ and $\sigma NN^*(1440)$ coupling constants*
  B. Juliá-Díaz, A. Valcarce, P. González, F. Fernández.
  Phys. Rev. C 66, 024005, (2002).

- *Quark model study of the triton binding energy*
  B. Juliá-Díaz, J. Haidenbauer, A. Valcarce, and F. Fernández.
  Phys. Rev. C 65, 034001, (2002).

- *Microscopic derivation of the NN*(1440) potential*
  B. Juliá-Díaz, P. González, F. Fernández, and A. Valcarce.
  Phys. Rev. C 63, 024006, (2001).

- *$NN^*(1440)$ in a constituent quark model*
  B. Juliá-Díaz, P. González, A. Valcarce, F. Fernández.
  "The Physics of the Roper Resonance", Trento ECT* 2002.

- *$\pi NN^*(1440)$ and $\sigma NN^*(1440)$ coupling constants from a microscopic $NN \rightarrow NN^*(1440)$ potential*
  P. González, B. Juliá-Díaz, A. Valcarce, F. Fernández.
  Baryons 2002, JLab, Newport News (USA), 4-8 March, 2002.
  xxx:nucl-th/0206066

- *Quark model study of the triton bound state*
  B. Juliá-Díaz, A. Valcarce, F. Fernández, J. Haidenbauer.
  Mesons and Light Nuclei'01, Prague, July 2001.
  AIP Conf.Proc. 603 (2001) 263.

- *Quark model study of $NN^*(1440)$ components on the deuteron*
  B. Juliá-Díaz, D. R. Entem, F. Fernández, A. Valcarce.
  Mesons and Light Nuclei'01, Prague, July 2001.
  AIP Conf.Proc. 603 (2001) 267.

- *NN^* interactions from a constituent quark cluster model*
  B. Juliá-Díaz.
  Contributed to the School, *Understanding the structure of hadrons*, Prague July 9-13 2001.
  Czech J. Phys. 52 B181 Suppl. B (2002).

- *Quark model description of the NN*(1440) potential*
  B. Juliá, F. Fernández, P. González y A. Valcarce.
  XVII European conference in few body problems in physics, Evora (Portugal), September 2000.
  Nuclear Physics A, 689, 31 (2001).

- *La interacción NN* en un modelo quark no relativista*
  B. Juliá, F. Fernández y A. Valcarce.
  XXVII Reunión Bienal de la Real Sociedad Española de Física, Valencia, September 1999.